Aus dem

Institut für Medizinische Psychologie

Institut der Ludwig-Maximilians-Universität München

The circadian clock and G-protein-coupled receptor signaling: RGS16 and how it controls chronotype

Dissertation
zum Erwerb des Doktorgrades der Medizin
an der Medizinischen Fakultät
der Ludwig-Maximilians-Universität München

vorgelegt von
Tanja Schwarzmeier

aus
Pfaffenhofen a. d. Ilm

Jahr
2025

Mit Genehmigung der Medizinischen Fakultät der
Ludwig-Maximilians-Universität München

Erstes Gutachten:	Prof. Dr. Dr. Martha Merrow
Zweites Gutachten:	Prof. Dr. Jürgen Bernhagen
Drittes Gutachten:	Prof. Dr. Jan Rémi

Dekan: Prof. Dr. med. Thomas Gudermann

Tag der mündlichen Prüfung: 20.11.2025

Table of Contents

Zusammenfassung

Viele Vorgänge im Körper sind unter der Kontrolle der inneren Uhr, deren Synchronisierung mit unserer Umgebung dazu führt, dass viele Verhaltensweisen einer 24-Stunden-Periodik unterliegen. Unsere Schlaf- und Aktivitätspräferenz wird Chronotyp genannt. Beeinflusst wird dieser unter anderem durch externe Faktoren wie Lichtexposition, aber es gibt auch eine genetische Komponente. Mehrere genomweite Assoziationsstudien haben RGS16, „Regulator of G-protein Signaling 16“, als ein potentielles Chronotyp-Gen identifiziert. RGS16 spielt eine wichtige Rolle in den zentralen Schrittmacherzellen der inneren Uhr. Es ist ein Modulator von Signalwegen der G-Protein-gekoppelten Rezeptoren (GPCRs), welche im gesamten Körper vorkommen und Informationen über die Umgebung an die Zelle und den Organismus weitergeben. Daher wäre es möglich, dass GPCRs und RGS16 eine allgemeinere Rolle in den Input-Wegen der Uhr spielen. In dieser Arbeit soll das Zusammenspiel zwischen der inneren Uhr, RGS16 und GPCRs erforscht und hierdurch möglicherweise eine Erklärung für interindividuelle Unterschiede im Chronotyp gefunden werden.

RGS16 wurde in humanen Osteosarkomzellen (U-2 OS) und adulten retinalen Pigmentepithelzellen (ARPE-19) mittels Knock-down (KD) herunterreguliert und der Effekt auf Schlüsselmerkmale der inneren Uhr, also Periodenlänge des Rhythmus in konstanten Bedingungen, Phase in Bezug auf den Umgebungszyklus und Temperaturunabhängigkeit der Rhythmen, charakterisiert. Hierbei zeigten sich je nach Zelllinie und Bedingungen unterschiedliche Effekte sowohl in U-2 OS als auch in ARPE-19 Zellen, was für eine allgemeinere Rolle von RGS16 im Uhrnetzwerk spricht. RGS16 selbst steht ebenfalls unter dem Einfluss der Uhr, unter anderem durch Änderungen der Proteinmenge und der Lokalisation über den Tag. Außerdem reagiert es auf Temperaturänderungen, und ein KD führt zu einer erhöhten Temperaturempfindlichkeit der Zellen. Dies legt eine Beteiligung in der Input-Regulierung nahe, möglicherweise durch die Beeinflussung des cAMP-Signalwegs. Es konnten zirkadiane cAMP-Rhythmen in U-2 OS Zellen gezeigt werden, welche durch den KD beeinflusst wurden. Passend hierzu war die cAMP-Antwort nach GPCR-Stimulation unterschiedlich, je nachdem, ob zu einer Zeit hoher oder niedriger RGS16-Level stimuliert wurde. Die cAMP-Spiegel beeinflussen wiederum viele bekannte Uhr-Gene.

Insgesamt scheint RGS16 in mehreren Zellarten eine Rolle für die innere Uhr zu spielen. Die Daten weisen auf eine Beteiligung am Input des Uhrnetzwerks hin. Dies macht RGS16 zu einem sogenannten Zeitnehmer, da es sowohl als Input als auch als Output der Uhr fungiert, und so Zeit-Informationen an die Zellen weitergibt. Die Daten unterstützen weiterhin die in anderen Arbeiten publizierten Ansichten, dass RGS16 über die Regulierung von cAMP-Leveln am Netzwerk der Uhr beteiligt ist, und erweitert diese um weitere Zellen und Gewebe.

Abstract

Many processes in the body are under the control of the circadian clock. The entrainment of the clock to our 24 h environment results in rhythmic behaviours, called chronotype. Chronotype is influenced by external factors such as light, but it also has a genetic basis. Several genome-wide association studies (GWAS) have identified RGS16, Regulator of G-protein Signaling 16, as a potential chronotype-influencing gene. RGS16 has been shown to be crucial for keeping the rhythm in the central pacemaker cells in the brain. It is a modulator of G-protein-coupled receptor (GPCR) signaling. As GPCRs are ubiquitous throughout the body, where they relay information about the environment to the cell and the organism, we hypothesized that they may be involved in modulating zeitgebers of the circadian clock in a more generalized way, too. In this work, we wished to explore the interplay between the clock, RGS16, and GPCRs as part of the mechanism to explain interindividual variations in chronotype.

RGS16 was knocked down in human osteosarcoma (U-2 OS) and adult retinal pigment epithelium (ARPE-19) cells to determine its effect on key circadian properties, namely free-running period, phase of entrainment, and temperature compensation. Here, the knockdown (KD) leads to a variety of changes, demonstrating that RGS16 indeed plays a role in the function of the clock in peripheral cells. Changes were observed in U-2 OS cells as well as in ARPE-19 cells, suggesting an involvement in several tissues, although the exact effect differs depending on the cell line and the conditions. RGS16 itself is also influenced by the clock, with fluctuations in abundance and localization depending on the time of day. It also responds to temperature changes, and a KD makes the system more susceptible to temperature variations, which serve as important zeitgebers in the body. This suggests an involvement of RGS16 in the zeitgeber input pathway. Circadian rhythms in cAMP levels in free-running conditions could also be shown in U-2 OS cells, which were impacted by a KD of RGS16, reinforcing an involvement in cAMP signaling. In accordance with this, the cAMP response elicited by GPCR activation at different times of day is influenced by RGS16 levels. Many clock genes have cAMP response elements in their promoter regions, so fluctuating cAMP levels act as clock inputs.

Overall, RGS16 seems to play a role in the circadian clock in several cells and tissues, with the data suggesting an involvement in the zeitgeber input pathway of the clock. By being part of both input and output of the clock network, RGS16 acts as a zeitnehmer and passes on timing information to the cells. Our findings support previous research that RGS16 acts on the circadian clock through involvement in the regulation of cAMP levels, and expands the knowledge about its role to other cells and tissues.

List of Figures

List of Tables

List of Abbreviations

BMAL1: Brain and muscle arnt-like protein 1

cAMP: cyclic adenosine monophosphate

CRE: cAMP response element

CoG: Center of Gravity

ExT: External time

FFT-NLLS: Fast Fourier Transform Nonlinear Least Squares fit

FRP: Free-running period

GPCR: G-protein-coupled receptor

GTP: Guanosine triphosphate

IF: Immunofluorescence

JTK_cycle: Jonckheere-Terpstra-Kendall cycles test for rhythmicity

KD: Knockdown

N-CHA: N^6-cyclohexyladenosine

PCC: Pearson's Correlation Coefficient

RGS16: Regulator of G-protein signaling 16

RKD: RGS16 KD

SCN: Nucleus Suprachiasmaticus

shRNA: short hairpin RNA

WB: Western Blot

1. Introduction

The circadian clock, deriving its name from “circa diem”, meaning “about a day”, is an endogenous temporal program which orchestrates the daily regulation of physiology, metabolism and behavior of almost all living organisms. It evolved as an adaptation to the earth’s 24h rotation, which leads to a highly rhythmical environment with aspects such as light quality and intensity, ambient temperature, nutrient availability and predator exposure recurring in regular time frames. Therefore, most organisms have evolved a system, or clock, that enables them to anticipate and respond to this predictable cycling environment, which has been shown to be evolutionarily advantageous (Dodd et al., 2005; Ouyang et al., 1998). As a result, many processes are clock-regulated, from molecular mechanisms such as DNA repair to physiology including core body temperature and behaviour like the sleep-wake cycle and feeding times. Disruption of the circadian clock leads to disease, consistent with the demonstrations that the clock provides an evolutionary advantage (Roenneberg & Merrow, 2016). Additionally, circadian clocks impact health care in another way: the targets of many pharmaceuticals are expressed with a daily rhythm, which brings the circadian clock into focus for the development and administration of medical treatments (Roenneberg & Merrow, 2016; Zhang et al., 2014). About 1/3 of all newly approved drugs target some level of GPCR signaling (Rask-Andersen et al., 2011; Sriram & Insel, 2018). Knowing when a GPCR targeted for drug treatment is expressed – knowing its circadian rhythm – can have critical effects on therapy: drug treatment given at a time of low target receptor expression can result in lower efficacy and higher side effects.

Circadian rhythms have three key properties: they have an endogenous free-running period of about 24 hours under constant conditions; they entrain to external stimuli; the rhythms are temperature-compensated, meaning they remain stable over a wide range of temperatures (Edery, 2000). A free-running circadian rhythm is described by Pittendrigh in the Cold Spring Harbour Symposium of 1960 as an endogenous and self-sustained biological rhythm whose period approximates the period of the earth’s rotation (24h) (Pittendrigh, 1960). Free-running periods can tell us something about the configuration of a system, but the phase of entrainment is what is important in a cycling environment. Circadian rhythms must be entrainable, which means their periodicity is influenced by external cues such as temperature and light (so-called zeitgebers, which translates from German as “time-giver”) (Aschoff, 1960; Pittendrigh, 1960; Pittendrigh, 1981). Under normal conditions, biochemical reactions are temperature-dependent. With rising temperatures, due to the increased energy levels of the molecules, the reactions

typically occur faster. The circadian clock, however, needs to remain stable over a variety of temperatures, therefore the system has to be temperature-compensated (Pittendrigh, 1960; Sweeney & Hastings, 1960).

We know quite a bit about the molecular mechanism of eukaryotic circadian clocks. At the core of the mammalian circadian clock, there are so-called central clock genes which regulate their own expression via a transcription-translation negative feedback loop (Takahashi, 2017). The molecular clock exists in almost all cells, but its individual components, inputs and outputs vary between different tissues and organisms (Takahashi, 2017). For example, which mRNAs or proteins are cycling and at what time is hugely tissue- and organism-specific (Zhang et al., 2014). Numerous molecular layers influence the clock, and many have not been fully understood yet. For instance, links to metabolism and to redox state have been described, but they are difficult to explore with typical molecular genetic tools and thus it is not entirely clear how much these states impact the clock (Asher et al., 2008; Milev et al., 2015). In a simplified model, also referred to as the Eskin model or Eskinogram, the clock mechanism can be described as containing three main components: an input, an oscillator, and an output (Eskin, 1979). This is a considerable simplification though, since the various outputs can in turn act as inputs for the same or other clocks (so-called zeitnehmers, translated from the German word for “time-takers”), and the numerous layers of the oscillators are intertwined (McWatters et al., 2000; Roenneberg & Merrow, 2005; Takahashi, 2017).

The circadian clock in mammals (at the level of the organism) is mainly relying on light as its primary input. The light information is sensed in the intrinsically photosensitive retinal ganglion cells (ipRGC) and then passed on to the suprachiasmatic nucleus (SCN), a region in the hypothalamus just above the optic chiasm (Berson et al., 2002; Peirson & Foster, 2009). The SCN acts as a central pacemaker which synchronizes the other clocks in the body via the regulation of the sleep-wake cycle, hormone secretion, and body temperature, among others (Doi et al., 2011). However, there are still many unanswered questions regarding the complex regulation und synchronization of peripheral clocks, as light is not the only input to the circadian clock and there exists an SCN-independent food-entrainable oscillator as well whose anatomical location is still unknown (Balsalobre et al., 1998; Escobar et al., 2009; Mendoza, 2007; Mistlberger, 2009). The liver has also increasingly gained attention for its role in regulating metabolism in a circadian fashion, with food intake being the main synchronizer for many of its rhythms (Balsalobre et al., 1998; Daniels et al., 2023; Hayasaka et al., 2011).

The most well-known output of the mammalian clock is sleep timing: being "a morning person" or "lark" vs. being an "owl", as the most extreme chronotypes are often called. "Chronotype" refers to an organism's habitual behaviour in regard to the time of day when certain events (e.g. sleeping and waking) occur. It is an indicator of the phase of entrainment of an organism relative to the external 24 h zeitgeber cycle at a behavioural level. Chronotype is near-normally distributed in humans. It is influenced by the environment (mainly light exposure) as wells as individual (for example age and gender) and genetic factors (Roenneberg et al., 2007; Roenneberg, Wirz-Justice, et al., 2003). Several genes have been discovered that influence chronotype. Some are known clock genes such as *PERIOD* or *CLOCK* (Ebisawa et al., 2001; Hamet & Tremblay, 2006; Katzenberg et al., 1998; Toh et al., 2001). For example, clock genes known from mice show up in pedigrees with early sleeping individuals (Jones et al., 1999). However, many elements still remain unidentified. Looking for chronotype genes using the MCTQ (Munich ChronoType Questionnaire) in a genome wide association study (GWAS) identified only sleep duration genes (Allebrandt et al., 2013; Allebrandt et al., 2010). Taking a high throughput approach, genome-wide association studies (GWAS) that were looking for alleles for "morningness" yielded several associated loci including RGS16. RGS16 ("Regulator of G-Protein Signaling 16") was identified as among the most significant hits (Hu et al., 2016; Jones et al., 2016; Lane et al., 2016). A follow-up study confirmed an RGS16 variation as a likely causal coding variant for morningness (Jones et al., 2019).

RGS16 is a known modulator of G-protein-coupled receptor (GPCR) signaling pathways. It belongs to the B/R4 subfamily of the Regulator of G Protein Signaling family, a highly abundant group of proteins involved in the regulation of diverse, central cellular processes. RGS16 has been shown to be involved in various pathways including immunity, inflammation, tumorigenesis, metabolism and coagulation (Tian et al., 2022). It increases the GTPase activity of G protein subunits ($G_{i/o}$ as well as G_q) by stimulating GTP hydrolysis (Bansal et al., 2007; Koelle, 1997; Masuho et al., 2020). GPCRs are a large family of cell surface receptors which transmit signals from the extracellular environment to the inside of the cells. Several levels of GPCR signaling are under circadian control (Doi et al., 2011; Roenneberg & Merrow, 2016). One example is melanopsin, a GPCR expressed in ipRGCs, which passes on the light information to the SCN where this information is processed and leads to the subsequent synchronization of the peripheral clocks in the body (Panda et al., 2005; Provencio et al., 2000). Another example for the direct relationship between the clock and GPCRs is melatonin, a hormone that has a strong circadian rhythm in mammals and exerts its effects through GPCRs

(Dubocovich, 2007). It is expressed in the beginning of the night and signals “darkness” to the organism (Pévet et al., 2006). Caffeine is another a molecule that acts via modulation of GPCR signaling and can heavily influence sleeping behaviour. It has been shown to lengthen the circadian rhythm of behavior as well as cellular rhythms in mammals (Burke et al., 2015; Oike et al., 2011). It conveys its effect among others through the Adenosine 1 receptor, a GPCR, by blocking the activation of the $G_{i/o}$ subunit by adenosine, thereby increasing the production of cAMP (Chen et al., 2013; Nehlig et al., 1992; Shryock et al., 1998). cAMP is an important second messenger molecule that conveys many different physiological functions.

RGS16 has also been shown to act through modifying cAMP levels (Doi et al., 2011). It interacts with the G_i subunit, which suppresses cAMP production via inhibition of the adenylyl cyclase (AC). RGS16 inhibits G_i, therefore allowing for cAMP production while RGS16 is present. By being expressed in a circadian fashion with its peak in the morning in the SCN, RGS16 leads to cycling circadian levels of cAMP (Doi et al., 2011). Many core clock genes such as BMAL1 also have a cAMP-response element (CRE) in their promoter region (Allen et al., 2017; Doi et al., 2011; Koyanagi et al., 2011; O'Neill et al., 2008). This could be a possible input pathway to the clock. In turn, RGS16 expression is also clock-regulated via D-box and E-box regions (Nakagawa et al., 2020). A knockdown or knockout of RGS16 results in an alteration of the locomotor behavior in mice, an established behavior under circadian regulation (Doi et al., 2011; Hayasaka et al., 2011). RGS16 has also been shown to be involved in the food-entrainable oscillator in the liver by being entrained by feeding rhythms and regulating glucose production and GPCR-stimulated fatty acid oxidation in hepatocytes (Hayasaka et al., 2011; Huang et al., 2006; Pashkov et al., 2011).

Therefore, RGS16 seems to be important for two of the major synchronizers of the body: SCN and liver, aka light and food input pathways. Since RGS16 is modulating GPCR signaling, and both GPCRs and RGS16 are ubiquitously expressed in the body, we propose a generalized role of RGS16 in the GPCR signaling cascade that feeds back on the clock, not only in the SCN or the liver, but in most cells of the body.

To explore what role RGS16 plays in peripheral (non-SCN) cells, I wish to answer two questions:

1. What effect does a knockdown of RGS16 have on the molecular circadian clock in peripheral cells, and is this a general principle?
2. How does RGS16 interact with the circadian clock in peripheral cells?

1.1 What effect does a knockdown of RGS16 have on the molecular circadian clock in non-SCN cells, and is this a universal principle?

Circadian rhythms have three key properties: they have an endogenous free-running period of about 24 hours under constant conditions; they entrain to external stimuli called zeitgebers; the frequencies of the rhythms are temperature-compensated (Edery, 2000). Here, we investigate the regulation of GPCR signaling by RGS16 and its effect on these key features of the circadian clock. This can help shed light onto the interaction between the circadian clock in cells and GPCRs. This information could eventually aid the fine-tuning of (chrono)pharmacotherapy.

To explore the role of RGS16 in non-SCN cells, human osteosarcoma cells (U-2 OS) and ARPE-19 (adult retinal pigment epithelium) cells were used. U-2 OS cells are a widely used model in circadian biology (Baggs et al., 2009; Hirota et al., 2008; Liu et al., 2007; Maier et al., 2009). ARPE-19 cells are non-photoreceptive retinal cells that are not involved in transmitting zeitgeber information, but are highly dependent on circadian regulation due to their direct rhythmic sun and heat exposure (DeVera et al., 2022).

For investigating the key circadian properties of cells, luciferase reporter cell lines are an established tool (Welsh et al., 2005; Yamazaki & Takahashi, 2005). Here, a luciferase gene is fused to the promoter of a core clock gene such as *Bmal1,* so the clock-regulated gene expression (as a measure of the circadian clock) can be quantified continuously via luminometry over several days. U-2 OS and ARPE-19 cell lines stably expressing luciferase from a *Bmal1* promoter fragment were used to establish RGS16 knockdown cell lines. Cells were transfected such that they stably expressed a luciferase construct that reports *Bmal1* expression (BMAL1::Luc) and in addition they expressed RGS16 shRNA. BMAL1::Luc cell lines transfected with a scrambled shRNA construct served as a negative control.
With these cell lines, experiments were performed to determine the following:

a) free-running period
b) phase of entrainment (in standard cold:warm 12:12 cycles as well as in different thermoperiods and T cycles)
c) temperature compensation (in free-run and entrainment)

1.2 How does RGS16 interact with the circadian clock in peripheral cells?

As opposed to SCN cells, little is yet known of how RGS16 interacts with the molecular clock in peripheral cells. RGS16 and the core circadian clock could be intertwined in a number of ways: RGS16 abundance may be temporally regulated, gating its activity; RGS16 may be localized to different compartments depending on the time of day, limiting its interaction partners; RGS16 may respond to temperature changes to convey this zeitgeber information to the cell, as it has been shown to be upregulated following heat pulses (Seifert et al., 2015); RGS16 may change localization in response to GPCR activation, which itself can be highly rhythmic in the body; RGS16 may modulate downstream signaling pathways of GPCRs, for example via cAMP, analogous to the SCN.

Human osteosarcoma cells (U-2 OS cells) are an established model for peripheral cells in molecular biology as well as in circadian biology and have well-documented, stable circadian rhythms (Maier et al., 2009). Therefore, this cell line was used for these experiments.

To investigate the interaction of RGS16 with the clock, the following experiments were performed:

a) Western blot time course to determine if the abundance of RGS16 is changing over the time of the day
b) Immunofluorescence time course to determine if the localization of RGS16 changes over the time of the day
c) Localization of RGS16 in response to temperature pulses
d) Localization of RGS16 in response to GPCR stimulation
e) Free-running period of *BMAL1* with and without a knockdown of RGS16 after the addition of caffeine
f) Explore baseline cAMP rhythms
g) Effect of a knockdown of RGS16 on baseline cAMP levels
h) Effect of RGS16 levels on the cAMP response after GPCR activation

2. Materials and Methods

2.1 Tables of Materials

2.1.1 Cell lines

The cell lines utilized in this work are listed in the following table.

Cell line	Description	Origin	Experiments
U-2 OS, here: "**native U-2 OS**"	Native U-2 OS cell line; human osteosarcoma cells	American Type Culture Collection [ATCC] # HTB-96	Protein time course; Immunocytochemistry: RGS16 and A1R localization
U2OS_Bmal1p-luc, here: "**U2OS BMAL1::Luc**"	U-2 OS with a *Bmal1* promoter fragment	A. Kramer, Charité, Berlin	Creation of RGS16 KD cell lines and controls
Selected U2OS_Bmal1p-luc_RKD, here: "**U2OS-RKD**"	U-2 OS with a *Bmal1* promoter fragment and RGS16 shRNA, selected	This work	Determine the effect of a KD of RGS16 on clock properties
Selected U2OS_Bmal1p-luc_scrRNA, here: "**U2OS-control**"	U-2 OS with a *Bmal1* promoter fragment and scrambled shRNA, selected	This work	Determine the effect of a KD of RGS16 on clock properties
Subcloned U2OS_Bmal1p-luc_RKD, here: "**Subcloned_U2OS-RKD**"	U-2 OS with a *Bmal1* promoter fragment and RGS16 shRNA, subcloned, single clone	This work	Determine the effect of a KD of RGS16 on clock properties
Subcloned U2OS_Bmal1p-luc_scrRNA, here: "**Subcloned_U2OS-control**"	U-2 OS with a *Bmal1* promoter fragment and scrambled RNA, subcloned, single clone	This work	Determine the effect of a KD of RGS16 on clock properties
U-2 OS_pGlo, here: "**U2OS_pGlo**"	U-2 OS with a Promega pGlo cAMP-Sensor	J. O'Neill, MRC Laboratory of Molecular Biology, Cambridge	Baseline cAMP rhythms; Creation of KD cell lines; cAMP stimulation experiments
Selected U-2OS_pGlo_RKD, here: "**pGlo_RKD**"	U-2 OS with a Promega pGlo cAMP-Sensor and RSG16 shRNA, selected	This work	Determine the effect of a KD of RGS16 on baseline cAMP rhythms
Selected U-2OS_pGlo_scrRNA, here: "**pGlo_control**"	U-2 OS with a Promega pGlo cAMP-Sensor and	This work	Determine the effect of a KD of RGS16 on baseline cAMP rhythms

	scrambled shRNA, selected		
ARPE-19_Bmal1p-luc, here: "**ARPE BMAL1::Luc**"	ARPE-19, human adult retinal pigment epithelium, with a *Bmal1* promoter fragment	G. Wildner, LMU Munich	Creation of RGS16 KD cell lines and controls
Selected ARPE-19_Bmal1p-luc_RKD, here: "**ARPE-RKD**"	ARPE-19 with a *Bmal1* promoter fragment and RGS16 shRNA, selected	This work	Determine the effect of a KD of RGS16 on clock properties
Selected ARPE-19_Bmal1p-luc_scrRNA, here: "**ARPE-control**"	ARPE-19 with a *Bmal1* promoter fragment and scrambled shRNA, selected	This work	Determine the effect of a KD of RGS16 on clock properties

2.1.2 Chemicals and Reagents

The chemicals and reagents, including media and antibiotics, that were used for buffers and experiments are listed in the following table.

Chemical	**Supplier**	**Order No.**
1 M TRIS/HCl buffer pH 6.8	AppliChem	A1087
10% APS Ammoniumpersulfate	Sigma-Aldrich	A3980
10% SDS	AppliChem	A1502
30% Acrylamide/Bis-acrylamide	Sigma-Aldrich	A3574
Bond Breaker TCEP Solution	Thermo Scientific	77720
Bromphenol blue sodium salt	USB	US12370
BSA Bovine Serum Albumin	Sigma-Aldrich	A7906
Caffeine	Abcam	ab120240
DAPI	Sigma-Aldrich	D9542
Dexamethasone	Sigma-Aldrich	D4902
DMEM Dulbecco's Modified Eagle Medium +4.5 g/L D-Glucose. No added Sodium Pyruvate, no Glutamine	Gibco	31053028
D-Luciferin	P.J.K.	102111
Dopamine hydrochloride	Sigma-Aldrich	H8502
Dulbecco's Modified Eagle's Medium/Nutrient Mixture F-12 Ham with 15 mM HEPES and sodium bicarbonate. Without L-glutamine and phenol red. Liquid, sterile-filteres. Suitable for cell culture (DMEM/F12. 1:1 mixcture)	Sigma-Aldrich	D6434
Ethanol	AppliChem	A3678
FCS inactivated 40min/56°C. sterile-filtered	Gibco	10270106

Formaldehyde Solution	Sigma-Aldrich	F8775
GlutaMAX (100X)	Gibco	35050061
Glycerol 100%	Sigma-Aldrich	G5516
Glycine (1.92 M)	Roth	3908.4
HCl 37%	Sigma-Aldrich	258148
Hygromycin B in PBS 50 mg/ml	Invitrogen	10687010
Immersion oil	Sigma-Aldrich	56822
Isoprenaline hydrochloride	Sigma-Aldrich	I6527
Isopropanol	AppliChem	131090.1211
KCl (2.7 mM)	AppliChem	A3980
Methanol	Thermo Scientific	10284580
Milk powder, nonfat	Spinnrad	002230048
N6-cyclohexyladenosine	Abcam	ab120472
NaCL (150 mM)	AppliChem	A2942
Opti-MEM Reduced Serum Medium	Gibco	31985062
PageRuler Plus Prestained Protein Ladder	Thermo Scientific	26619
Penicillin / Streptomycin	Gibco	15140122
Pierce ECL Western Blotting Substrate	Thermoe Scientific	32106
PBS Dulbecco's phosphate buffered saline. Modified, without calcium chloride and magnesium chloride	Sigma-Aldrich	D8537
PFA Paraformaldehyde 95%	Sigma-Aldrich	158127
Ponceau S	FLUKA	81460
Puromycin	Gibco	A1113803
R-phenylephrine hydrochloride	Sigma-Aldrich	P6126
Serotonin creatinin sulfate monohydrate	Sigma-Aldrich	H7752
Sodium Pyruvate 100mM 100x	Gibco	11360070
SuperSignal West Femto Maximum Sensitivity Substrate	Thermo Scientific	34095
TEMED: N N N N Tetramethylethylenediamine	Sigma-Aldrich	T9281
TripLE Express (no phenol red)	Gibco	12604013
TRIS base (250 mM)	Sigma-Aldrich	T1503
Triton X-100	Sigma-Aldrich	T8787
Trypan blue stain 0.4%	Gibco	15250061
Tween-20	Sigma-Aldrich	P9416

2.1.3 Consumables

The consumables, including materials, plasmids, transfection kits and antibodies that were used are listed in the following tables.

Consumable	**Supplier**
12 ml cell culture tube	cellstar greiner bio-one
96 well plate white: Nunclon Delta Surface	Thermo Scientific Nunc

Automated pipette automatic-Sarpette	Sarstedt
Blotting paper	Whatman
Cell scraper	Sarstedt
Cellstar tubes 50 ml	cellstar greiner bio-one
Cryopure tubes 1.8ml	Sarstedt
CytoOne 96 well plate clear, TC-treated	Star Lab
Eppendorf tubes 2.0 ml	Eppendorf
Glass bottom dish 35mm	ibidi
Gloves	Unifloves
Liquid nitrogen	Linde Gas
Parafilm	Bemis
Pipette tips 10µl - 1000 ml: TipOne Graduated Filter Tip	Star Lab
Pipettes: 2-50 ml	cellstar greiner bio-one
Pipettes: reference and research plus	Eppendorf
Plastic foil / disposable bags	Sarstedt
PVDF membrane: Immun-Blot PVDF Membranes for Protein Blotting	Bio-Rad
StarTub Reagent Reservoir 25 ml	Star Lab
Sponge	Bio-Rad
TC 6, 12, 24 well plates	Sarstedt
TC flask T25 and T75	Sarstedt
Transparent, evaporation-free cover (Optical Adhesive Covers)	Applied Biosystems
Tube 15 ml	Sarstedt

Plasmids and transfection		
Lipofectamine 3000 kit	Invitrogen	1946887
Promega pGlo sensor plasmid	Promega	E2301
shRNA RGS16 TL316695 plasmids	Origene	TL316695
shRNA scrRNA TL316695 plasmids	Origene	TL316695

Antibodies	**Supplier**	**Experiments**
Primary antibody A1R (rabbit) ab151523	Abcam	Western blot, Immunofluorescence
Primary antibody actin (mouse) ab14128	Abcam	Western blot
Primary antibody RGS16 (mouse) ab119424	Abcam	Western blot, Immunofluorescence
Primary antibody vinculin (mouse) V9264	Sigma-Aldrich	Western blot
Secondary antibody Goat Anti-Mouse IgG HRP 170-6516	Bio-Rad	Western blot
Secondary antibody Goat Anti-Rabbit IgG HRP 170-6515	Bio-Rad	Western blot
Secondary GFP-antibody to mouse (goat anti-mouse IgG H&L AlexaFluor 488) ab150113	Abcam	Immunofluorescence
Secondary RFP-antibody to rabbit (donkey anti-rabbit IgG H&L Alexa Fluor 647) ab150075	Abcam	Immunofluorescence

2.1.4 Equipment

The following table list the equipment that was used.

Equipment	Supplier
Astacus water purifyer	membraPure
Autoclave	Varioklav
Cell culture hood: Mars safety classe 2	Scanlaf
Centrifuge cell culture: Rotina 420R	Hettich Zentrifugen
Centrifuge wet lab: Eppendorf 5417 R	Eppendorf
Computers: cell culture / luminometers	ASUS
Computers: Microscope	hp
Computers: wet lab and analysis	Apple Mac
Electrophoresis chamber	Bio-Rad
Fluorescence Camera: DS-Qi2	Nikon
Freezer Premium NoFrost -20°C	Liebherr
Fridge 4°C	gorenje
Heat plate thermomixer C	Eppendorf
Imager for WB: ChemiDoc MP Imaging System	Bio-Rad
Incubator cell culture: New Brunswick Galaxy 170 R with 5% CO2	Eppendorf
Incubators for luminometry: Sanyo MIR-553 and MIR-154-PE	Panasonic
Luminescence Camera: iKon-M 934 CCD	Andor
Luminometer Berthold Centro LB960 XS3	Berthold
Microscope cell culture with fluorescence: Leica ICC50 HD	Leica
Mini Rocker-Shaker	Kisker
MiniSpin plus	Eppendorf
Nikon TI2-E microscope	Nikon
Scale	Sartorius
TC20 automated cell counter	Bio-Rad
Transfer apparatus	Bio-Rad
Vortex genie 2	Scientific Industries SI
Vortex V-1 plus	Kisker

2.1.5 Programs and Software

The following programs and software were used for acquiring and analyzing data.

Program / Software	Developer
BioDare2	Zielinski et al., 2014, University of Edinburgh, biodare2.ed.ac.uk
Center of Gravity	Díez-Noguera, 2013, https://github.com/luca-gas/center-of-gravity

ChronoSapiens9	Till Roenneberg, Chronsulting, LMU Munich
GraphPad Prism Version 8	GraphPad by Dotmatics, www.graphpad.com
ImageLab 5.1	BioRad Laboratories, Inc.
MikroWin 2000 and 2010	Labsis Laborsysteme
NIS-Elements AR 5.20.00 64-bit software	Nikon

2.1.6 Media, Buffers and Recipes

The recipes for buffers and media that were used are listed in the following tables.

Growing medium
DMEM Dulbecco's Modified Eagle Medium with 4.5 g/L D-Glucose
10% FCS
1% Glutamax
1% Sodium Pyruvate
100 U/ml penicillin
100 µg/ml streptomycin

Recording medium
DMEM:F12 (1:1) Dulbecco's Modified Eagle Medium/Nutrient Mixture F-12 Ham with 15 mM HEPES and sodium bicarbonate
10% FCS unless otherwise indicated
1% Glutamax
100 U/ml penicillin
100 µg/ml streptomycin
250 µM D-Luciferin unless otherwise indicated

1x Separating Gel Buffer: TRIS-HCl 1.5 M pH 8.8	
91 g	TRIS base
300 ml	H2Odd
adjust pH to 8.8	HCl 37%
fill to 100 ml	ddH2O

12% Separating Gel Solution	
2 ml	ddH2O
400 µl	1x Separating Gel Buffer (1.5 M TRIS-HCl pH 8.8)
600 µl	30% Acr Bis
36 µl	10% SDS
24 µl	10% APS
4 µl	TEMED

1x Running Gel Buffer: TRIS-HCl 1.5 M pH 6.8	
91 g	TRIS base

300 ml	H2Odd
adjust pH to 8.8	HCl 37%
fill to 100 ml	ddH2O

4% Stacking Gel Solution	
3 ml	ddH2O
2.1 ml	0.5 M TRIS-HCl pH 6.8
2.8 ml	30% Acr Bis
80 µl	10% SDS
56 µl	10% APS
6 µl	TEMED

4x SDS Protein Sample Buffer: Leammli	
2.5 ml	1 M TRIS-HCl buffer pH 6.8
4 ml	Glycerol 100%
4 mg	Bromphenol blue
0.8 g	SDS
fill to 10 ml	ddH2O
to 900 µl aliquots, freshly add 100 µl	TCEP

5x Running Buffer: TRIS-Glycin (TG) Buffer pH 8.3	
15 g	TRIS base 250 mM
94 g	Glycine 1.92 M
adjust pH to 8.3	HCl 37%
50 ml	10% SDS (0.1%)
fill to 1000 ml	

1x Running buffer	
150 ml	5x Running Buffer pH 8.3
600 ml	ddH2O

10x Transfer Buffer	
30.25 g	TRIS base 250 mM
142.5 g	Glycine 1.92 M
adjust pH to 8.9 - 8.3	HCl 37%
fill to 1 l	ddH2O

1x Transfer Buffer	
100 ml	10x Transfer Buffer
200 ml	Methanol (20%)
700 ml	ddH2O

10x TBS (TRIS-Buffered Saline) pH 8.0	
60 g	TRIS base 50 mM
80 g	NaCL 150 mM
2 g	KCl 2.7 mM
adjust pH to 8.0	HCl 37%
fill to 1000 ml	ddH2O

1x TBST	
100 ml	10x TBS
900 ml	ddH2O
1 ml	Tween-20 0.1%

1x PFA Paraformaldehyde	
80 ml	1x PBS
4 g	PFA Paraformaldehyde
raise pH until the solution is clear	1 M NaOH
adjust volume to 100 ml	ddH2O
adjust pH to 6.9	HCl 37%

2.2 Methods

2.2.1 Cell culture conditions

All cells were cultured in growing medium (DMEM Dulbecco's Modified Eagles Medium containing 10% FCS, 1% Glutamax, 1% Sodium-Pyruvate, 100 U/ml penicillin and 100 µg/ml streptomycin, all from Gibco). They were kept in an incubator (Galaxy 170 R New Brunswick, Eppendorf) with constant 37°C and 5% CO2. The U-2 OS cells were split 1-2 times per week. For this, the old medium was discarded before the cells were washed twice with PBS (Sigma). Then, the cells were covered with TripLE (Gibco) and incubated until they were completely detached. A 1:10 suspension in growing medium was made and the cells were split 1:10 before adding new medium. For ARPE-19 cells, the medium was changed 1-2 times per week by discarding the old medium and adding new medium without splitting.

2.2.2 Transfection and generation of stable knockdown cell lines

U-2 OS and ARPE-19 cell lines stably expressing luciferase from a *Bmal1* promoter fragment were used as a basis for most experiments. The "U2OS_Bmal1p-luc" cell line, in short here "U-2 OS", is described by Maier et al., 2009. The ARPE-19 cells were a kind gift from G. Wilder, LMU Munich, and were stably transfected with the same plasmid that was described

by Maier et al. according to the Lipofectamine 3000 (Invitrogen) protocol. RGS16 shRNA was purchased from Origene, the included scrambled shRNA served as a negative control.

Both cell lines were transfected with RGS16 shRNA or scrambled shRNA (controls) according to the Lipofectamine 3000 protocol and selected with puromycin to create a stable knockdown. Additionally, U-2 OS cells were subcloned and a single clone was used for further experiments. For the cAMP reporter cell lines, here "U2OS_pGlo", U-2 OS cells stably expressing the bioluminescent Promega pGlo sensor (Promega; a kind gift from J. O'Neill, MRC Laboratory of Molecular Biology, Cambridge) were used. For the knockdown experiments, they were similarly transfected with RGS16 shRNA and scrambled shRNA according to the Lipofectamine 3000 protocol and selected with Puromycin without subcloning.

The knockdown efficiency of all cell lines was assessed via western blot are shown in figure 34. KD efficiency in % = (1 – (RGS16 level of control / RGS16 level of KD)) x 100

Selected U-2 OS (U2OS_control / U2OS_RKD)	60%
Subcloned U-2 OS (subcloned_U2OS_control / subcloned_U2OS_RKD)	63%
Selected ARPE-19 (ARPE_control / ARPE_RKD)	81%
Selected U2OS_pGlo (pGlo_control / pGlo_RKD)	62%

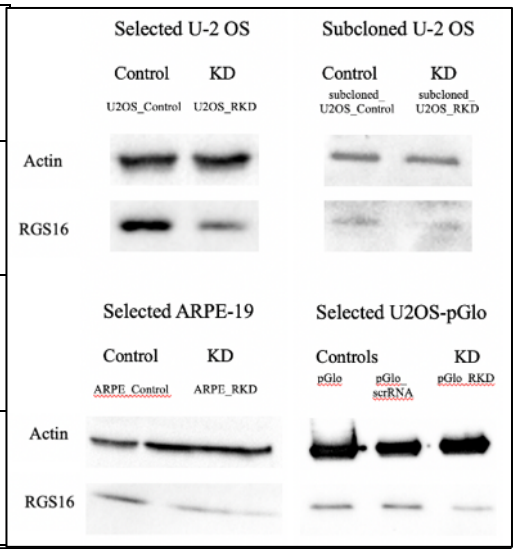

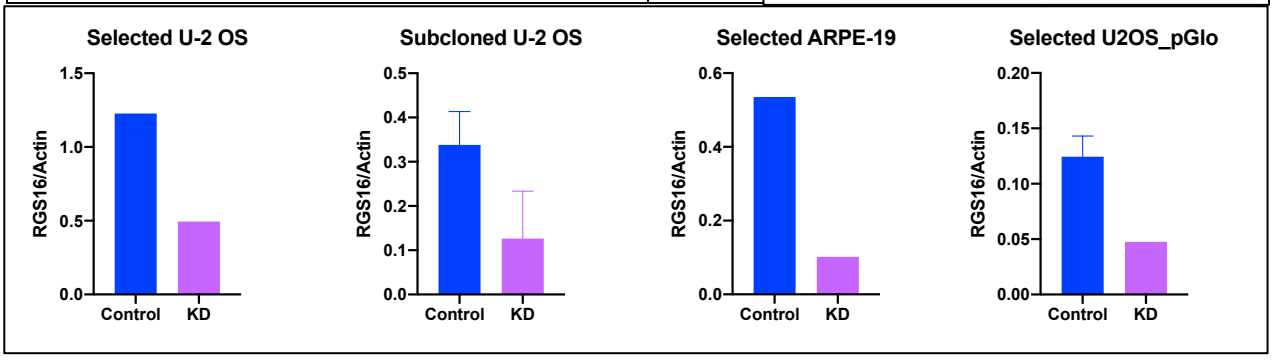

Western Blots and protein levels (RGS16/Actin) of KDs vs. Controls.

2.2.3 Bioluminescence recording of *Bmal1* expression

The U-2 OS and ARPE-19 cell lines used to analyze the effect of a knockdown of RGS16 on the clock all stably express luciferase from the *Bmal1* promoter fragment mentioned above (Maier et al., 2009). The cells were seeded onto a white 96-well plate (Nunclon Delta, Thermo Fisher Scientific) with a density of 20,000 cells per well in recording medium (DMEM/F12, Dulbecco's Modified Eagle's Medium/Nutrient Mixture F-12 Ham with 15 mM HEPES and sodium bicarbonate 1:1, Sigma, with 1% Glutamax, 100 U/ml penicillin and 100 µg/ml streptomycin, all from Gibco) containing 10% FCS. After the indicated preparation, described below, the plates were sealed with a transparent, evaporation-free cover (Optical Adhesive Covers, Applied Biosystems, Life Technologies). Then the plates were transferred to the luminometer (Berthold Centro LB960 XS3) inside a temperature-controlled incubator (Sanyo MIR-553 or MIR-154-PE, Panasonic, Japan). The temperature was either constant or cycling, as indicated. Luminescence was measured for 1s per well every 5, 10, 60 or 90 minutes (depending on the luminometer settings).

Preparation of the selected U-2 OS and ARPE-19 cell lines:

The selected U-2 OS and ARPE-19 cell lines (U2OS_RKD, U2OS_control, ARPE_RKD and ARPE_control) were directly seeded in 200 µl of recording medium containing 250 µM D-Luciferin (P.J.K.) and 10% FCS. The temperature was either constant (for free-run experiments) or cycling (for entrainment experiments), as indicated. For free-run experiments, 1 µM dexamethasone (Sigma) was added directly to the recording medium to synchronize the cells. The plate was then immediately transferred into the luminometer inside a temperature-controlled incubator.

Preparation of the subcloned U-2 OS cell lines:

For experiments in free-running conditions, the subcloned U-2 OS cell line (subcloned_U2OS_RKD and subcloned_U2OS_control) was synchronized for 30 minutes with 1 µM dexamethasone in 0% FCS medium the day after seeding. After washing twice with PBS, 200 µl of recording medium containing 10% FCS and 250 µM D-Luciferin was added to each well.

For temperature cycle experiments, the wells were washed twice with PBS and then recording medium containing 10% FCS and 250 µM D-Luciferin was added without dexamethasone synchronization the day after seeding.

Caffeine experiment:
For the experiment to determine the effect of caffeine on the circadian clock with and without a knockdown of RGS16, the selected U-2 OS cells (U2OS_RKD and U2OS_control) were seeded onto a white 96-well plate in recording medium containing 10% FCS with a density of 20,000 cells per well. The next day, the cells were synchronized with 1 µM dexamethasone and switched to serum-free recording medium containing 1 mM of caffeine (Abcam) vs. no caffeine, as indicated.

2.2.4 Western Blot

Western blots were used to quantify the effect of the knockdowns and to assess RGS16 and Adenosine 1 receptor (A1R) abundance over the course of the day.

For quantifying the knockdown efficiency, cells were seeded in T25 tissue culture flasks (Sarstedt) and harvested at full confluency.

For testing whether there is a free-running rhythm of RGS16 protein levels in U-2 OS cells, native U-2 OS cells were seeded in T25 tissue culture flasks with a total of 0,6 x 10^7 cells per flask in recording medium containing 10% FCS. The next day, the medium was replaced by serum-free recording medium containing 1 µM dexamethasone. After 30 min, the cells were washed twice with PBS and recording medium containing 10% FCS was added. Starting 12 h after the stimulation, the cells were harvested every 4 h.

To analyze RGS16 and Adenosine 1 Receptor (A1R) abundance over the time of day in entrainment, U-2 OS cells were seeded in T25 tissue culture flasks with a total of 0,6 x 10^7 cells per flask in recording medium containing 10% FCS. Then they were entrained in 12:12 34/37°C for 5 days and then harvested every 4 h over 24 h.

For harvesting, the cells were washed twice with ice cold PBS, scraped off with a cell scraper (Sarstedt) and transferred to 1.5 ml Eppendorf tubes (Eppendorf). Then they were centrifuged at 1500 rpm for 5 min in 4°C (Centrifuge 5417 R, Eppendorf). The supernatant was discarded, the pellet was frozen in liquid nitrogen (Linde Gas) and then stored in -80°C or directly treated with Laemmli buffer. 100 µl of 4X Laemmli buffer were added to the pellets and diluted to 1X before loading the sample and a loading marker (PageRulerPlus Prestained Protein Ladder, Thermo Fisher Scientific) on a 12% SDS page gel. The SDS page was run for 90 min at 120 V

in running buffer in the electrophoresis chamber (Bio-Rad). A PVDF membrane (Bio-Rad) was cut to the appropriate size and then activated in methanol. The transfer sandwich was made using a sponge (Bio-Rad), 3 sheets of blotting paper (Whatman), the gel, the PVDF membrane, another 3 sheets of blotting paper, and another sponge. The transfer sandwich was then put into the transfer apparatus (Bio-Rad) containing the transfer buffer and ice inside the refrigerator. The electrotransfer was run for 1 h at 80 V. After the transfer, the membrane was incubated in Ponceau S stain for 5 min before imaging with the ChemiDoc MP Imaging System (Bio-Rad). Then the membrane was blocked in 5% milk (Spinnrad) for 1 h in 37°C. The primary antibody, diluted 1:2000 in TBST-milk (Tween-20: Sigma), was added and left on the membrane overnight at 4°C. After washing 3 times for 20 min each with TBST, the secondary antibody, diluted 1:1000 in TBST-milk, was added and left on the membrane for 1 h at 37°C. The membrane was then washed 3 times in TBST for 20 min each. After addition of the chemiluminescent substrate (SuperSignal West Femto Maximum Sensitivity Substrate for low-intensity bands, and Pierce ECL Western Blotting Substrate for high-intensity bands, both from Thermo Scientific), the images were taken with the ChemiDoc MP Imaging System and analyzed with ImageLab 5.1 (Bio-Rad).

All antibodies used are listed in the antibody table in 5.1.3.

2.2.5 Immunofluorescence

For immunofluorescence (IF) experiments, native U-2 OS cells were seeded in 35 mm microscopy dishes (ibidi) in recording medium containing 10% FCS.

For the IF time course to detect the localization of RGS16 at different times of day, cells were seeded at a density of 20.000 cells per dish before the dish was sealed with parafilm (Bemis). The cells were then entrained in a 12:12 temperature cycle of 34/37°C for 5 days before being released to constant 34°C or 37°C for 3 days. The dishes were collected at specific time points every 4 h over 12 h, when they were washed twice with PBS before fixation in 4% paraformaldehyde-PBS (PFA from Sigma-Aldrich) for 10 min at room temperature. Then they were washed with PBS for 3 times for 5 min each. For permeabilization, the cells were incubated in 0.2% Tween-20 in PBS at room temperature for 5 min. Then they were washed with PBS for 3 times for 5 min each. After that, the cells were blocked in 2% BSA (Sigma) for 1 h at room temperature. Then the primary antibody (mouse anti-RSG16, Abcam) was added with a dilution of 1:100 overnight at 4°C. All antibodies were prepared in 1% BSA. Then the

dishes were washed with PBS 3 times for 10 min each. Next, the secondary antibody (AlexaFluor 488, Abcam) was added at a dilution of 1:500 and incubated for 1 h at 37°C. Then the dishes were washed with PBS 3 times for 10 min each before removing excess liquid and imaging.

For the temperature pulse experiment to assess RGS16 localization in response to temperature pulses, cells were grown to semi-confluency in 35 mm microscopy dishes in recording medium containing 10% FCS. The next day, the cells were subjected to temperature pulses of 27°C, 39°C or 43°C for 4 h as indicated by putting the dishes in an incubator with the respective temperatures. Then the same protocol as above was applied for IF preparation and imaging.

For the IF experiments to analyze RGS16 localization after addition of different GPCR ligands, the cells were grown to semi-confluency in 35 mm microscopy dishes in recording medium containing 10% FCS. The next day, 100 µM each of caffeine (Abcam), N6-cyclohexyladenosine (N-CHA, Abcam), dopamine (Sigma-Aldrich), serotonin (Sigma-Aldrich), isoprenaline (Sigma-Aldrich), and phenylephrine (Sigma-Aldrich), were used to bind adenosine, dopamine, serotonin, β-adrenergic and α1-adrenergic receptors, respectively. The indicated ligands were added to the cells for 5 min, and the localization of RGS16 was subsequently assessed via immunofluorescence. Additionally, A1R localization was analyzed after caffeine and N-CHA addition as well as in controls. The medium containing the ligands was removed after the indicated times, and the protocol described above was used for fixation and imaging. When A1R was determined as well, the A1R primary antibody (rabbit anti-A1R antibody, Abcam) was added simultaneously to the mouse RGS16 antibody, and the secondary RFP anti-rabbit antibody (AlexaFluor 647, Abcam) was added simultaneously to the GFP anti-mouse antibody. Additionally, DAPI (Sigma) was added for visualization of the nucleus before washing the dishes again 3x with PBS before imaging.

For imaging, the Nikon TI2-E microscope was used with a Nikon DS-Qi2 camera for fluorescence detection. The images were then analyzed with the FIJI software (Schindelin et al., 2012) and the data was transferred to Prism for further analysis. The images were converted to 8bit grey-scale and thresholding was applied as indicated. For colocalization analysis, the Pearson's correlation coefficient was calculated with the JACoP Plugin (Bolte & Cordelières, 2006).

2.2.6 Determination of cAMP levels and rhythms by real-time microscopy

U2OS_pGlo cells were put into constant 30°C to determine if there is a cAMP rhythm in single U-2 OS cells. The cells stably transfected with the bioluminescent Promega GloSensor were a kind from the O'Neill Laboratory. This system allows for real-time measurement of cAMP levels by a post-translational cAMP intramolecular complementation biosensor (firefly luciferase). The cells were seeded at 10-50% confluency in 35 mm microscopy dishes containing recording medium with 10% FCS. After 1-3 days, the medium was changed to serum-free recording medium containing 1 µM dexamethasone and 1 mM luciferin. The dish was sealed with parafilm, put into the microscope at constant 30°C and left to acclimate there for several hours before the imaging series was started. For imaging, the Nikon TI2-E microscope was used with an Andor iKon-M 934 CCD camera (Andor) for bioluminescence. The images were taken every 2 h for 50-74 h, as indicated, with 30 min exposure time and 4x4 binning. The first hour was discarded for analysis due to light pollution. The images were then analyzed with the Nikon NIS-Elements AR 5.20.00 64-bit software (Nikon). The images were thresholded to remove the background. Single cells that were discernible across the time series were traced over the time of the experiment and a time profile of the sum intensity of the individual cells was calculated by the Nikon software. The data was then transferred to BioDare2 for further analysis.

2.2.7 Determination of cAMP levels and rhythms by luminometry

To test for baseline cAMP rhythms in U-2 OS cells via luminometry, U2OS_pGlo cells were seeded at 20,000 cells/well onto white 96-well plates in recording medium with 10% FCS containing 1 µM dexamethasone and 1 mM luciferin. The plates were then sealed with a transparent, evaporation-free cover and put into the luminometer at constant 34°C. Luminescence was measured for 1s per well every 10 minutes. The first 2 h where the cells were acclimating to the new temperature were removed, and the following 72 h of data were analyzed. The data was transferred to BioDare2 for further analysis.

2.2.8 cAMP stimulation at times of high and low RGS16 levels

To assess cAMP levels after A1R stimulation at times of high vs. low RGS16 protein levels, U2OS_pGlo cells were stimulated with 50 nM N-CHA (N6-cyclohexyladenosine), a selective A1R agonist. The peak and trough of RGS16, at ExT 2 and ExT 14, respectively, were determined by the western blot time course and confirmed by repeated sampling and western blots at the respective time points. The cells were seeded onto white 96-well-plates at 20,000

cells/well in recording medium containing 10% FCS. Then the plates were sealed and entrained for 5 days in 34/37°C. At ZT 8 and 20, they were taken out of the luminometer on a thermally controlled plate from the Thermomixer C (Eppendorf) and stimulated with 50 nM N-CHA. The controls were stimulated with serum-free medium. Then, they were sealed again and put back into the luminometer. Luminescence was measured for 0.5 s every 76 s for 1h in constant 30°C. Two-way ANOVAs were performed for the fold change N-CHA/medium stimulation for peak vs trough.

The same experiment was then repeated with U-2 OS cells containing the pGlo sensor and a knockdown of RGS16 via shRNA (pGlo_RKD) to assess whether the knockdown of RGS16 abolishes the time-of-day effect of the A1R stimulation on cAMP levels.

2.2.9 Statistical analysis

Unless otherwise specified, data are expressed as mean ± SD. Sample sizes are indicated in the figure legends. One sample equals one well, unless otherwise indicated.

The graphs were generated using ChronoSapiens version 9 (Chronsulting) and GraphPad Prism version 8.4.2 (GraphPad Software, La Jolla, CA).

The statistical analyses were performed with Prism 8.4.2.

For normality tests, Shapiro-Wilk tests were applied. When the values were normally distributed, Student's t tests with 95% confidence intervals were used for comparing two groups, and when they were not normally distributed, Mann-Whitney tests were used. For analyzing the change across several time points, one-way ANOVAs were performed in normally distributed samples, and the Kruskal-Wallis test was used for not-normally distributed samples. For the analysis of more than two groups, two-way ANOVAs were used, followed, where indicated, by post-hoc Sidak's multiple comparisons tests.

Rhythmicity Test

For assessing rhythmicity, the Jonckheere-Terpstra-Kendall (JTK) cycle test for rhythmicity was applied with the following settings: Classic JTK, cosine 2H, linear detrending, $P<0.05$ with Benjamini Hochberg correction.

Period Analysis

For analyzing periods in clean datasets that did not have much background noise (all U-2 OS data except for the caffeine and cAMP experiments), the data was transferred to ChronoSapiens9 and analyzed with the following settings: 2 hour smooth, 24 h trend correction, T = 24. Then, the autocorrelation method was used for the indicated days. For the period analysis, the first 24 h were removed to account for acute effects of stimulation and transfer.

For noisier or short datasets (ARPE-19 cells, the U-2 OS caffeine experiment, and the cAMP experiments), the period was calculated using the Fast Fourier Transform nonlinear least squares (FFT-NLLS) function of the BioDare2 suite (Zielinski et al., 2014). This is generally the recommended method for noisier or shorter datasets. The detrending that yielded the best fit was applied (baseline for ARPE-19 experiments, linear for the cAMP luminometry experiment, and cubic for the cAMP microscopy experiment). The first 24 h were removed for all datasets except for the cAMP experiments. Here, only 2 h were removed due to a quick dampening and therefore shorter datasets. Periods were considered as circadian when their duration was between 18 and 34 hours.

The period results were then transferred to Prism 8, where outliers were removed (ROUT = 1) and the indicated statistical analyses applied.

Phase Analysis

For analyzing phase, the center of gravity was calculated as described by Díez-Noguera using the formulas shown below (Díez-Noguera, 2013).

$$a = \frac{\sum_{i=1}^{n} y_1 \cos\frac{2\pi i}{n}}{\sum_{i=1}^{n} y_1}; b = \frac{\sum_{i=1}^{n} y_1 \sin\frac{2\pi i}{n}}{\sum_{i=1}^{n} y_1}; \frac{b}{a} = \frac{\sum_{i=1}^{n} y_1 \sin\frac{2\pi i}{n}}{\sum_{i=1}^{n} y_1 \cos\frac{2\pi i}{n}}$$

The code of the software that was developed for calculation is available at https://github.com/luca-gas/center-of-gravity. The results were then transferred to Prism 8, where outliers were removed (ROUT = 1) and the indicated statistical analyses applied.
The phase data is graphed and calculated according to External time, meaning that the 0 time point is defined as the middle of the cold phase (mid-cold).

For analyzing the Q_{10}, the standard formula below was used after reversing the reaction rate R1 and R2, as a longer free-running period means a slower reaction rate. T1 represents the lower temperature, T2 the higher temperature.

$$Q_{10} = \left(\frac{R_1}{R_2}\right)^{\frac{10}{T_1 - T_2}}$$

An alternative way of calculation can be found at https://github.com/dxda6216/q10 which uses SciPy Optimize non-linear least squares fit on Google Colab to calculate the Q_{10} for circadian datasets using the following formula:

$$\mathrm{Tau}_t = \mathrm{Tau}_{37} / (Q_{10} ** ((t - 37) * 0.1))$$

$$\tau_t = \frac{\tau_{37}}{Q_{10}^{\left(\frac{t-37}{10}\right)}}$$

For both calculation methods, the phase was transposed by +24 to avoid negative values.

3. Results

3.1 Effect of a knockdown of RGS16 on key circadian properties

To explore the role of RGS16 in the clockwork of the molecular circadian clock in non-SCN cells, RGS16 shRNA was stably transfected into U-2 OS and ARPE-19 cells containing a *Bmal1* luciferase reporter (BMAL1::Luc) to establish knockdown (KD) cell lines. BMAL1::Luc cells transfected with a scrambled shRNA construct were used as a negative control. The knockdown efficiency of the cell lines was assessed via western blot (Figure 1). RGS16 levels were normalized to the corresponding actin levels in the same lane, and the KD efficiency was calculated as follows:

KD efficiency in % = (1 – (RGS16 level of control / RGS16 level of KD)) x 100.

The KD efficiency was 60% in the selected U-2 OS cells, 63% in the subcloned U-2 OS cells, and 81% in the selected ARPE-19 cells.

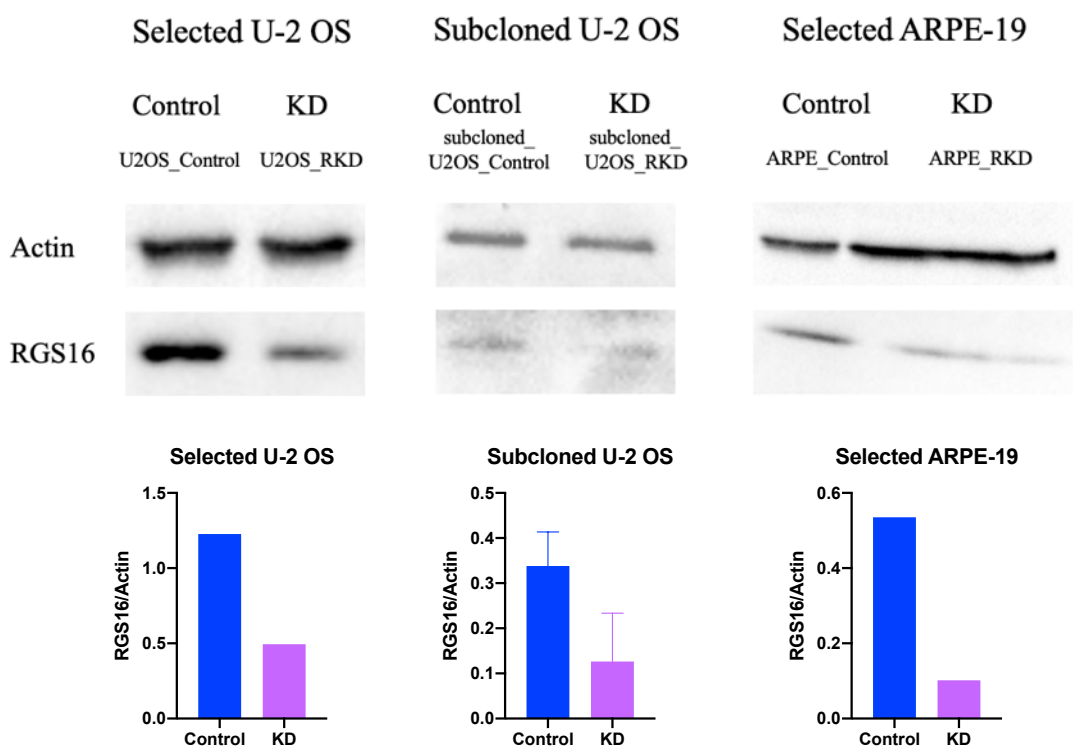

Figure 1: Western blots and bar graphs showing reduced RGS16 protein levels after KD with stably transfected RGS16 shRNA.
Shown are actin (loading control) and RGS16 protein levels of controls (scrambled shRNA) vs. RGS16 KD cells (RGS16 shRNA) in selected U-2 OS BMAL1::Luc cells ("U2OS_control" and "U2OS_RKD"), subcloned U-2 OS BMAL1::Luc cells ("subcloned_U2OS_control" and "subcloned_U2OS_RKD"), and selected ARPE-19 BMAL1::Luc cells ("ARPE_control" and "ARPE_RKD"). RGS16 levels were normalized to the corresponding actin levels in the same lane. The KD efficiency was 60% in the selected U-2 OS cells, 63 % in the subcloned U-2 OS cells, and 81% in the selected ARPE-19 cells.

With these cell lines, a number of experiments were conducted to determine the effects of a KD of RGS16 on the key circadian properties. It could be observed that the KD impacts two of the three key circadian properties: the knockdown cell lines show an impairment of the free-running period of the core clock gene *BMAL1*, as well as an altered phase of entrainment across several conditions. It could be shown that both U-2 OS and ARPE-19 cells remain temperature-compensated after a KD of RGS16 in both free-run and entrainment.

3.1.1 Free-running period

A common way to quantify the circadian clock in cells and tissues is to measure the free-running period ("FRP" or "period") of core clock genes in constant 37°C across several days. To assess the FRP in U-2 OS and ARPE-19 cells, the cells were synchronized with 1 µM dexamethasone and subsequently measured over 5 days at 37°C. The free-running period was significantly different between KDs and controls in all cell lines (Figure 2).

In the selected U-2 OS cells, the period was shortened (P=0.0107) (Figure 2A). The subcloned U-2 OS KD cell line, however, had a significantly longer free-running period compared to controls (P<0.0001) (Figure 2B). The selected ARPE-19 cells showed an overall longer FRP than the U-2 OS cells, and the period of the KD cells was shortened compared to controls (P<0.0001) (Figure 2C). When comparing the selected with the subcloned cells, the subcloned controls had a shorter free-running period in U-2 OS cells and a longer FRP in KDs (both P<0.0001) (Figure 2D).

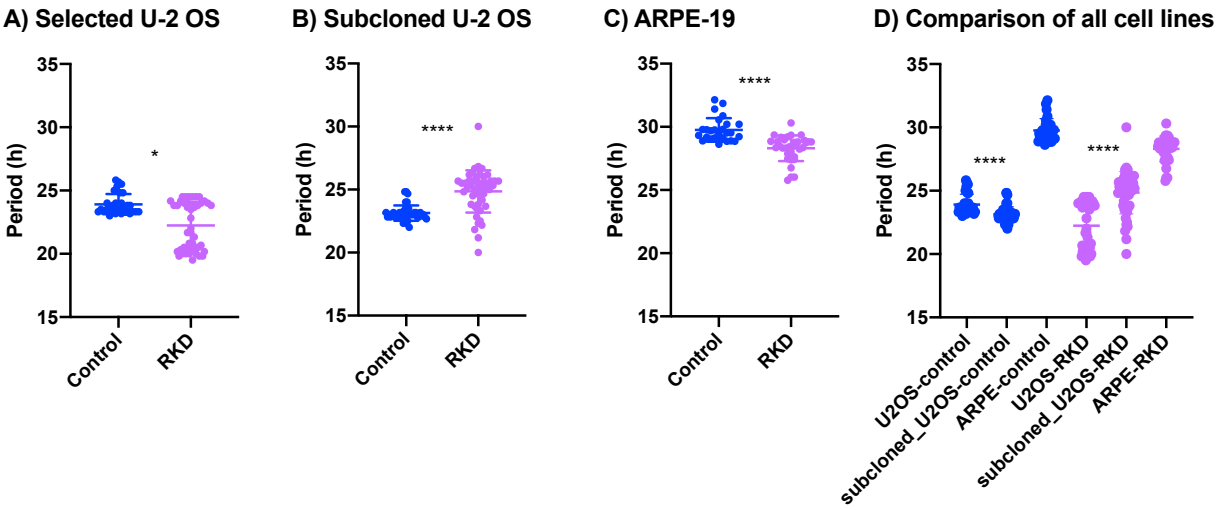

Figure 2: A KD of RGS16 impairs the free-running period in U-2 OS and ARPE-19 cells.
*The free-running period of a luciferase reporter of Bmal1 promoter activity was measured on days 2 to 5 in constant 37°C after synchronization with dexamethasone. Shown is the period with mean and SD for the RGS16 knockdowns (pink) vs the controls (blue) for the different cell lines. * = Significance determined by Mann-Whitney tests. Outliers were removed by Prism (ROUT = 1).*

A) The selected U-2 OS cells showed a shortened FRP compared to controls (Controls: 23.91 ± 0.8186 h, KD: 22.24 ± 1.867 h, P=0.0107). N=31 for controls and N=46 for RGS16 KD cells.
B) The subcloned U-2 OS KD cells had a significantly longer FRP than controls (Controls: 23.13 ± 0.6018 h, KD: 24.85 ± 1.670 h, P<0.0001). N=42 for controls and N=49 for RGS16 KD cells.
C) The selected ARPE-19 cells showed an overall longer FRP than the U-2 OS cells, and the period of the KD cells was shortened compared to controls (Controls: 29.76 ± 0.9341 h, KD: 28.30 ± 1.014 h, P<0.0001). N=26 for controls and N=34 for RGS16 KD cells.
D) Comparison of the selected vs. subcloned U-2 OS cell lines and ARPE-19 cell line. ARPE-19 showed a longer free-running period than U-2 OS cells, and the period after a KD of RGS16 was shortened in ARPE-19, analogous to the selected U-2 OS cells.

3.1.2 Phase of Entrainment

The phase of entrainment defines the relationship of a predefined phase marker with the cycle of its environment (zeitgeber cycle). Common phase markers are the onset, offset, peak or trough of a curve, but these can be easily influenced by acute responses to temperature changes, for example. To reduce this problem, the center of gravity can be used instead, which defines the "temporal center" of a times series by including averages of angles of different phase markers in a cycle rather than only using a single reference point (Díez-Noguera, 2013). The phase of entrainment can still be 'masked' by acute responses to temperature changes, meaning that the change of temperature itself leads to changes in phase that obscure the real circadian phase (Mrosovsky, 1999; Roenneberg et al., 2005). To test the robustness of phase markers in relation to temperature transitions, a variety of entrainment protocols can be used to pull apart the system. These include T cycles, variations in thermoperiods and in zeitgeber strength, which are described in the following paragraphs.

In cultured cells, a commonly used zeitgeber is a temperature cycle (Buhr et al., 2010; Prolo et al., 2005). A standard protocol entrains cells to 12 hours of cool temperature followed by 12 hours of warmth for several days (Figure 3). A stable phase of entrainment is usually reached after around 3-5 days.

There are also variations of that protocol, for example T cycles, meaning cycles with different "day" lengths, to assess how far the system can be pushed to entrain to a non-24h cycle. Normally, a circadian system cannot entrain to extremely short or long cycles (Aschoff, 1960; Bruce, 1960; Kleitman & Kleitman, 1953; Roenneberg, Daan, et al., 2003). Cells with a "slower" internal clock, usually manifesting in a longer free-running period, are sometimes able to entrain to longer T cycles but show deficiencies in entraining to shorter T cycles (Aschoff, 1960; Aschoff & Pohl, 1978; Burt et al., 2021; Duffy et al., 2001; Hoffmann, 1963; Pittendrigh & Daan, 1976; Rémi et al., 2010). To determine whether this is also the case when RGS16 is

knocked down, the RGS16 KD cells (U-2 OS and ARPE-19) were tested in several T cycles (Figures 4-6).

There is also a phenomenon called frequency demultiplication. It describes the observation that an oscillator can entrain to a cycle that is a harmonic of the frequency of the internal cycle. For the circadian clock with its internal period of about 24 h, one such harmonic is 12 h. It has been shown that the circadian clock can use a 12 h cycle to entrain and show a 24 h rhythm under certain circumstances (Browman, 1944; Bruce, 1960; Merrow et al., 1999; Roenneberg, Daan, et al., 2003). To test whether this phenomenon also exists in U-2 OS and ARPE-19 cells and whether there was an impairment when RGS16 was knocked down, the cells were entrained in cycles of 6 h of cold followed by 6 h of warm temperatures (Figure 7).

Another variation to dissect the phase of entrainment is exposing the cells to different "daylengths". Instead of 12 hours of dark or cold ("night") and 12 hours of light or warmth ("day"), the cells can be exposed to varying lengths of "night" and "day". Through this, it becomes possible to assess the relationship of the phase within the different stages of the temperature cycle (Aschoff, 1960; Bruce, 1960; Burt et al., 2021; Merrow et al., 1999; Rémi et al., 2010; Tan et al., 2004). To assess this in RGS16 KD cells, the U-2 OS and ARPE-19 cells were entrained in 16 hours of cold and 8 hours of warm, and vice versa (Figures 8 and 9).

Lastly, entrainment can be tested by increasing or reducing the strength of the zeitgeber, e.g., the amplitude of the temperature cycle. Normally, the stronger the zeitgeber, the faster and more efficient the entrainment (Aschoff, 1960; Aschoff & Pohl, 1978; Burt et al., 2021). Inversely, by reducing the amplitude of the temperature cycle, it is expected that it takes the system longer to entrain, and the phase may change. If the zeitgeber strength is too low, entrainment may fail. If RGS16 is involved in the detection and reaction to temperature changes, as could be suggested by its increased expression after heat shock, it could make the whole system more susceptible to temperature changes and therefore lead to a change in the reaching of a stable phase of entrainment, especially in lower amplitude cycles (Seifert et al., 2015). To assess whether this is true, RGS16 KD cells and controls were exposed to temperature cycles with a temperature difference of Δ3°C vs. Δ1.5°C (Figure 10).

The goal of all these experiments was to obtain information about what role RGS16 plays for the circadian clock "in the real world", where it encounters zeitgebers, which loss of its

functions can be buffered by the system, and what could be deduced by these findings on its role in the molecular clockwork.

The data is graphed and calculated according to External time, meaning that the 0 time point is defined as the middle of the cold phase (mid-cold), analogous to midnight (Daan et al., 2002).

3.1.2.1 Temperature Cycles in 12:12

First, the cells were entrained in a 12:12 35.5/38.5 °C temperature cycle (Figure 3). The data was then analyzed by calculating the center of gravity for day 5, by which time the cells were all stably entrained.

In the selected U-2 OS cell line, the KD cells were entraining to a later phase compared to controls (P=0.0185) (Figure 3A). In the subcloned U-2 OS cell line, the KD cells were entraining to an earlier phase compared to controls (P=0.0002) (Figure 3B). In the selected ARPE-19 cell line, the KD cells were entraining to a later phase, but the difference was not statistically significant (P=0.3039) (Figure 3C).

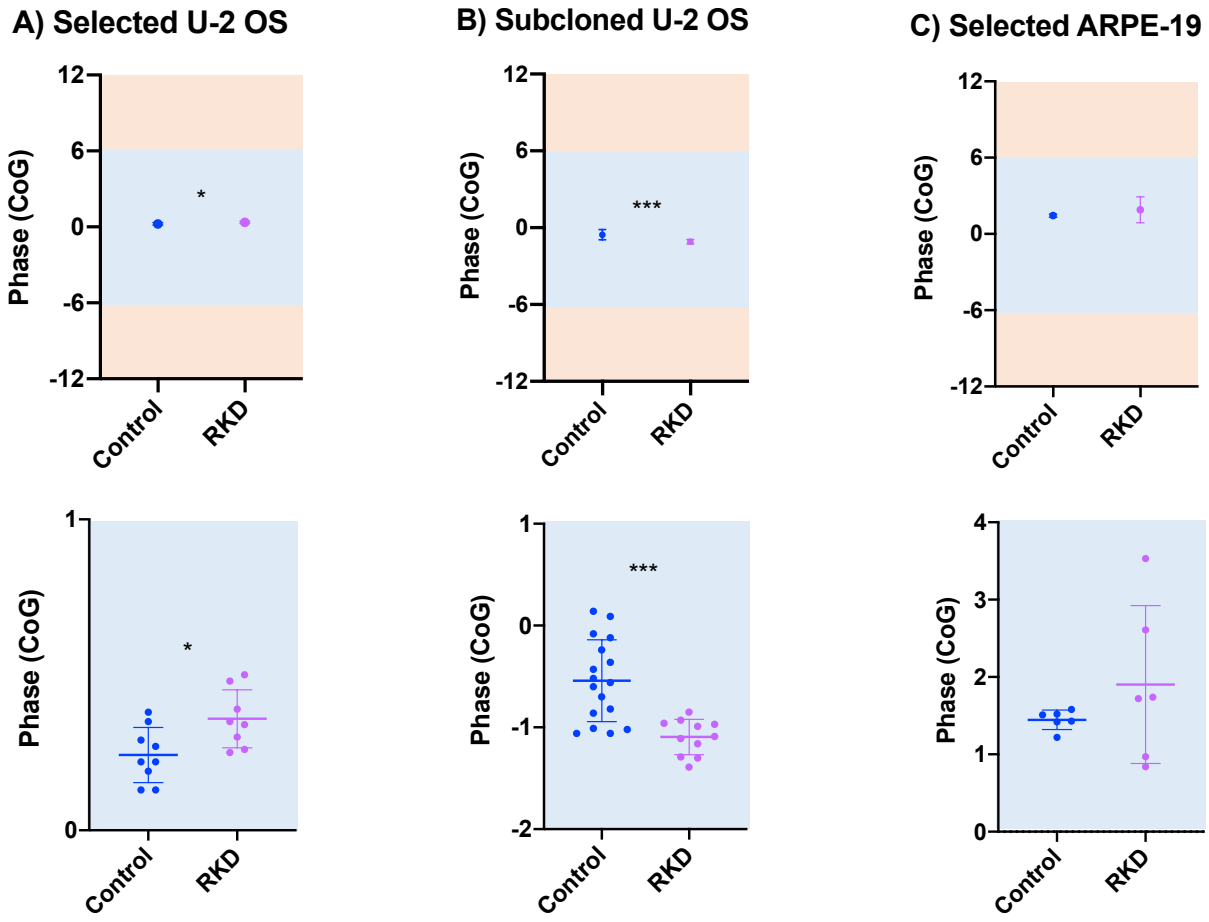

Figure 3: A KD of RGS16 impairs the phase of entrainment in 12:12 35.5/38.5°C.
*Shown is the phase of the Center of Gravity of Bmal1 promoter activity with mean and SD for the RGS16 knockdowns (pink) vs the controls (blue) for the different cell lines on day 5. The 0 timepoint indicates mid-cold. Upper panel: y axis scale -12 to 12 h, lower panel: y axis optimized for magnification. Time point 0 indicates mid-cold (External time). * = significance determined by t tests. Outliers were removed by Prism (ROUT = 1).*

A) In the selected U-2 OS cell line, the KD cells showed a later phase compared to controls (Controls = -0.2422 ± 0.08843 h, KDs = 0.3588 ± 0.09342 h, P=0.0185). N=9 for controls and N=8 for RGS16 KD cells.
B) In the subcloned U-2 OS cell line, the KD cells were entraining to an earlier phase compared to controls (Controls = -0.5418 ± 0.4019 h, KDs = -1.095 0.1743 h, P=0.0002). N=17 for controls and N=11 for RGS16 KD cells.
C) In the selected ARPE-19 cell line, the KD cells were entraining to a later phase, but the difference was not statistically significant (Controls = 1.447 ± 0.1261 h, KDs = 1.902 ± 1.021 h, P=0.3039, ns). N=6 for both cell lines.

3.1.2.2 T Cycles

We also tested the phase of entrainment in several cycle lengths, so-called T cycles. For evaluating T cycles, the cells were entrained in the indicated temperature cycles and the phase (Center of Gravity) was calculated for days 3 to 6.

In the selected U-2 OS cell line, the cells were entrained in temperature cycles of 35.5/38.5 °C (Figure 4). In 13:13, the KD cells were entrained to a significantly earlier phase on day 3 compared to controls (P<0.0001) (Figure 4A). The two-way ANOVA showed a significant difference between the cell lines (F (1, 63) = 67.73, P<0.0001). In 12:12, the KDs showed a significantly later phase of entrainment on days 3 and 6 (P<0.0001 and P=0.0010, respectively) (Figure 4B). There was a significant difference between KDs and controls (F (1, 63) = 28.62, P<0.0001). In 11:11, the KDs entrained to a significantly later phase on days 3 and 4 (P<0.0001 and P=0.0478, respectively), and to a significantly earlier phase on day 6 (P=0.0056) (Figure 4C). There was a significant difference between KDs vs controls (F (1, 63) = 12.73, P=0.0007).

Overall, there were significant differences in the different T cycles between the cell lines. In 12:12, the KDs showed a later phase of entrainment despite having a shorter free-running period, where an earlier phase due to a supposedly “faster” clock would be expected. In the shorter cycle, the entrained phase of the KDs was earlier than in controls, in accordance with the shorter free-running period and “faster” clock. Both cell lines showed increasingly later phases in longer cycles. The KDs seem to entrain faster to their stable phase of entrainment in the shorter cycle than in the long cycle, and to entrain faster than the controls. In the longer cycle, the controls reach their stable phase faster than the KDs. When graphing the phase according to real vs. modulo tau (24/T), both lines show a similar pattern of advance of the phase in longer T cycles, showing that they can entrain to the imposed T cycles (Figure 4D and E).

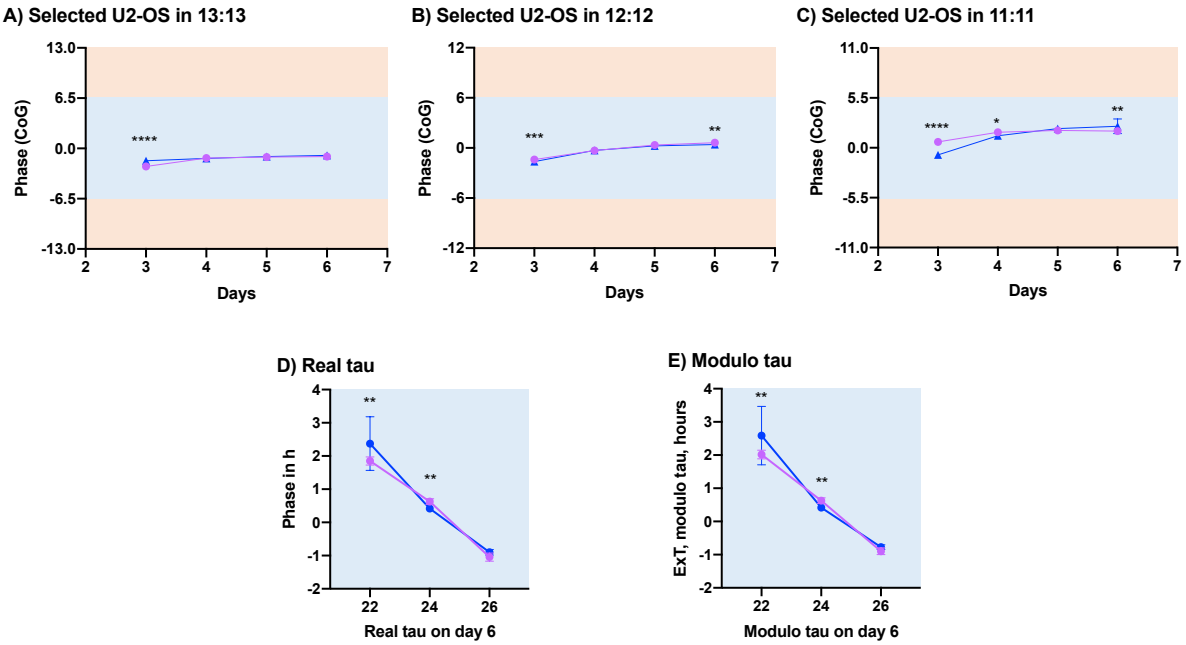

Figure 4: Phase of the Center of Gravity of Bmal1 promoter activity in the selected U-2 OS cell line in different zeitgeber (T cycle) lengths in 35.5/38.5°C as indicated.
*Shown is the phase with mean and SD for the RGS16 knockdowns (pink) vs the controls (blue) for the different cell lines. Time point 0 indicates mid-cold (External time). * = significance in post hoc Sidak's test in entrainment (after day 3). Outliers were removed by Prism (ROUT = 1).*
A) 13:13: Controls: N=9 for all days; KDs: N=9 for days 3, 4, and 6, N=8 for day 5.
B) 12:12: Controls: N=9 for all days; KDs: N=9 for days 3, 4, and 6, N=8 for day 5.
C) 11:11: Controls: N=9 for all days; KDs: N=9 for days 3-5, N=8 for day 6.
D) Real and E) modulo (24/T) tau for days 6 of each cycle length.

In the subcloned U-2 OS line, cells were entrained in temperature cycles of 34/37 °C (Figure 5).

In 12:12, the U-2 OS KDs entrained to a significantly later phase compared to controls on all days ($P<0.0001$, $P<0.0001$, $P=0.0061$, $P=0.0107$, and $P<0.0001$ on days 3, 4, 5, 6, and 7 respectively) (Figure 5A). In the two-way ANOVA, there was a significant difference between KDs and controls ($F(1, 182) = 121.1$, $P<0.0001$).

In 11:11, the KDs entrained to a significantly later phase than controls on day 3 ($P<0.0001$), and to an earlier phase on days 5 and 6 (both $P<0.0001$) (Figure 5B). Again, there was a significant difference between KDs and controls ($F(1, 182) = 20.74$, $P<0.0001$).

In 10:10, again, the KDs entrained to a later phase than controls on day 3 ($P<0.0001$), and to an earlier phase on days 5 and 6 ($P=0.0006$ and $P=0.0041$, respectively) (Figure 5C). Here, there was no significant difference between the two cell lines ($F(1, 218) = 0.8061$, $P=0.3703$).

In 9:9, the KDs entrained to a significantly earlier phase on days 6 through 9 ($P=0.0015$, $P=0.0003$, $P=0.0006$, and $P<0.0001$ for days 6, 7, 8, and 9, respectively) (Figure 5D). The two-way ANOVA showed a significant difference between KDs and controls ($F(1, 291) = 64.35$, $P<0.0001$).

In 8:8, the KDs entrained to a significantly earlier phase on days 6 through 10 (P=0.002, P=0.001, P<0.0001, P<0.0001, P=0.0017 for days 6, 7, 8, 9, and 10, respectively) (Figure 5E). There was a significant difference between KDs and controls (F (1, 292) = 89.38, P<0.0001).

Generally, in 12:12, the RGS16 KD cells entrained to a later phase than the control cells. This trend is reversed for shorter T cycles, where the KD cells entrained to an earlier phase despite having a longer free-running period, where a later phase of entrainment due to a "slower" clock would be expected. Overall, the phase of the center of gravity shifts from mid-cold in 12:12 towards the later warm phase in shorter cycles. As shown in panel F and G, there seems to be a systematic entrainment to an earlier phase in the KDs, and interestingly, both KD and WT seem to be able to entrain to cycles as short as 8:8. Usually, it is assumed that the clock cannot entrain to such short T cycles, so these experiments are rarely performed for human cells.

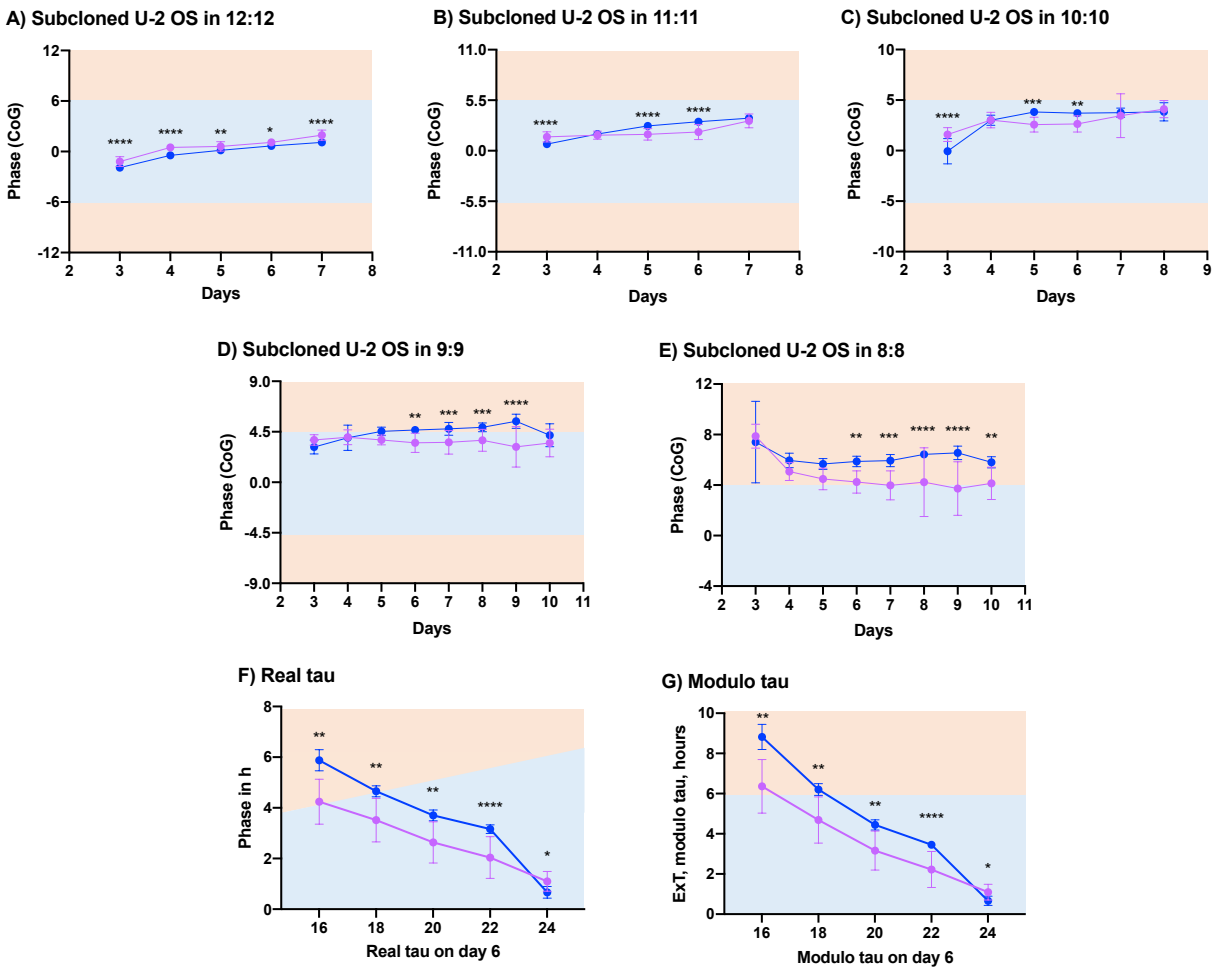

Figure 5: Phase of the Center of Gravity of Bmal1 promoter activity in the subcloned U-2 OS cell line in different zeitgeber (T cycle) lengths in 34/37°C as indicated.
*Shown is the phase with mean and SD for the RGS16 knockdowns (pink) vs the controls (blue) for the different cell lines. Time point 0 indicates mid-cold (External time). * = significance in post hoc Sidak's test in entrainment (after day 3). Outliers were removed by Prism (ROUT = 1).*
A) 12:12: Controls: N=18 for all days; KDs: N=21 for days 3, 4 and 5, N=20 for day 5, N=19 for day 6.

B) 11:11: Controls: N=18 for all days; KDs: N21 for days 3 and 7, and N=20 for days 4-6.
C) 10:10: Controls: N=18 for days 3, 4 6, and 7, and N=17 for days 5 and 8; KDs: N=21 for days 3-7, N=19 for day 8.
D) 9:9: Controls: N=18 for days 3 and 4, N=17 for day 5, N=15 for day 6, N=18 for days 7-10; KDs: N=21 for days 3-9, and N=20 for day 10.
E) 8:8: Controls: N=18 for days 3-7 and day 10, N=17 for days 8 and 9; KDs: N=21 for days 3-6, 8, and 10.
F) Real and G) modulo (24/T) tau for days 6 of each cycle length.

In the selected ARPE-19 line, the cells were entrained in temperature cycles of 35.5/38.5 °C (Figure 6). In 13:13 and 12:12, there was no significant difference between the cell lines (F (1, 39) = 0.6193, P=0,4361, and F (1, 39) = 0.09676, P=0.7574, respectively) (Figure 6A and B). In 11:11, the KDs showed a significantly earlier phase than the controls on day 3 (P=0.0003), and a significantly later phase on day 6 (P=0.0047) (Figure 6C). The two-way ANOVA showed a significant difference between KDs and controls (F (1, 40) = 6.358, P=0.0158).
Generally, there were only mild differences between the ARPE-19 cell lines, with significant differences only in the shorter cycle. When entrained in the 11:11 cycle, the KDs show a later phase of entrainment despite showing a shorter free-running period with a supposedly "faster" clock. Both cell lines showed later phases in the 11:11 cycle than in 13:13 cycle. When graphed according to real vs. modulo tau (24/T), both lines show a similar pattern of advance of the phase in longer T cycles, showing that they can entrain to the imposed T cycles (Figures 6D and E).

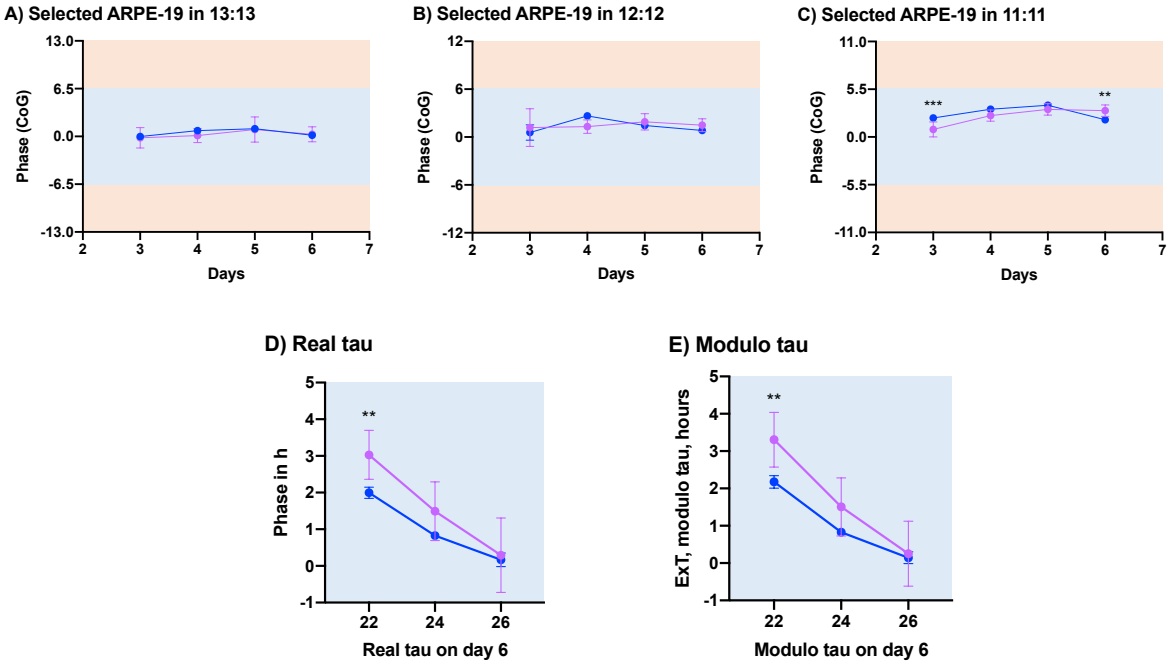

Figure 6: Phase of the Center of Gravity of Bmal1 promoter activity in the selected ARPE-19 cell line in different zeitgeber (T cycle) lengths in 35.5/38.5°C as indicated.
*Shown is the phase with mean and SD for the RGS16 knockdowns (pink) vs the controls (blue) for the different cell lines. Time point 0 indicates mid-cold (External time). * = significance in post hoc Sidak's test in entrainment (after day 3). Outliers were removed by Prism (ROUT = 1).*

A) 13:13: N=6 for all except KDs on Day 5, there N=5.
B) 12:12: Controls: N=6 for days 3, 5, and 6, and N=5 for day 4; KDs: N=6 for all days.
C) 11:11: N=6 for all.
D) Real and E) modulo (24/T) tau for days 6 of each cycle length.

3.1.2.3 Frequency Demultiplication

To test whether frequency demultiplication occurs in U-2 OS and ARPE-19 cells and whether there is an impairment when RGS16 was knocked down, the KD cells and controls were entrained in 6:6 cold:warm cycles and the graphs then checked for signs of 12 h and 24 h rhythms (Figure 7). Overall, the underlying 24 h rhythm showed up throughout the cell lines as a major peak every 24 h with a minor peak every 12 h. The extent of the frequency demultiplication varied among cell lines (Figure 7 and table 1).

The selected U-2 OS control cells show a main 24 h rhythm until the 12 h and 24 h peaks are equal in size on day 5 (Figure 7A). The 12 h peak appears in the double plot on day 3. In the KDs, the 24 h rhythm is dominant until day 4, where the second peak appears in the double plot and is equal in size compared to the 24 h peak (Figure 7A). However, the 12 h peaks are visible in both cell lines after day 1 in the line graphs.

Both subcloned U-2 OS cell lines show an additional 12 h rhythm in addition to the 24 h rhythm from day 2 in the Δ3°C cycle (Figure 7B). The size of both peaks was equal around day 3 in both cell lines.
In order to elucidate the property of frequency demultiplication better, the cells were put in a 6:6 cycle with a low amplitude zeitgeber (only Δ0.5°C). Here, the controls kept their 24 h rhythm with only hints of a second peak around day 4, while a second peak emerged around day 2 in the KD cells which was equal in size to the first peak around day 5 (Figure 7C). This shows that the circadian clock of the control U-2 OS cells is robust enough to keep its 24 h rhythm for the duration of the experiment, while the KDs fails to demultiply by day 5.
Also it could be observed that in the KDs, the main peak progressed gradually across the day, as is expected in circadian entrainment (double plots of Figures 7B and C), while the curve showed increased squaring, indicating stronger masking by the shift in temperature (particularly visible in the line graphs, Figures 7B and C). This was the case for both high and low amplitude cycles.

In the frequency demultiplication protocol, the selected ARPE-19 cells first showed a 24 h rhythm, which then converted to a 12 h rhythm after 2 days in both controls and KDs (Figure 7D).

Overall, all cell lines showed frequency demultiplication. The 24 h rhythm in the controls usually persisted longer in controls than in the KDs, which can be seen both in the onset of the second (12 h) peak, as well as in the time by which there was no difference in peak size anymore. This suggests that the clock is less robust in RGS16 KD cells. This was more pronounced in the U-2 OS cells than in the ARPE-19 cells.

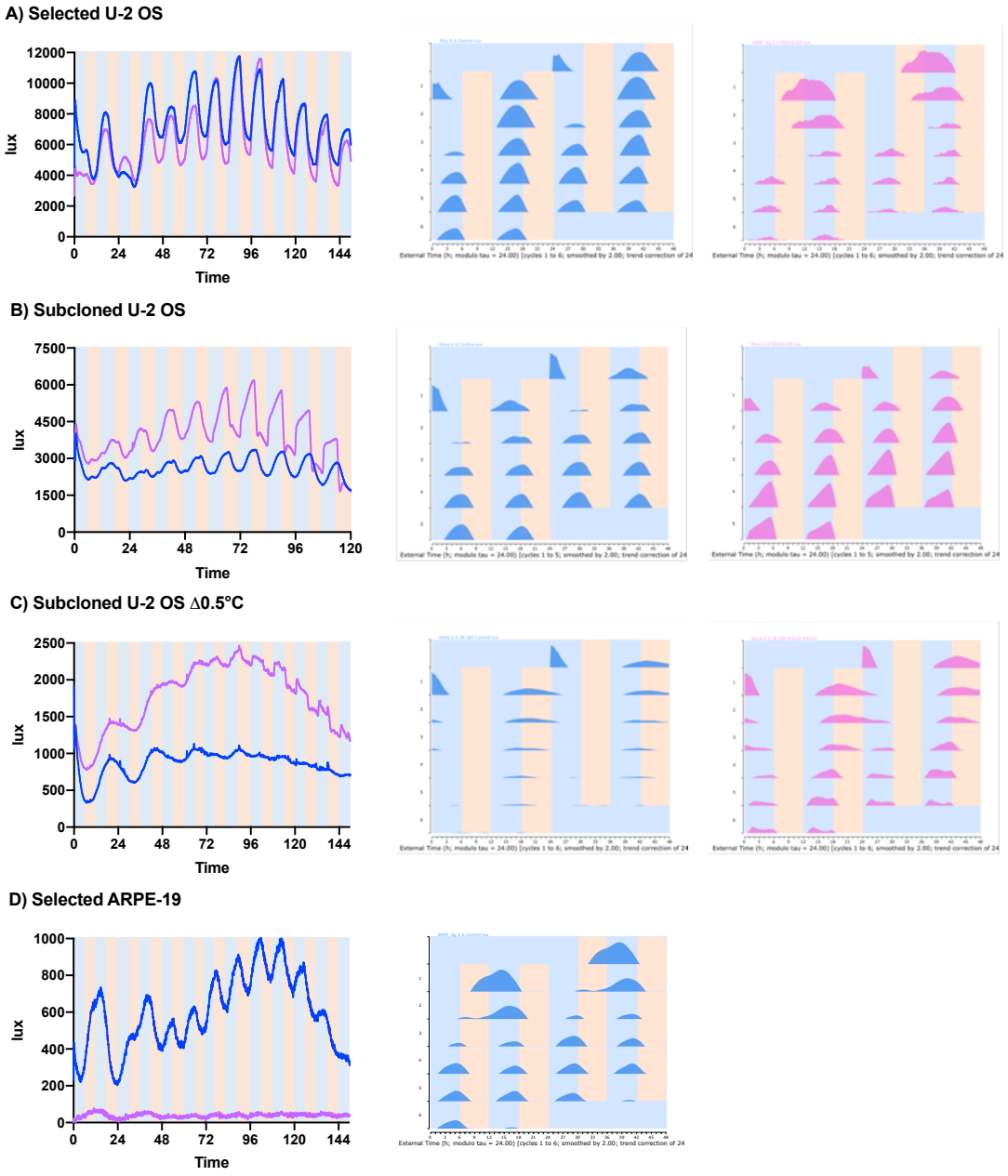

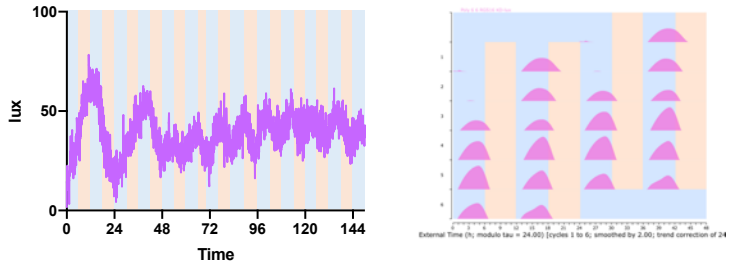

Figure 7: Both U-2 OS and ARPE-19 cells show frequency demultiplication with and without a KD of RGS16. Line graphs (linear detrending, Biodare; left) and double plots (2h smooth, 24h trend correction, T=24, ChronoSapiens; right) for the RGS16 knockdowns (pink) vs the controls (blue) in 6:6. Double plots show 48 h in a row to better visualize the changes across several cycles.
A) Selected U-2 OS cell line, 35.5/38.5°C. N=9 for both;
B) Subcloned U-2 OS cell line, 34/37°C. N=18 for controls and N=21 for KDs;
C) Subcloned U-2 OS cell line, 36/36.5°C. N=18 for controls and N=21 for KDs;
D) Selected ARPE-19 cell line, 35.5/38.5°C. N=6 for both.

Day by which second (12 h) peak emerges

A)	Selected U-2 OS	Subcloned U-2 OS	Subcloned U-2 OS, Δ0.5°C	Selected ARPE-19
Control	3	2	4	2
KD	4	2	2	3

Day by which size of the peaks is equal

B)	Selected U-2 OS	Subcloned U-2 OS	Subcloned U-2 OS, Δ0.5°C	Selected ARPE-19
Control	5	3	-	3
KD	4	3	5	3

Table 1: Frequency demultiplication in U-2 SO and ARPE-19 cells.
Shown is the day by which the second peak appears in the different cell lines (A) and the day by which the peaks are equal in size (B).

3.1.2.4 Thermoperiods

For evaluating the changes in the phase of entrainment in relationship to the cold/warm and warm/cold transitions, different thermoperiods were used to test the selected U-2 OS and ARPE-19 cells (8:16, 12:12, and 16:8 in 35.5/38.5 °C) (Figures 8 and 9). These experiments can also be used to assess how and if the cells show masking effects with this zeitgeber. As human body temperature variations are normally not a symmetrical 12:12 cycle, but instead usually show a shorter cold phase than warm phase, the 8:16 cycle is the more physiological protocol (Aschoff, 1983). The center of gravity was calculated and outliers were removed in Prism (ROUT=1). Day 6 of entrainment was used for analysis.

In the selected U-2 OS cell line, the controls and knockdowns entrained significantly differently across the different conditions (Figure 8). In 16:8 and 12:12, the KD cells were entraining to a later phase compared to controls (P=0.0148 and P=0.0001, respectively) (Figures 8A and B). In 8:16, the KDs were entraining to an earlier phase compared to controls (P=0.0001) (Figure 8C). In increasingly shorter "nights", the phases of the center of gravity of both cell lines moved closer to the cold-warm-transition ("dawn") and further away from the warm-cold transition ("dusk") (Figure 8D).

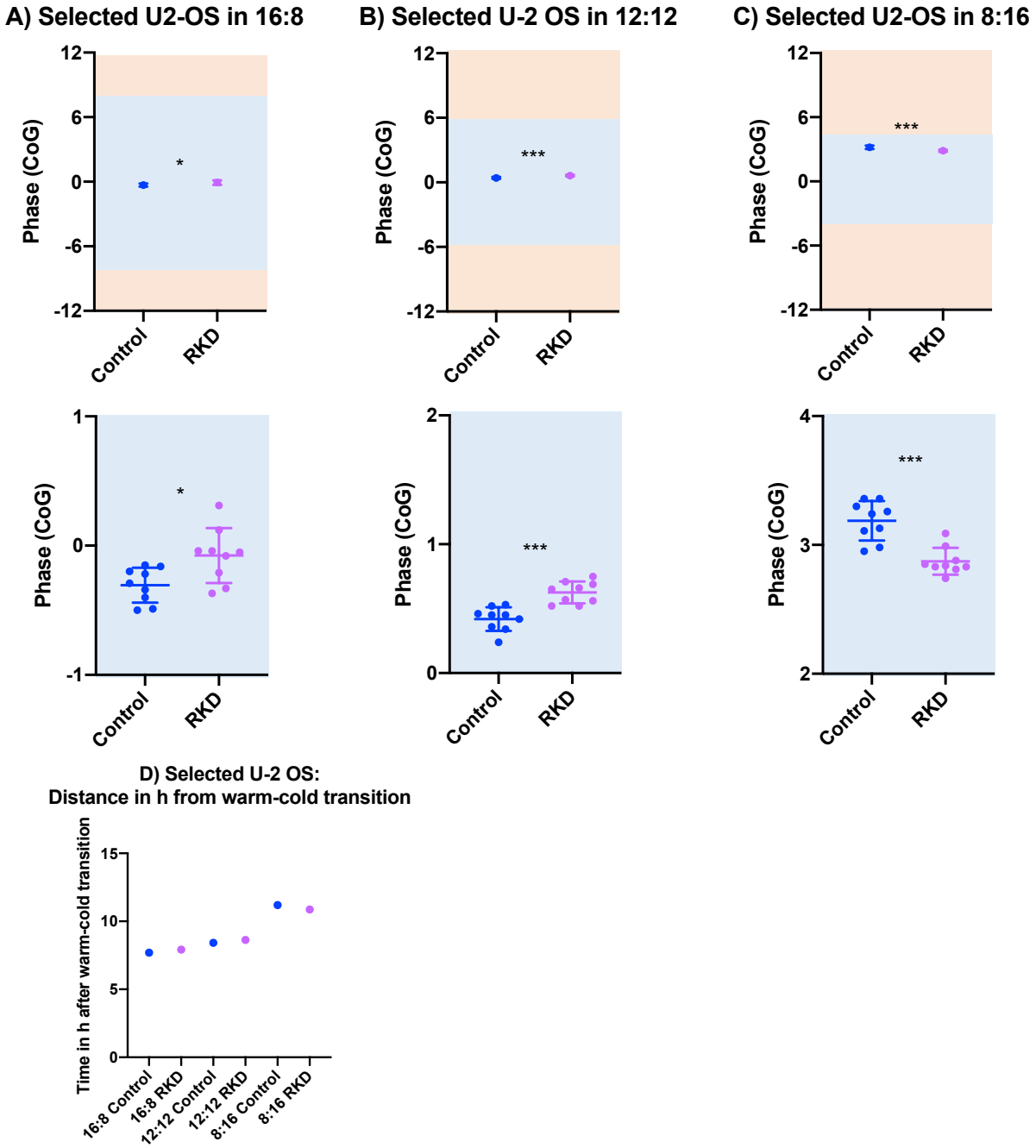

Figure 8: Phase of the Center of Gravity of Bmal1 promoter activity in the selected U-2 OS cell line in different thermoperiods in 35.5/38.5°C as indicated.
*Shown is the phase with mean and SD for the RGS16 knockdowns (pink) vs the controls (blue) for the different cell lines. Time point 0 indicates mid-cold (External time). * = significance determined by t tests. Outliers were removed by Prism (ROUT = 1).*

A) 16:8: The KDs have a later phase than controls (Controls = -0.3056 ± 0.1351 h, KDs = -0.07667 ± 0.2120 h. P=0,0148). N=9 for controls and RGS16 KD cells.
B) 12:12: The KDs have a later phase than controls (Controls = 0.4189 ± 0.09212 h, KDs = 0.6256 ± 0.08531 h. P=0.0001). N=9 for controls and RGS16 KD cells.
C) 8:16: The KDs have an earlier phase than controls (Controls = 3.188 ± 0.1537 h, KDs = 2.873 ± 0.1048 h. P=0.0001). N=9 for controls and RGS16 KD cells.
D) Distance (in hours) of the phase from the warm-cold transition for the different conditions.

In the selected ARPE-19 cell line, the controls and knockdowns were also significantly different in several different conditions (Figure 9). In 16:8, the KD cells were entraining to a later phase compared to controls (P=0.0227 for 16:8) (Figure 9A). In 8:16, the KD cells were entraining to a significantly earlier phase compared to controls (P=0.0162) (Figure 9C). Again, in increasingly shorter cold phases, the phases of the center of gravity of both cell lines moved closer to the cold-warm-transition and further away from the warm-cold transition (Figure 9D).

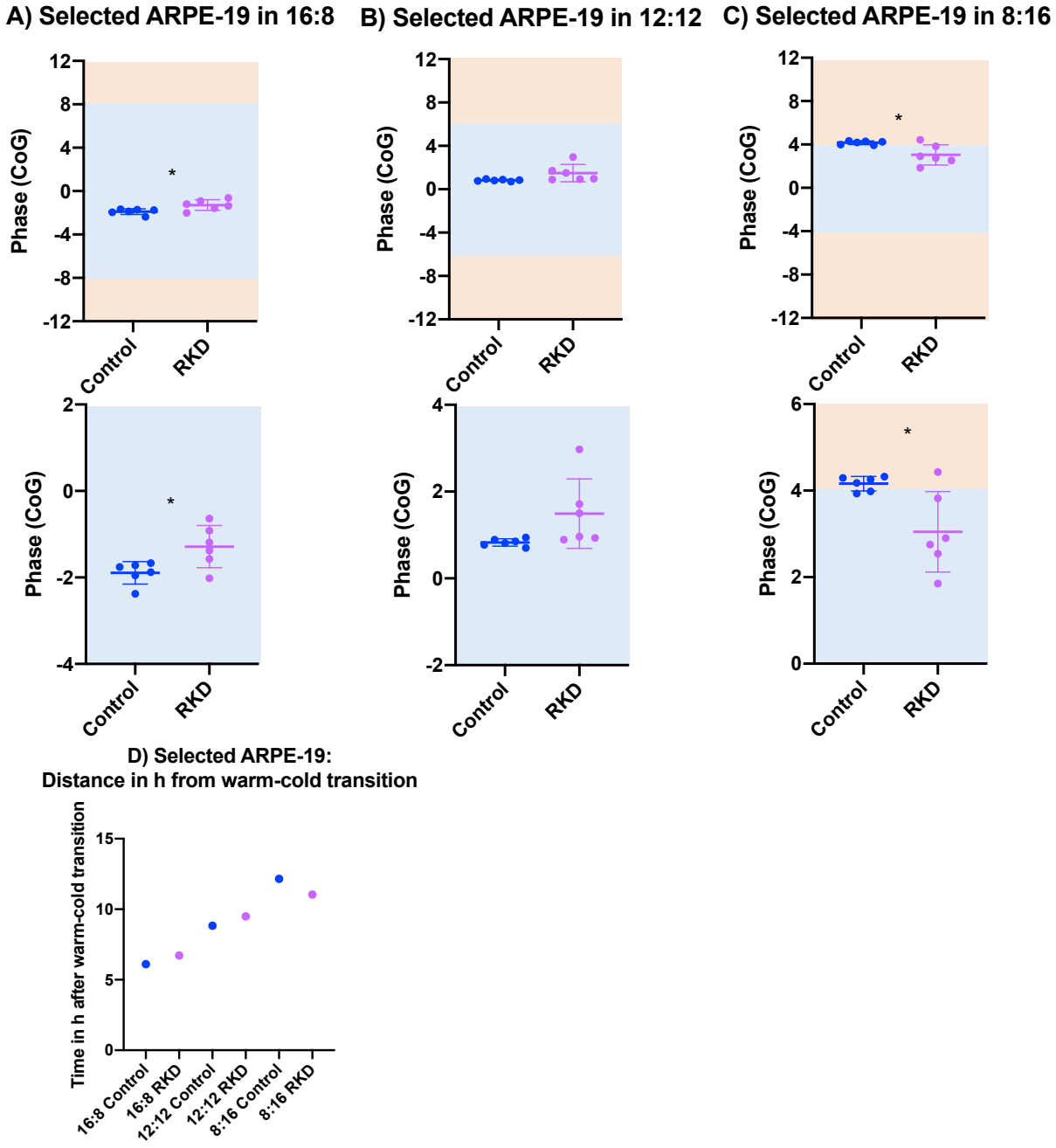

Figure 9: Phase of the Center of Gravity of Bmal1 promoter activity in the selected ARPE-19 cell line in different thermoperiods in 35.5/38.5°C as indicated.
*Shown is the phase with mean and SD for the RGS16 knockdowns (pink) vs the controls (blue) for the different cell lines. Time point 0 indicates mid-cold (External time). * = significance determined by t tests. Outliers were removed by Prism (ROUT = 1).*
A) 16:8: The KDs have a significantly later phase than controls (Controls = -1.893 ± 0.2600 h, KDs = -1.287 ± 0.4876 h. P=0.0227). N=6 for controls and KD cells.
B) 12:12: The KDs have a later phase than controls, although the difference was not statistically significant (Controls = 0.8267 ± 0.08595 h, KDs = 1.493 ± 0.7992 h. P=0.0696). N=6 for controls and KD cells.
C) 8:16: The KDs have a significantly earlier phase than controls (Controls = 4.160 ± 0.1663 h, KDs = 3.048 ± 0.9284 h, P=0.0162). N=6 for controls and RGS16 KD cells.
D) Distance (in hours) of the phase from the warm-cold transition for the different conditions.

3.1.2.5 Entrainment to different zeitgeber strengths

To evaluate whether a KD of RGS16 leads to an increased susceptibility to temperature changes and thus to a faster entrainment, the subcloned RGS16 KD U-2 OS cells and controls were exposed to temperature cycles with a "standard" amplitude (with a temperature difference of Δ3°C) vs. a low amplitude (Δ1.5°C) (Figure 10). The cell lines were compared across the entire time course (days 1-6) as well as in the entrained state only (days 3-6).
The time point when the cells reached a stable phase of entrainment was different, as was the phase angle. In Δ3°C, both the controls and the KDs reached a stable phase at day 3 (Figure 10A). In Δ1.5°C, the controls reached a stable phase at day 3, the KDs at day 2 (Figure 10B). Therefore, the KDs seemed to entrain faster to the new phase in Δ1.5°C.

For cycles with Δ3°C, there was no significant difference between the controls and the KDs when looking at days 1-6 in the two-way ANOVA ($F(1, 267) = 0.03970$, $P=0.5292$), but the interaction factor was significantly different ($F(5, 267) = 9.419$, $P<0.0001$), and on day 1, the KDs showed a significantly later phase compared to controls in the post hoc Sidak's multiple comparisons test ($P<0.0001$) (Figure 10A). When only looking at the entrained state (days 3 to 6), there was a significant difference between KDs and controls in the two-way ANOVA ($F(1, 160) = 12.12$, $P=0.0006$).

For cycles with Δ1.5°C, the two-way ANOVA showed a significant difference between KDs and controls across the whole experiment (days 1-6) as well as in the entrained state (days 3-6) ($F(1, 215) = 309.0$, $P<0.0001$, and $F(1, 141) = 25.43$, $P<0.0001$, respectively) (Figure 10B). The post hoc Sidak's multiple comparisons test showed a significantly later phase of entrainment on days 1, 2, and 3 ($P<0.0001$ for days 1 and 2, and $P=0.0001$ for day 3).

The use of a weaker zeitgeber allowed a visualization of systematic entrainment in control and KD cells (relative to a strong zeitgeber). Overall, it could be observed that the KD cell lines seem to entrain faster to a weaker zeitgeber, thus they are apparently more susceptible to temperature as a zeitgeber than controls.

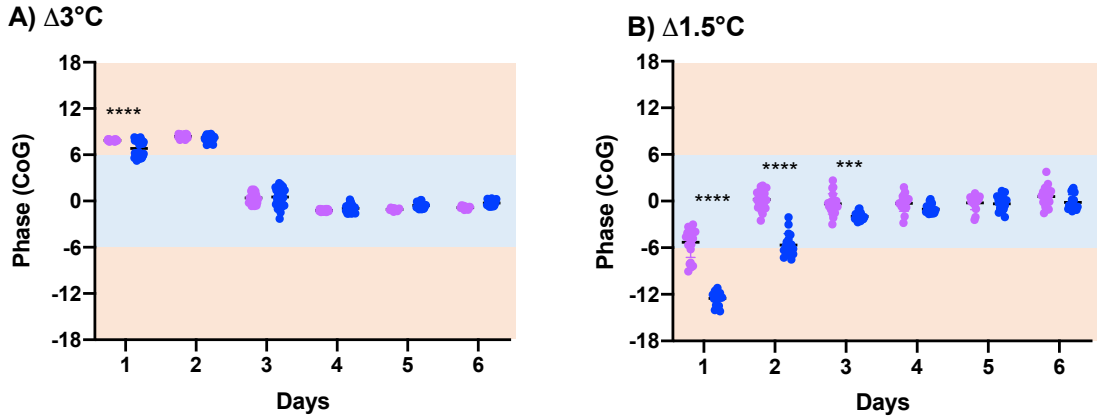

Figure 10: Phase of the Center of Gravity of Bmal1 promoter activity of the subcloned U-2 OS cell line in 12:12 35.5/38.5°C and 36/37.5°C.
*Shown is the phase with mean and SD for the RGS16 knockdowns (pink) vs the controls (blue). Time point 0 indicates mid-cold (External time). * = significance in post hoc Sidak's test (days 1-6). Outliers were removed by Prism (ROUT = 1).*
A) Δ3°C: The cells all reached a stable phase of entrainment on day 3. Controls: N=34 for day 1, 3 and 4, N=33 for day 2, N=17 for day 5 and 6. KDs: N=22 for days 1-4 N=11 for day 5 and 6.
B) Δ1.5°C: The KDs reached a stable phase of entrainment on day 2, the controls on day 3. Controls: N=18 for days 1-5, N=17 for day 6. KDs: N=21 for days 1-3, N=20 for days 4 and 6, N=17 for day 5.

3.1.3 Temperature Compensation

By definition, circadian rhythms are temperature-compensated (Pittendrigh, 1960), although much less has been tested in homeotherms. To test whether RGS16 could play a role in temperature compensation, U-2 OS and ARPE-19 KD cells were tested in a variety of temperatures, in free-run as well as in entrainment conditions (Figures 11 and 12).

To quantify the temperature sensitivity of a system, the Q_{10} is calculated. It is the rate of chemical or biological change over 10°C and is calculated via the following formula:

$$Q_{10} = \left(\frac{R_2}{R_1}\right)^{\frac{10}{T_2 - T_1}}$$

T1 represents the lower temperature, T2 the higher temperature. R1 and R2 represent the rate of the reaction. Since a longer free-running period means a slower reaction rate, R1 and R2 need to be reversed, which results in the following formula, which was used for the Q_{10} calculations:

$$Q_{10} = \left(\frac{R_1}{R_2}\right)^{\frac{10}{T_1 - T_2}}$$

The Q_{10} stays around 1 over a range of physiological temperatures in temperature compensated systems, while the rate for normal biochemical reactions usually lies around 2-3 or higher (Avery, 1974; Sweeney & Hastings, 1960).
The standard formula for the Q_{10} only takes into account the highest and the lowest value and thus it misses non-linear trends. An alternative way of calculating it by using a non-linear fit yielded similar results and is shown in the Supplementary Materials. Further, the Q10 is not meant for circular data such as the phase values. The formula is meant for positive values only, so for phase calculations, the data was transposed to +24.

3.1.3.1 Temperature compensation in free-run

Typically, temperature compensation is tested by assessing the free-running period over several constant temperatures. For this, the cells were synchronized with dexamethasone and then measured in constant 31°C, 34°C, 37°C and 40°C as indicated. Then, the Q_{10} was calculated using the formula shown above. Even though there were trends towards slight over- (Q_{10} of <1) or under-compensation (Q_{10} > 1), both U-2 OS and ARPE-19 always qualify as temperature-compensated even after a KD of RGS16 (Figure 11). The periods and Q_{10} values are shown in table 2 and 3, respectively.

In the selected U-2 OS control cell line, the period was slightly longer in both high and cold temperatures in the controls (Figure 11A). The Q_{10} was 1.02, so the cells were well compensated. The KDs showed a longer free-running period in colder temperatures. This is generally termed under-compensated, but the Q_{10} of 1.28 still qualifies as temperature compensated.

In the subcloned U-2 OS cell line, the controls show a shortening of the FRP in colder temperature with a minimally over-compensated Q_{10} of 0.98 (Figure 11B). The KDs, however, were slightly under-compensated with the period increasing in colder temperatures and a Q_{10} of 1.31.

In the selected ARPE-19 cell line, the controls had a significantly shorter free-running period in low and high temperatures, the Q_{10} was 1.03 (Figure 11C). The KDs were similarly well compensated with a Q_{10} of 1.02 and a relatively stable period across all temperatures.

Overall, the KDs seem to trend more towards under-compensation in U-2 OS, while they show very similar compensation in ARPE-19 cells (Figure 11D).

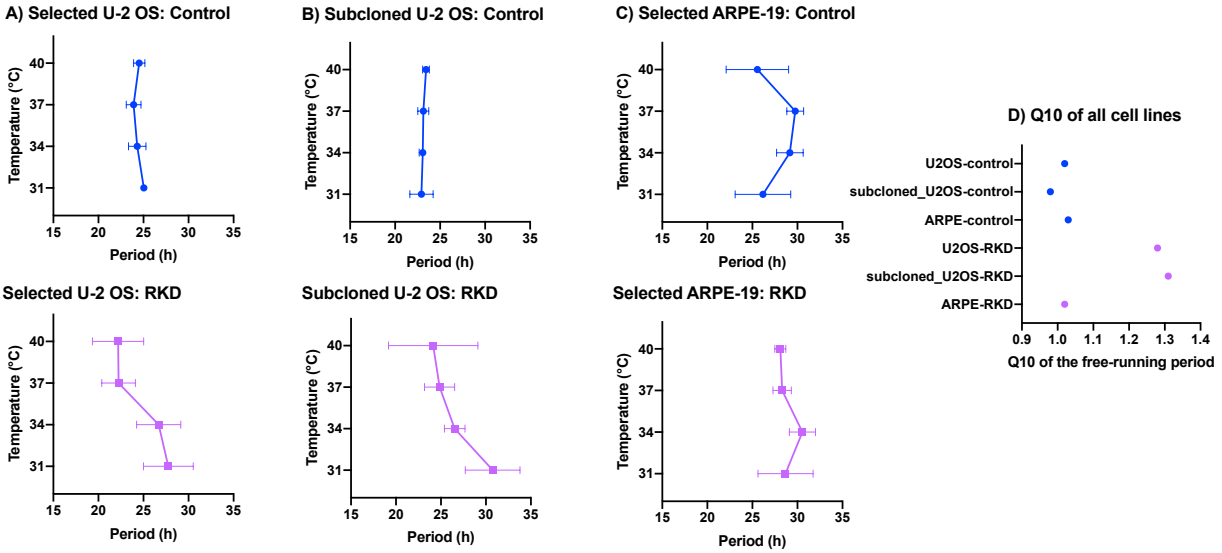

Figure 11: Temperature compensation of the free-running period is not impaired by a KD of RGS16 in U-2 OS and ARPE-19 cells.
Shown is the free-running period of Bmal1 promoter activity with mean and SD for the RGS16 knockdowns (pink) vs the controls (blue) in different constant temperatures. Outliers were removed by Prism (ROUT = 1).
A) Selected U-2 OS cell line. Controls: N=24 for 31°C, N=23 for 34°C, N=31 for 37°C, N=23 for 40°C; KDs: N=23 for 31°C, N=24 for 34°C, N=46 for 37°C, N=24 for 40°C. Kruskal-Wallis test: P<0.0001 for both controls and KDs.
B) Subcloned U-2 OS cell line. Control: N=52 for 31°C, N=34 for 34°C, N=42 for 37°C, N=18 for 40°C; KDs: N=50 for 31°C, N=38 for 34°C, N=49 for 37°C, N=21 for 40°C. Kruskal-Wallis test: P<0.0121 for controls and P<0.0001 for KDs.
C) Selected ARPE-19 cell line. Controls: N=9 for 31°C, N=17 for 34°C, N=26 for 37°C, N=13 for 40°C; KDs: N=19 for 31°C, N=20 for 34°C, N=34 for 37°C, N=11 for 40°C. Kruskal-Wallis test: P<0.0001 for both controls and KDs.
D) Q_{10} of the free-periods of all cell lines.

Free-running period at…	**31°C**	**34°C**	**37°C**	**40°**
U2OS_Control	25.05 ± 0.3561	24.31 ± 0.9696	23.91 ± 0.8186	24.53 ± 0.6249
U2OS_RKD	27.76 ± 2.761	26.69 ± 2.448	22.24 ± 1.867	22.19 ± 2.845
Subcloned_U2OS_Control	22.93 ± 1.293	23.07 ± 0.3917	23.13 ± 0.6018	23.44 ± 0.3755
Subcloned_U2OS_RKD	30.75 ± 3.038	26.53 ± 1.146	24.85 ± 1.670	24.14 ± 4.970
ARPE_Control	26.17 ± 3.089	29.17 ± 1.481	29.76 ± 0.9341	25.55 ± 3.469
ARPE_RKD	28.68 ± 3.059	30.55 ± 1.450	28.30 ± 1.014	28.10 ± 0.6065

Table 2: The mean ± SD in h of the free-running period of Bmal1 promoter activity in the different cell lines at the different temperatures.

Usually, temperature compensation is analyzed looking at the lowest vs. the highest temperature. Since the circadian clock is a dynamic, temperature-compensated system, the Q_{10} of the longest vs. shortest free-running period was also tested to look for systematic changes (Table 3). In most cases, both analyses yielded similar results.

Q_{10} at…	lowest vs. highest temperature	Longest vs. shortest FRP
U2OS_Control	1.02	1.08
U2OS_RKD	1.28	1.28
Subcloned_U2OS_Control	0.98	0.98
Subcloned_U2OS_RKD	1.31	1.31
ARPE_Control	1.03	1.67
ARPE_RKD	1.02	1.15

Table 3: The Q10 of the means of the free-running period of Bmal1 promoter activity in the different cell lines at the lowest vs. highest temperature and at the longest vs. shortest free-running period of the different temperatures.

3.1.3.2 Temperature compensation in entrainment

Further, temperature compensation of cells under entrainment was analyzed. Here, temperature cycles with a mean of 31°C, 34°C, 37°C and 40°C and a temperature difference of Δ3°C were used to entrain the cells, and day 5 was analyzed to calculate the center of gravity. Both U-2 OS and APRE-19 showed later phases in high and low temperatures, but they still remained temperature-compensated after a KD of RGS16 (Figure 12). The phases and the calculated Q_{10} values for lowest vs. highest temperatures and earliest vs. latest phase are shown in table 4 and 5, respectively.

The selected U-2 OS control cells showed a Q_{10} of 1.02, while the KD cell line had a similar Q_{10} of 1.00 (Figure 12A). This was similar when comparing the earliest vs. latest phase instead of lowest vs. highest temperature (Table 5).

The subcloned U2- OS cells were over-compensated with a Q_{10} of 0.85 in controls and 0.75 in KDs (Figure 12B). This was even more pronounced when comparing the earliest vs. latest phase instead of the lowest vs. highest temperature (Table 5).

The selected ARPE-19 cells were well compensated with a Q_{10} of 1.05 in controls and 1.04 in KDs (Figure 12C). Here, they showed under-compensation when comparing the earliest and latest phase (Table 5).

Overall, the subcloned U-2 OS cells trended more towards over-compensation than the other two cell lines (Figure 12D).

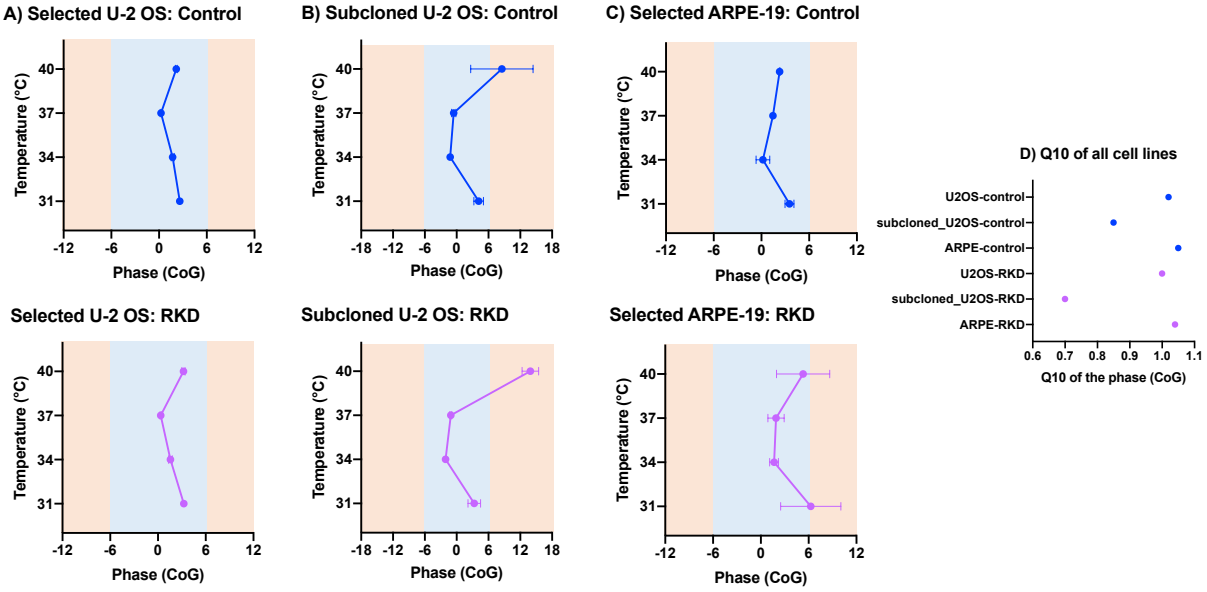

Figure 12: The phase of entrainment of U-2 OS and ARPE-19 remains temperature-compensated after a KD of RGS16.
The phase of the Center of Gravity of Bmal1 promoter activity was determined in different temperatures: 29.5/32.5°C, 32.5/35.5°C, 35.5/38.5°C, 38.5/41.5°C, in 12:12. Shown is the phase with mean and SD for the controls (blue, upper panel) and the RGS16 knockdowns (pink, lower panel) for the different cell lines. Time point 0 indicates mid-cold (External time). Outliers were removed by Prism (ROUT = 1).
A) Selected U-2 OS cell line. N=9 for all except KDs in 37°C, there N=8. One-way ANOVA: P<0.0001 for both controls and KDs.
B) Subcloned U-2 OS cell line. Controls: N=18 for 31°C, N=18 for 34°C, N=17 for 37°C, N=18 for 40°C; KDs: N=12 for 31°C, N=12 for 34 °C, N=11 for 37°C, N=12 for 40°C. Kruskal-Wallis test: P<0.0001 for both controls and KDs.
C) Selected ARPE-19 cell line. N=6 for all except Controls 34°C, there N=5. Kruskal-Wallis test: P=0.0001 for controls and P=0.0010 KDs.
D) Q_{10} of the phase of entrainment of all cells.

Center of Gravity at mean temperature of…	**31°C**	**34°C**	**37°C**	**40°**
U2OS_Control	2.608 ± 0.1537	1.719 ± 0.1984	0.2422 ± 0.0884	2.173 ± 0.1132
U2OS_RKD	3.251 ± 0.3991	1.573 ± 0.2409	0.3588 ± 0.0934	3.206 ± 0.2123
Subcloned_U2OS_Control	4.155 ± 0.8855	-1.226 ± 0.1824	-0.5418 ± 0.4019	8.536 ± 5.877
Subcloned_U2OS_RKD	3.323 ± 1.184	-2.075 ± 0.1698	-1.095 ± 0.1743	13.90 ± 1.554
ARPE_Control	3.532 ± 0.5659	0.1920 ± 0.8527	1.447 ± 0.1261	2.298 ± 0.04579
ARPE_RKD	6.270 ± 3.781	1.663 ± 0.5445	1.902 ± 1.021	5.312 ± 3.347

Table 4: The mean ± SD in h of the phase of the Center of Gravity of Bmal1 promoter activity in the different cell lines at the different temperatures (29.5/32.5°C, 32.5/35.5°C, 35.5/38.5°C, 38.5/41.5°C) in 12:12.

Q_{10} at…	lowest vs. highest temperature	latest vs. earliest phase
U2OS_Control	1.02	1.17
U2OS_RKD	1.00	1.21
Subcloned_U2OS_Control	0.85	0.55
Subcloned_U2OS_RKD	0.70	0.40
ARPE_Control	1.05	1.54
ARPE_RKD	1.04	1.73

Table 5: The Q10 of the means of phase of the Center of Gravity of Bmal1 promoter activity in the different cell lines at the lowest vs. highest temperature and at the latest vs. earliest phase of the different temperatures. 29.5/32.5°C, 32.5/35.5°C, 35.5/38.5°C, 38.5/41.5°C, in 12:12. For calculating the Q_{10}, all phases were transposed to +24 to exclude negative values.

3.1.3.3 Free-running Period vs. Phase of Entrainment

The relationship between free-running period and phase of entrainment is still not completely understood. Generally, it is assumed that a shorter free-running period correlates with an earlier phase of entrainment, and a longer free-running period correlates with a later phase of entrainment (Hamblen-Coyle et al., 1992; Rémi et al., 2010). However, this rule has been increasingly considered incomplete (Lee et al., 2017).

Both the KDs and the controls showed persisting temperature compensation in all three cell lines. However, the relationship between the free-running period and the phase of entrainment was not always the same (Figure 13). The periods and phases can be found in table 6.

In the selected U-2 OS cell line, the controls were well compensated with a Q_{10} of 1.02 both in the free-running period and in the phase of entrainment (Figure 13A). Here, in both high and low temperatures, the longer FRPs correlated with a later phase of entrainment, while moderate temperatures led to shorter periods and earlier phases.
The KDs had a Q_{10} of 1.28 in the free-running period and a Q_{10} of 1.00 in the phase of entrainment (Figure 13E). Here, the cells were slightly under-compensated in the free-run with an increase in period with a decrease in temperature. The phase showed a similar pattern to the controls with a later phase in both high and low temperatures, so the shorter period in high temperatures did not lead to a later, but to an earlier phase of entrainment.

In the subcloned U-2 OS cell line, the controls showed slight over-compensation with a Q_{10} of 0.98 in the free-running period and 0.85 in the phase of entrainment (Figure 13B). Here, the

period increased in higher temperatures, correlating with a later phase, but the shortened period in cold temperatures did not correlate with an earlier, but with a later phase of entrainment.

The KDs had a Q_{10} of 1.31 in the free-running period and a Q_{10} of 0.70 in the phase of entrainment (Figure 13F). Here, analogous to the selected cell line, the cells showed slight under-compensation in the free-run with an increase in period with a decrease in temperature, which correlated with a later phase of entrainment. In high temperatures, however, the shortened period correlated with a later, not an earlier phase again.

In the selected ARPE-19 cells, the controls had a Q_{10} of 1.03 in the free-running period and a Q_{10} of 1.05 in the phase of entrainment (Figure 13C). Free-running period and phase of entrainment showed opposing patterns, with shorter periods and later phases in high and low temperatures, and longer periods and earlier phases in moderate temperatures. The KDs had a Q_{10} of 1.02 for the free-running period and a Q_{10} of 1.04 for the phase of entrainment (Figure 13G). The pattern was the same as in the controls.

Overall, both KDs and controls did not always follow the rule that longer periods correlate with later phases and that shorter periods correlate with earlier phases (Figures 13D and H).

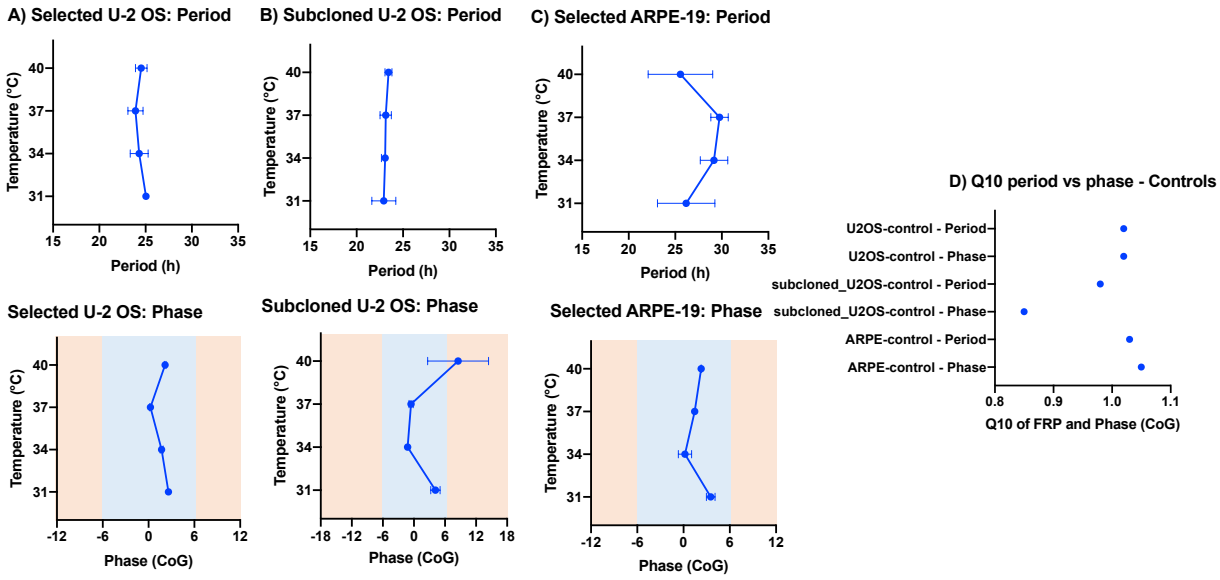

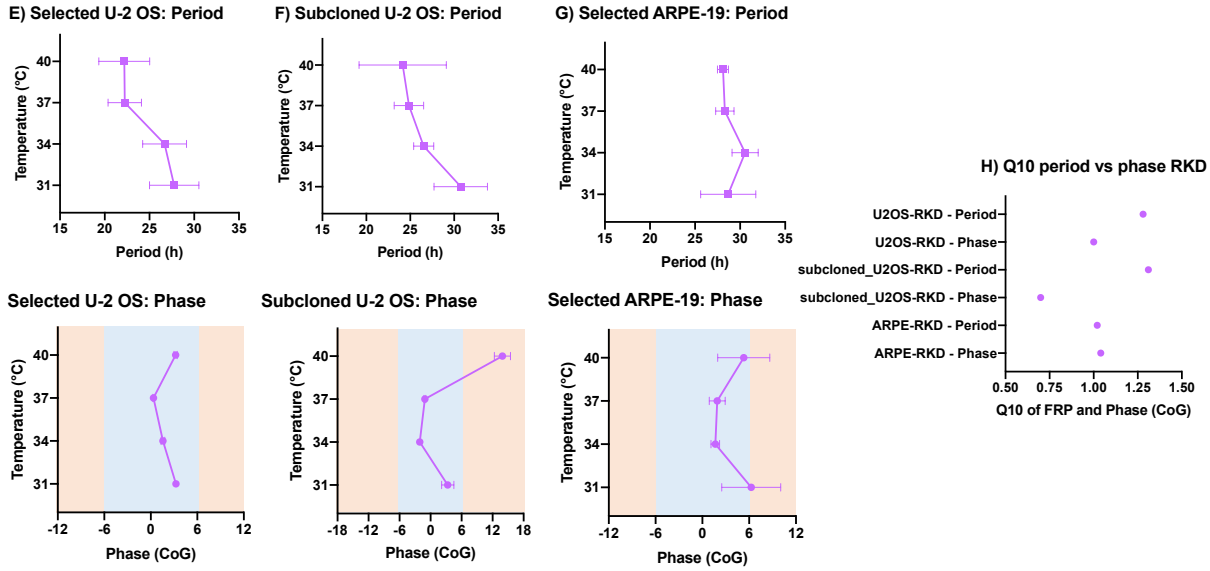

*Figure 13: Free-running period vs. phase of entrainment in controls (blue) and RGS16 KD cells (pink). Shown is the free-running period (above) and phase of entrainment of the Center of Gravity (below) of Bmal1 promoter activity with mean and SD in different temperatures (constant, above, or mean with a temperature difference of Δ3°C, below). Time point 0 indicates mid-cold (External time). * = significance in post hoc Sidak's test. Outliers were removed by Prism (ROUT = 1).*
A) Selected U-2 OS cell line, controls.
B) Subcloned U-2 OS cell line, controls.
C) Selected ARPE-19 cell line, controls.
D) Q_{10} of the periods and phases of the control cell lines.
E) Selected U-2 OS cell line, KDs.
F) Subcloned U-2 OS cell line, KDs.
G) Selected ARPE-19 cell line, KDs.
H) Q_{10} of the periods and phases of the KD cell lines.

The KDs also differed significantly from the controls in the different temperatures (Figure 14). In the selected U-2 OS cell line, the two-way ANOVA showed a significant interaction between temperature and cell line for the free-running period ($F(3, 210) = 26.83$, $P<0.0001$) (Figure 14A). The KDs showed a significantly longer free-running period in lower temperatures ($P<0.0001$ for both 31°C and 34°C), and a shorter free-running period in higher temperatures ($P=0.0005$ and $P<0.0001$ for 37°C and 40°C, respectively). For the phase, there was a difference in the interaction between temperature and cell line ($F(3, 63) = 27.76$, $P<0.0001$) as well as between the cell lines themselves ($F(1, 63) = 66.88$, $P<0.0001$). The KDs entrained to a significantly later phase than the controls in high and low temperatures ($P<0.0001$ for both 31°C and 40°C).

In the subcloned U-2 OS cell line, when looking at the free-running period, there was a significant difference in the interaction between temperature and cell line ($F(3, 296) = 47.85$, $P<0.0001$) as well as between KDs and controls ($F(1, 296) = 185.5$, $P<0.0001$) (Figure 14B). There was no significant difference in 40°C, but the KDs showed a longer free-running period

relative to controls in 31°C, 34°C, and 37°C (P<0.0001, P<0.0001, P=0.0003, respectively). There was a difference in the interaction between temperature and cell line in the phase as well (F (3, 110) = 11.40, P<0.0001). Here, the KDs showed a significantly later phase only in high temperatures (P<0.0001 for 40°C).

In the free-running period of the selected ARPE-19 cell line, there was a significant difference in the interaction between temperature and cell line (F (3, 141) = 10.13, P<0.0001) as well as for KDs vs. controls (F (1, 141) = 13.20, P=0.0004) (Figure 14C). The KDs had a significantly longer free-running period in low and high temperatures (P=0.0064 for 31°C and P=0.0062 for 40°C). In 37°C, the free-running period of the KDs was significantly shorter (P=0.0173). The phase was significantly different between the cell lines (F (1, 39) = 12.12, P=0.0012). The KDs entrained to a later phase than the controls, but the difference was only statistically significant in high temperatures (P=0.0340 for 40°C).

Generally, in lower temperatures, the KD lengthens the period compared to controls in U-2 OS cells. The KDs seem to be under-compensated compared to the controls.
In ARPE-19 cells, the period of the KDs is longer in high and low temperatures, and shorter in 37°C. Here, interestingly, the KD cells seem to be better compensated than the controls.
The phases seem to be well compensated, especially in physiological temperatures. In low and especially in high temperatures, however, the cells, especially the KDs, seem to be less well compensated and show a later phase of entrainment than controls.

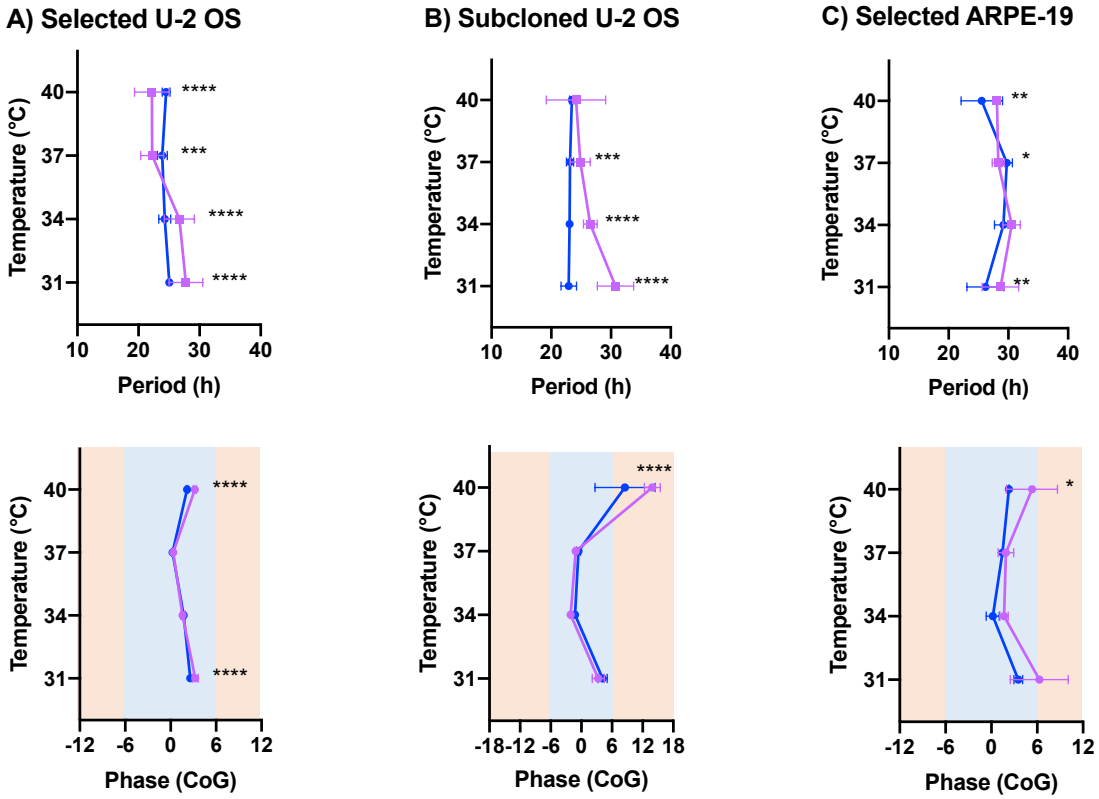

*Figure 14: Comparison between the RGS16 KD (pink) and control (blue) cell lines in different temperatures. Shown is the free-running period (above) and phase of entrainment of the Center of Gravity (below) of Bmal1 promoter activity with mean and SD in different temperatures (constant, above, or mean with a temperature difference of Δ3°C, below). Time point 0 indicates mid-cold (External time). * = significance in post hoc Sidak's test. Outliers were removed by Prism (ROUT = 1).*
A) Selected U-2 OS cell line.
B) Subcloned U-2 OS cell line.
C) Selected ARPE-19 cell line.

Q_{10} at…	**lowest vs. highest temperature - Period**	**lowest vs. highest temperature - Phase**	**longest vs. shortest Period**	**latest vs. earliest Phase**
U2OS_Control	1.02	1.02	1.08	1.17
U2OS_RKD	1.28	1.00	1.28	1.21
Subcloned_U2OS_Control	0.98	0.85	0.98	0.55
Subcloned_U2OS_RKD	1.31	0.70	1.31	0.40
ARPE_Control	1.03	1.05	1.67	1.54
ARPE_RKD	1.02	1.04	1.15	1.73

Table 6: Temperature compensated period and phase of the different cell lines.
Shown is the Q_{10} of the means of the free-running period and the phase of the Center of Gravity of Bmal1 promoter activity in the different cell lines at the lowest vs. highest temperature, and at the longest vs. shortest period and the latest vs. earliest phase of the different temperatures.

3.2 Interaction of RGS16 with the circadian clock in peripheral cells

3.2.1 Abundance of RGS16 in peripheral cells

It has been shown that RGS16 mRNA as well as protein abundance is regulated by the circadian clock in the SCN and the liver (Doi et al., 2011; Hayasaka et al., 2011). We tested whether there was a time-of-day difference in RGS16 abundance in U-2 OS cells as well (Figures 15 and 16).

For determining whether there is a free-running rhythm in RGS16 protein amounts, the cells were synchronized using dexamethasone, a potent resetter of the cellular circadian clock, and harvested every 4 h for 24 h starting 12 h after dexamethasone stimulation (Figure 15). The western blot images were analyzed with Image Lab (Figure 15A) and the individual dataseries were graphed in Prism. The RGS16 levels were normalized to actin and to time point 1 of each

individual blot (Figure 15B). There was a significant difference between the peak and the trough (P=0.0362) (Figure 15C).

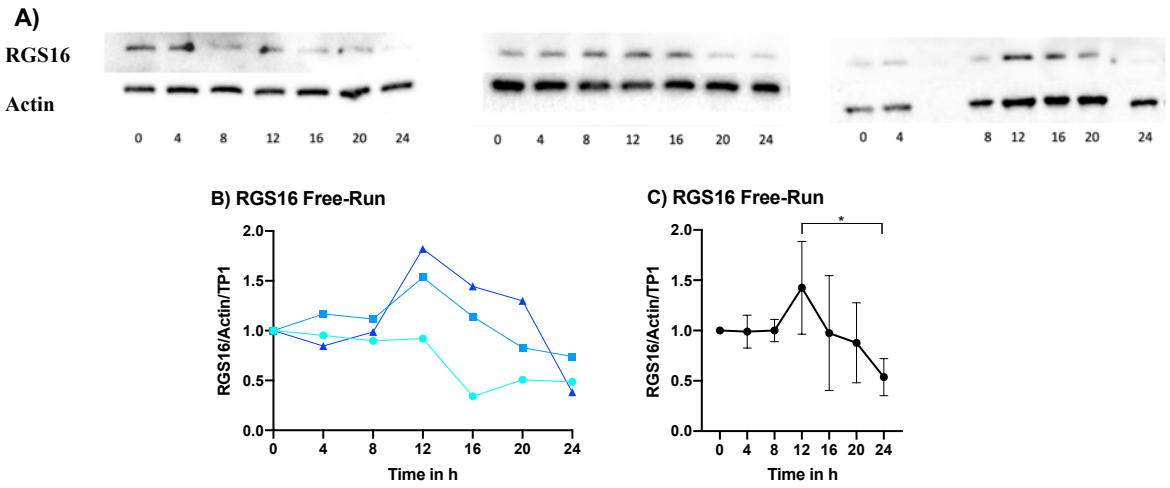

Figure 15: Abundance of RGS16 over 24h in U-2 OS in constant 37°C after synchronization with dexamethasone. The cells were synchronized with dexamethasone and then harvested every 4 h starting after 12 h after synchronization. The RGS16 levels were normalized to the vinculin levels and to time point 1 of each individual blot.
A) Western blots with RGS16 and Actin antibodies.
B) Single blots, normalized.
C) Mean ± SD, normalized. The student's t test showed a significant difference between maximum (TP 12, 24 h after synchronization) and minimum (TP 24, 36 h after synchronization), P=0.0362.

To test if the abundance of RGS16 changes over the time of day under entrainment conditions, U-2 OS cells were cultured in anticyclic 24 h temperature cycles (12h:12h 34/37°C or 37/34°C) for 5 days and then simultaneously harvested every 4 h over 12 h (Figure 16). The western blot images were analyzed with Image Lab (Figure 16A) and the individual and average dataseries were graphed in Prism (Figures 16B and C). The RGS16 levels were normalized to vinculin and to time point 1 of each individual blot.

RGS16 levels vary over the time of day in U-2 OS cells, with a peak around ExT 2 and a trough around ExT 14 (P=0.0029) (Figure 16D).

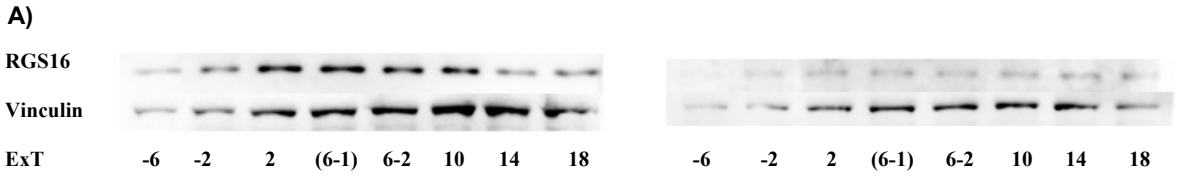

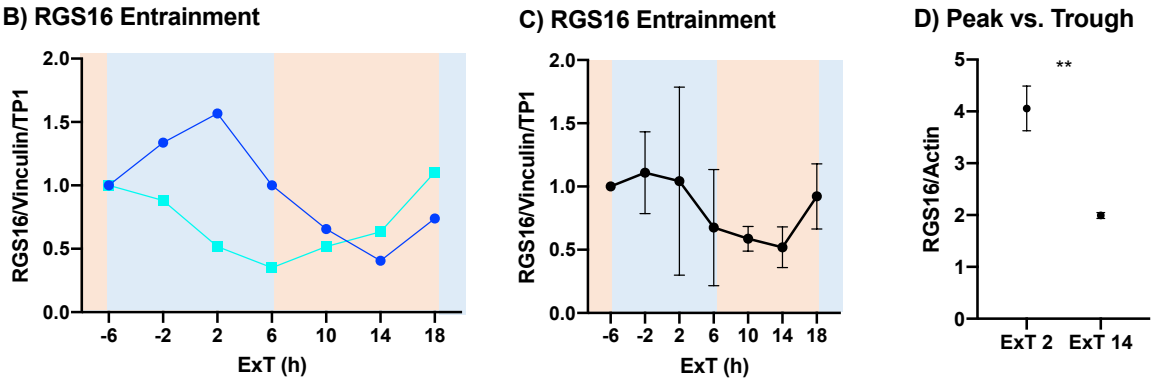

Figure 16: Abundance of the RGS16 over 24 h in U-2 OS in entrainment.
The cells were entrained in 34/37°C 12:12 and harvested every 4 h on day 5. ExT = External Time; time point 0 indicates mid-cold. The RGS16 levels were normalized to the vinculin levels and to time point 1 of each individual blot.
A) Western blots with RGS16 and Vinculin antibodies.
B) Single blots, normalized.
C) Mean ± SD, normalized.
D) Peak (ExT 2) and trough (ExT 14), normalized to actin. The student's t test showed a significant difference between the two time points (P=0.0029). N=2 for ExT 2 and N=3 for ExT 14.

3.2.2 Localization of RGS16 in different conditions

RGS16 is mainly found in the cytoplasm. However, it also has a membrane anchor and has been found in the membrane (Chen et al., 1999; Druey et al., 1999; Hiol et al., 2003; Osterhout et al., 2003). Therefore, we hypothesized that RGS16 may localize to different areas in different conditions or at different times of day. The spatiotemporal distribution of RGS16 in a 24 h temperature cycle was characterized, as well as its localization in response to temperature changes and to stimulation of GPCRs (Figure 17-23). This was done via immunocytochemistry. The regions of interest were drawn and the intensities were measured with FIJI. The region comprising 75 pixels around the nucleus was defined as 'perinuclear'; the outer 25 pixels of the cells were defined as 'membrane-adjacent'.

3.2.2.1 Localization over the time of day

To determine the spatiotemporal distribution of RGS16, cells were again cultured in anticyclic 24 h temperature cycles (12h:12h 34/37°C or 37/34°C) for 5 days and then released to constant 34°C or 37°C for 3 days. Then, the cells were harvested every 4 h over 12 h and immediately fixed, permeabilized, and incubated with an anti-RGS16 antibody for immunofluorescence microscopy (Figure 17).

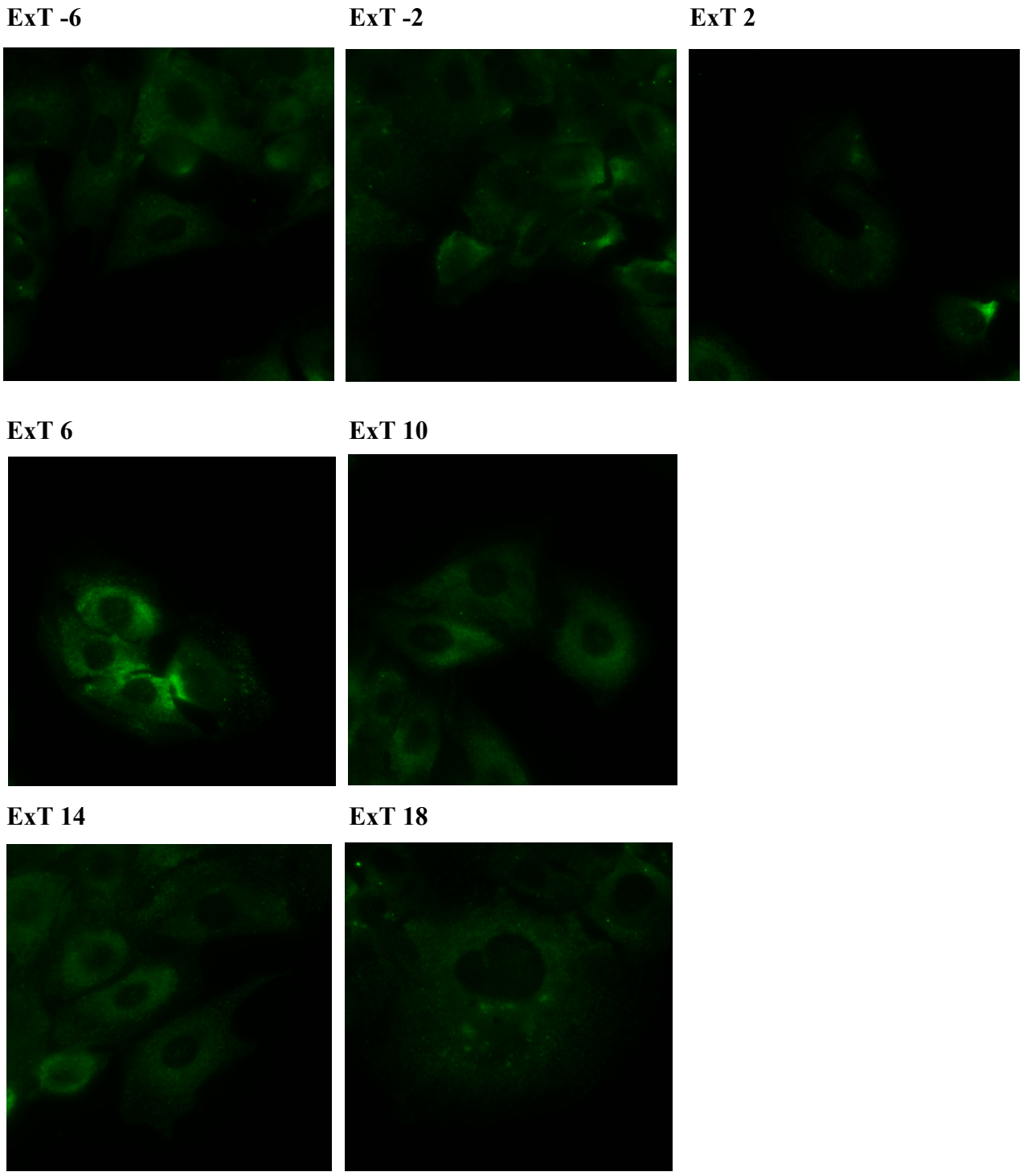

Figure 17: Immunofluorescence of GFP-stained RGS16 protein over 24 h in entrainment.
The cells were entrained in 34/37°C 12:12 and then released into 34°C or 37°C for 3 days before harvesting. ExT = External Time; time point 0 indicates mid-cold. Representative images were selected; the rest can be found in the supplementary materials.

Overall, RGS16 was localized primarily in the cytoplasm, as was expected, but there were some changes over the day (Figure 18). The mean intensity of the individual cells differed across the time course and peaked around the cold-warm transition at ExT 6 ($P<0.0001$) (Figure 18A).

Additionally, there was an antiphasic pattern of RGS16 localization with peak nuclear and perinuclear levels around ExT 2 and simultaneously low levels of membrane-adjacent RGS16 (Figures 18B-D, respectively). The fluctuation in RGS16 localization over the time course was significant for all three subcellular areas (One-way ANOVA P=0.0004 for the nucleus, and P<0.0001 for the perinuclear region and for the membrane).

Since the signal distribution and granulation within the cytoplasm was difficult to analyze with traditional methods, a visual scoring system was established to objectify the changes (see Supplementary Materials, 7.2.4, for details). Here, the cells were randomized and evaluated for the overall signal distribution within the cell as well as the number of bright spots / clusters of RGS16 protein (Figures 18E and F). Most cells showed a primarily perinuclear RGS16 distribution, but especially in the cold phase, the cells showed an increased signal enrichment in one or more corners of the cells (Figure 18E). Interestingly, when looking at the existence of bright spots or clusters of RGS16, the pattern was in phase with the amount of membrane-adjacent RGS16 levels, meaning when there were low levels of membrane-adjacent RGS16 (ExT 2, ExT 18), there was a simultaneous increase in the number of bright spots within the cells (Figure 18F). This could indicate an increased clustering of RGS16 at these times.

Overall, this suggests that the circadian clock influences RGS16 distribution within the cells.

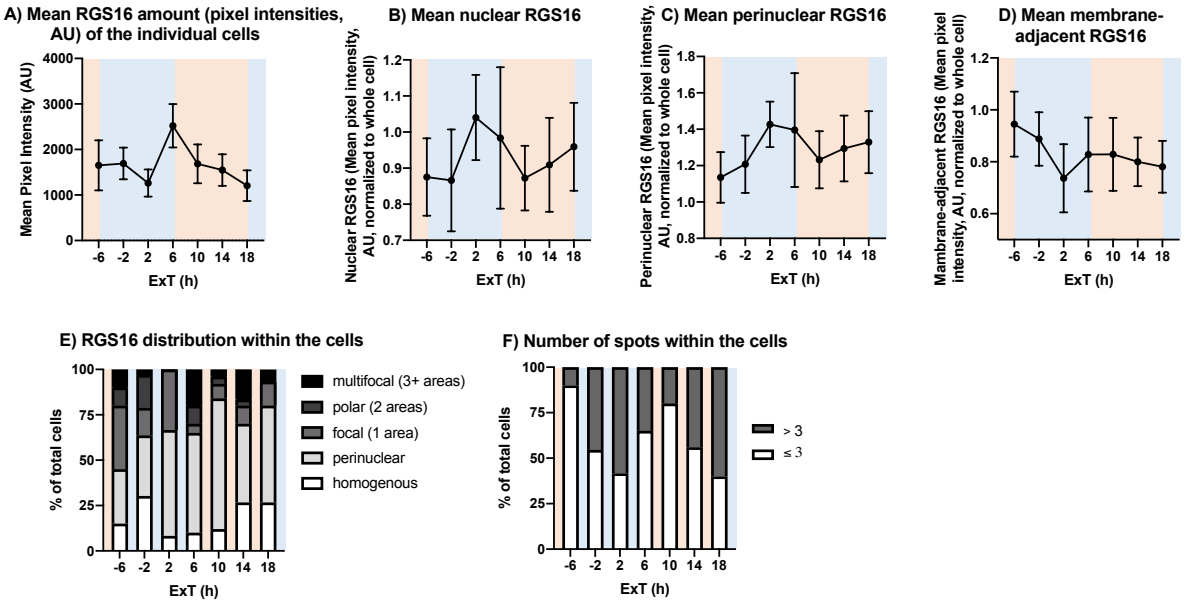

Figure 18: Immunofluorescence of GFP-stained RGS16 protein over 24 h in entrainment.
The cells were entrained in 34/37°C 12:12 and then released into 34°C or 37° for 3 days before harvesting. For A-C, the mean pixel intensities (AU, Arbitrary Units) of the individual cells were calculated in FIJI and the distribution in different compartments relative to the whole cell was analyzed. Outliers were removed in Prism (ROUT = 1), overall statistical significance was determined via one-way ANOVAs. For E-G, cells were scored visually to determine signal and spot distribution.
A) The amount of RGS16 (mean pixel intensity) of the cells was significantly different across the different time points, with a peak around ExT 6 (P<0.0001).
B) The RGS16 concentration in the nucleus was highest in the late cold phase with a peak around ExT 2 (P=0.0004).

C) The concentration in the perinuclear region was also highest in the late cold phase with a peak around ExT 2 (P<0.0001).
D) The highest amount of RGS16 that was located close to the membrane was in the beginning of the cold phase, the lowest around ExT 2 (P<0.0001).
E) Percentage of cells that (visually) had their main signal concentrated in the indicated area(s).
F) Percentage of cells that had more than 3 (gray) vs. up to 3 (white) bright spots.

3.2.2.2 Localization in response to temperature pulses

RGS16 has been shown to be upregulated following heat stress (43°C for 4h) (Seifert et al., 2015). Therefore, we hypothesized that it may be part of the cellular response to temperature changes that occur reliably each day and thus may change localization in response to heat or cold pulses. To explore this, cells were grown to semi-confluency in microscopy dishes at 37°C and then stimulated with high-amplitude pulses of 27°C and 43°C for 4 h each by putting them in an incubator with the respective temperatures. After the indicated times, the cells were immediately fixed, permeabilized, and incubated with an anti-RGS16 antibody for immunofluorescence microscopy (Figure 19).

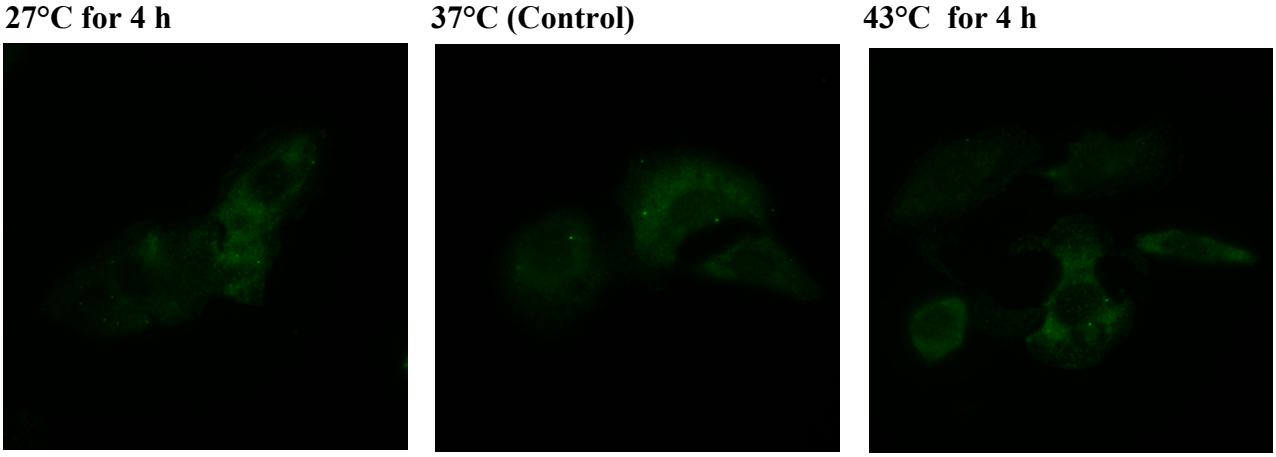

Figure 19: Immunofluorescence of GFP-stained RGS16 protein after temperature pulses of 27°C and 43°C for 4 h.
The cells were kept in 37°C and then exposed to the indicated temperatures for 4 hours. There were differences in the localization and amount of RGS16 across the different conditions. Representative images were selected; the rest can be found in the supplementary materials.

When the cells were exposed to 27°C and 43°C, the mean intensity of the signal decreased (P=0.0241 and P=0.0002, respectively) (Figure 20A). After both cold and heat exposure, RGS16 showed a decrease in nuclear and an increase in membrane-adjacent localization compared to controls (nucleus: P=0.0178 and P=0.0020 for 27°C and 43°C, respectively; membrane: P=0.0018 and P=0.0006 for 27°C and 43°C, respectively), while the amount of perinuclear RGS16 did not change significantly (Figures 20B, D and C). The overall expression remained homogenous, without relevant clustering or granulation (see Figure S10,

Supplementary Materials). In summary, both heat and cold exposure led to small but similar changes in RGS16 distribution, indicating a more general response to thermal zeitgeber signals.

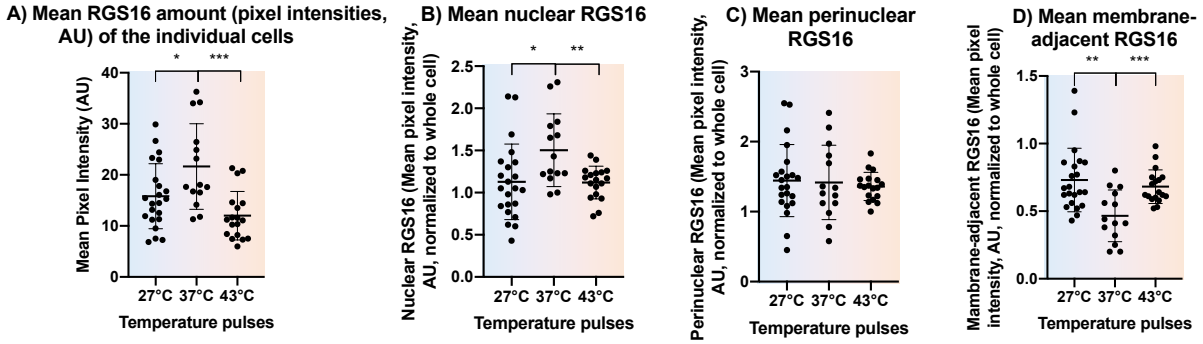

Figure 20: Immunofluorescence of GFP-stained RGS16 protein after temperature pulses of 27°C and 43°C for 4 h.
The cells were kept in 37°C and then exposed to the indicated temperatures for 4 hours. For A-C, the mean pixel intensities of the cells were calculated in FIJI and the distribution in the different areas relative to the whole cell was analyzed. Outliers were removed in Prism (ROUT = 1), statistical significance was determined via t tests and Mann-Whitney tests.
A) The amount of RGS16 (mean pixel intensity) of the cells was significantly lower after 4 h of 27°C and 43°C (P=0.0241 and P=0.0002, respectively).
B) The RGS16 concentration in the nucleus was significantly lower compared to the controls after being exposed to 4 h of 27°C and 43°C (P=0.0178 and P=0.0020, respectively).
C) The concentration in the perinuclear region showed no significant difference across the different conditions.
D) The amount of RGS16 that was located close to the membrane was increased after exposure to 4 h of 27°C and 43°C (P=0.0018 and P=0.0006, respectively).

3.2.2.3 Localization of RG16 in response to pharmacological stimulation of GPCRs

RGS16 is a regulator of G protein signaling and has been found in the cytosol and in the plasma membrane (Chen et al., 1999; Druey et al., 1999; Hiol et al., 2003; Osterhout et al., 2003). RGS proteins can change localization after expression and stimulation of GPCRs (Dulin et al., 1999; Leontiadis et al., 2009; Roy et al., 2003). Therefore, we hypothesized that RGS16 may change its localization in response to GPCR activation.

For investigating this, the localization of RGS16 was examined after the addition of ligands of $G_{i/o}$-coupled receptors: caffeine, N^6-cyclohexyladenosine (N-CHA), dopamine, and serotonin. After treatment with N-CHA and caffeine, the localization of their targeted Adenosine 1 receptor was determined in addition to RGS16, and the degree of colocalization was calculated. In addition to $G_{i/o}$, RGS16 also shows a preference for G_q proteins, so the G_q-coupled α1-adrenergic receptor agonist phenylephrine was also tested. Isoprenaline, which stimulates the G_s-coupled β-adrenergic receptor, was used as a negative control.

For this experiment, the U-2 OS cells were grown to semi-confluency and treated with 100 µM of caffeine (Abcam), N-CHA (Abcam), dopamine (Sigma-Aldrich), serotonin (Sigma-Aldrich), phenylephrine (Sigma-Aldrich), or isoprenaline (Sigma-Aldrich) as indicated for 5 min.

After the indicated treatments, the cells were fixed, permeabilized, and incubated with an anti-RGS16 GFP antibody (Figure 21A-G) and, after treatment with A1R ligands, simultaneously with an anti-A1R RFP antibody for immunofluorescence microscopy (Figure 21A-C).

A) Control

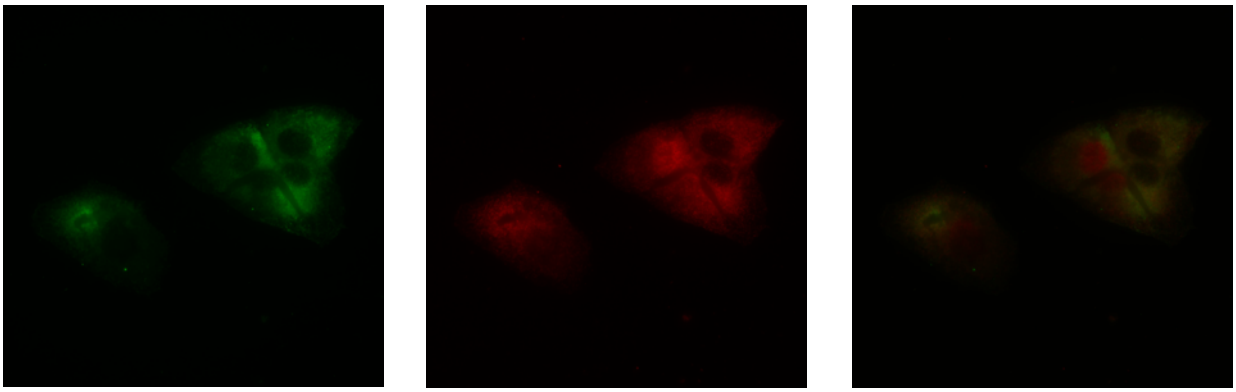

B) Caffeine

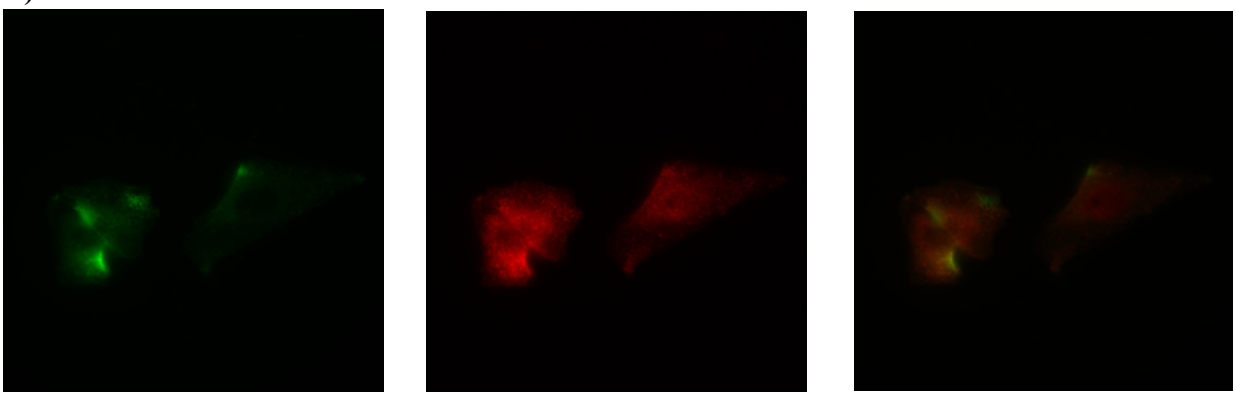

C) N-CHA

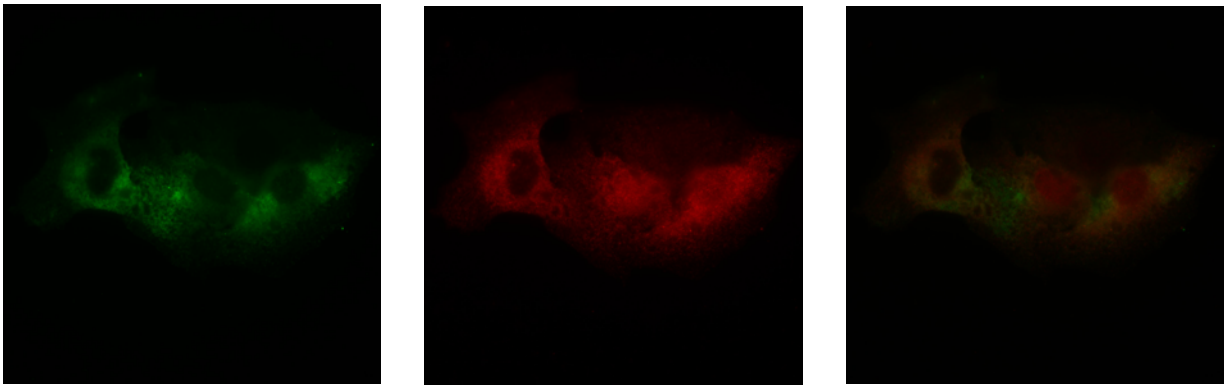

D) Dopamine **E) Serotonin**

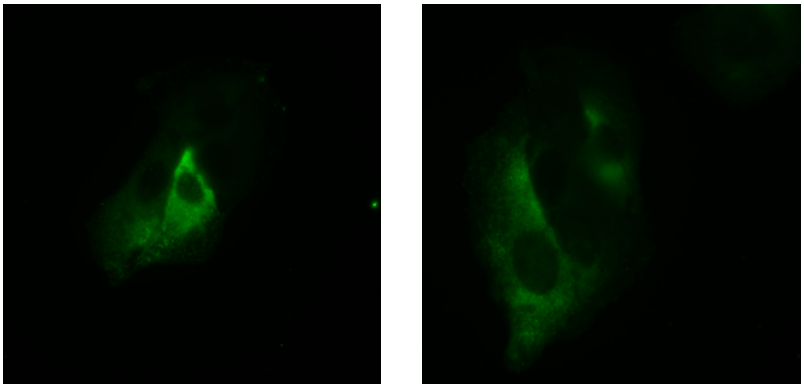

F) Phenylephrine **G) Isoprenaline**

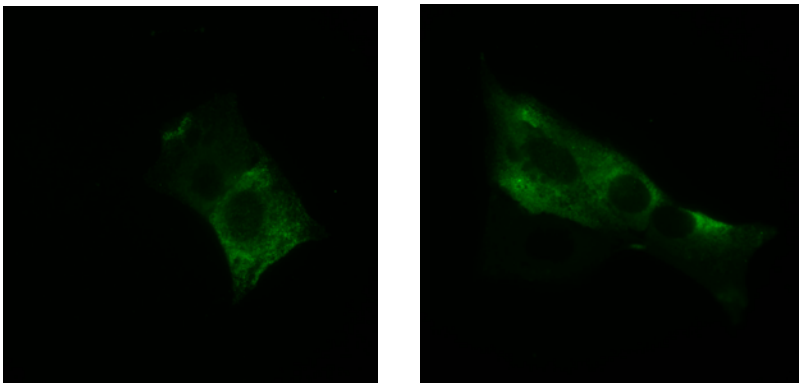

Figure 21: Immunofluorescence RGS16 (green, GFP) and A1R (red, RFP) after treatment with 100 µM of caffeine, N6-cyclohexyladenosine, dopamine, serotonin, phenylephrine, or isoprenaline as indicated for 5 min. Representative images were selected; the rest can be found in the supplementary materials.
A) Control; left to right: RGS16, A1R, overlay.
B) Treatment with caffeine; left to right: RGS16, A1R, overlay.
C) Treatment with N-CHA; left to right: RGS16, A1R, overlay.
D, E, F, G) Treatment with dopamine, serotonin, phenylephrine, and isoprenaline, respectively; RGS16 only.

When the cells were treated with caffeine, N^6-cyclohexyladenosine, dopamine, serotonin, phenylephrine, or isoprenaline, there were few changes in the amount of RGS16 in the different compartments (Figure 22A-C). Overall, most cells showed a homogenous signal distribution with the brightest signal in the perinuclear region. There was a small but significant reduction of RGS16 in the perinuclear region after the addition of caffeine or serotonin (P=0.0071 and P=0.0110, respectively) (Figure 22B). In these cells, there was also a shift towards a more polar expression pattern of the signal (see Figure S11, Supplementary Materials).

The Adenosine 1 receptor showed no significant change in distribution after treatment with caffeine or N-CHA (Figure 22G-I). The cells presented a homogenous signal distribution with no relevant clustering or bright spots (see Figure S11, Supplementary Materials).

Overall, the addition of GPCR ligands led to only small changes in RGS16 distribution and to no relevant changes in A1R distribution.

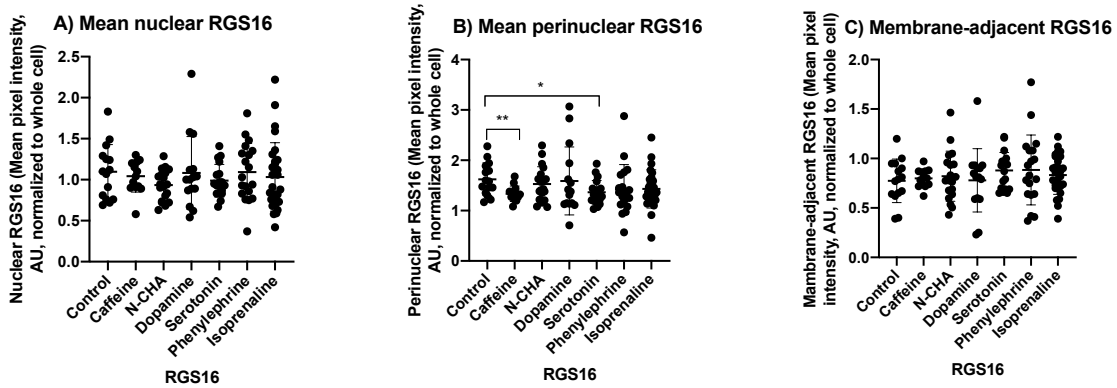

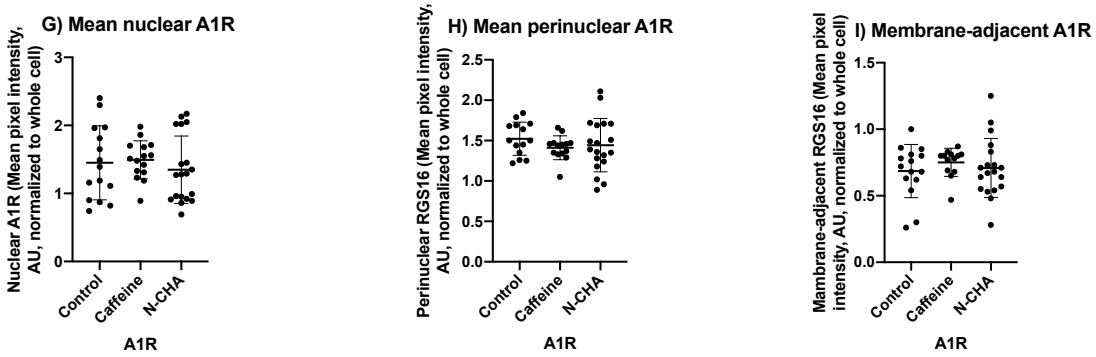

Figure 22: Immunofluorescence of GFP-stained RGS16 protein and RFP-stained A1R protein after treatment with 100 µM of caffeine, N6-cyclohexyladenosine, dopamine, serotonin, phenylephrine, or isoprenaline as indicated for 5 min.
For A-C and G-I, the mean pixel intensities of the cells were calculated in FIJI for GFP-stained RGS16 (top) and RFP-stained A1R (bottom) and the distribution in different compartments was analyzed. Outliers were removed in Prism (ROUT = 1), statistical significance was determined via t tests and Mann-Whitney tests.
A) There was no significant change in the amount of RGS16 in the nucleus after treatment with caffeine, N^6-cyclohexyladenosine, dopamine, serotonin, phenylephrine, or isoprenaline.
B) There was a significant reduction of RGS16 localized in the perinuclear region after treatment with caffeine and serotonin (P=0.0071 and P=0.0110, respectively).
C) There was no significant difference in the amount of RGS16 localized near the membrane after the indicated treatments.
D, E, F) There was no significant difference in A1R distribution after the addition of caffeine or N-CHA.

Further, it was analyzed how much RGS16 and the Adenosine 1 receptor colocalize after treatment with A1R ligands. For this, the Pearson's correlation coefficient (PCC) between GFP-stained RGS16 and RFP-stained A1R in the different regions was compared between treatment with caffeine or N-CHA vs. controls (Figure 23). Generally, the degree of correlation was very high, with both proteins being abundantly expressed, and did not change significantly when looking at the whole cell (Figure 23A). Only when analyzing the compartments separately, there were significant changes visible (Figures 23B-D). The administration of caffeine lead to a decrease in colocalization in the perinuclear and membrane-adjacent areas (P=0.0236 and P=0.0051, respectively), while the addition of N-CHA lowered the PCC in the nuclear region (P=0.0238). Generally, relative nuclear expression was higher for A1R than for RGS16, while the protein levels in the perinuclear and membrane-adjacent areas were comparable.

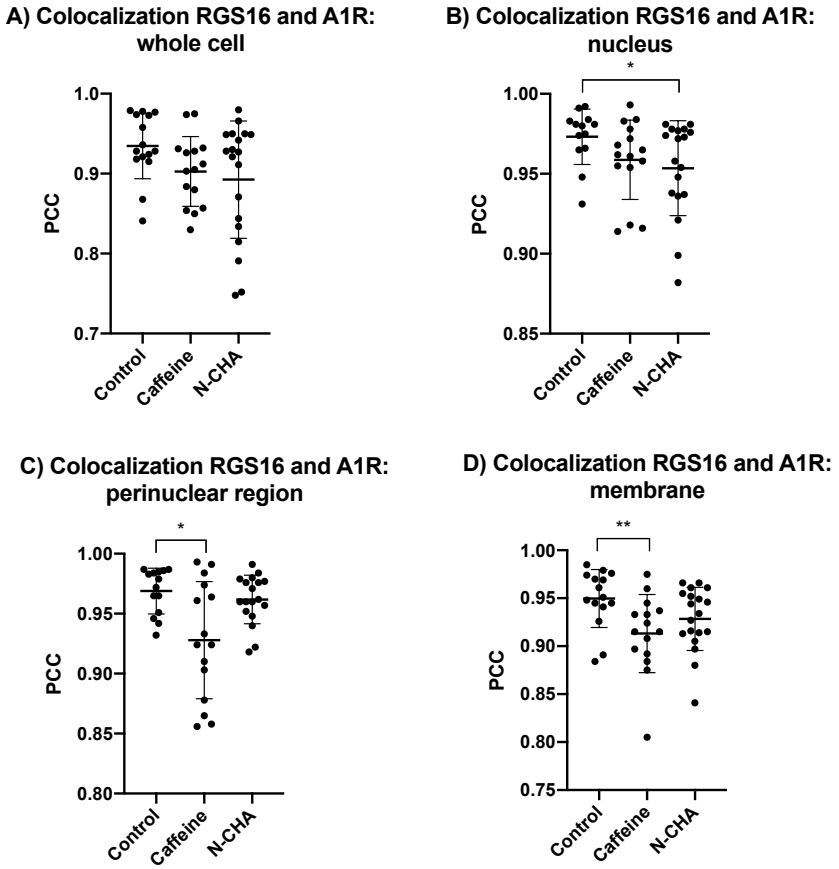

Figure 23: Pearson's correlation coefficient (PCC) of RGS16 and A1R localization after immunostaining with GFP and RFP after treatment with 100µM of caffeine or N6-cyclohexyladenosine for 5 min as indicated.
The images were imported in FIJI, and the Pearson's correlation coefficient was calculated for the separate regions. Outliers were removed in Prism (ROUT = 1), statistical significance was determined via t tests and Mann-Whitney tests.
A) The degree of colocalization did not differ significantly when the whole cells were analyzed.
B) When only the nuclear region was analyzed, there was no change in colocalization after the addition of caffeine, and less colocalization after the addition of N-CHA (P=0.0238).
C) When only the perinuclear region was analyzed, there was no change in colocalization after the addition of N-CHA, and less colocalization after the addition of caffeine (P=0.0236).
D) The same was true for the membrane-adjacent areas, where there was no change after the addition of N-CHA, but a decrease in colocalization after the addition of caffeine (P=0.0051)

In summary, the addition of caffeine led to a decreased amount of RGS16 in perinuclear areas; for A1R, there were no significant changes. The colocalization of RGS16 and A1R in the perinuclear and in the membrane-adjacent regions was decreased. The addition of N-CHA did not lead to any significant changes for either RGS16 or A1R, except for a small but significant decrease in their colocalization degree in the nuclear region.

3.2.3 Free-running period of *Bmal1* with and without a KD of RGS16 after the addition of caffeine

Caffeine has been shown to lengthen the circadian rhythm of behavior as well as cellular rhythms in mammals (Burke et al., 2015; Oike et al., 2011). As previously mentioned, it exerts its effect through the Adenosine 1 receptor by blocking the activation of $G_{i/o}$ by adenosine, thereby increasing the production of cAMP (Chen et al., 2013; Nehlig et al., 1992; Shryock et al., 1998). Since RGS16 acts on Gi-coupled receptors and has been shown to influence cAMP levels in the SCN as was described by Doi et al., we wanted to test whether the addition of caffeine has an effect of the period of U-2 OS cells in controls and in knockdowns, and whether the effect is additive to a knockdown of RGS16 (Doi et al., 2011). The selected *Bmal1* luciferase reporter cells with RGS16 shRNA (U2OS_RKD) were compared to controls transfected with the scrambled shRNA (U2OS_control) with and without the addition of 1mM caffeine to the medium (Figure 24).

The addition of caffeine and a KD of RGS16 both lengthened the free-running period of the cells significantly (P=0.0010 for caffeine vs. no caffeine, and P=0.0494 for KD vs. controls). The interaction factor was not significant (F (1, 46) = 0.001091, P=0.9173), suggesting that caffeine affects the period independently of a KD of RGS16.

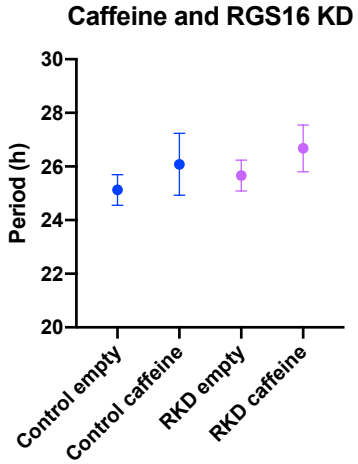

Figure 24: Free-running period on days 2 to 5 of a luciferase reporter of Bmal1 promoter activity of the selected U-2 OS cells in constant 37°C after synchronization with dexamethasone, with and without the addition of 1mM caffeine.
Shown is the RGS16 knockdown cell line (pink) vs a control cell line (blue).
The addition of caffeine lengthened the free-running period of the control cells (26.08 ± 1.154 h with caffeine vs 25.13 ± 0.5702 h without) as well as of the RGS16 KD cells (26.68 ± 0.8711 h with caffeine vs 25.66 ± 0.5776 h without). N=8 for Controls without caffeine, N=7 for KDs without caffeine, N=16 for Controls with caffeine, N=19 for KDs with caffeine.

3.2.4 RGS16 and cAMP signaling in U-2 OS cells

When RGS16 is expressed in the SCN, it allows for the rise of cAMP by antagonizing the inhibition of the adenylyl cyclase by G_i. Therefore, it is responsible for the cycling levels of cAMP in the SCN (Doi et al., 2011). cAMP is an important second messenger molecule that conveys many physiological functions, and many core clock genes have a CRE in their promoter region (Allen et al., 2017; Doi et al., 2011; Koyanagi et al., 2011; O'Neill et al., 2008). This could be a possible input pathway to the clock. We hypothesize that a similar mechanism to the one in the SCN is present in peripheral cells.

3.2.4.1 cAMP rhythms in U-2 OS cells

To test this hypothesis, baseline cAMP in U-2 OS cells were analyzed. So far, no clear circadian baseline rhythm of cAMP has been published in U-2 OS cells. U-2 OS cells stably transfected with the bioluminescent Promega GloSensor were obtained from a collaborating laboratory (O'Neill Laboratory). This system allows for real-time measurement of cAMP levels by a post-translational cAMP intramolecular complementation biosensor (firefly luciferase). The luminescence signal significantly decreases in higher temperatures, so the experiments were conducted in lower temperatures. Single-cell rhythms were assessed using real-time microscopy (Figure 25). Then, the overall rhythm of controls vs. KDs was assessed in the luminometer (Figure 27).

3.2.3.1.1 Single-cell real-time microscopy

To explore if there is a baseline cAMP rhythmicity in U-2 OS cells, the rhythm of individual cells was assessed by real-time microscopy (Figure 25). Images were taken every 2 h (examples shown in Figure 25B). About 62% of the single cells that showed luminescence signals over several hours were deemed rhythmic (Biodare; Classic JTK_Cycle test, cosine 2H, linear detrending, $p<0.05$, with Benjamini Hochberg correction). A period between 18 and 34 hours was called circadian, which was the case for 79% of the rhythmic cells. The average period was 25.88 ± 2.924 h (determined by FFT-NLLS after cubic detrending) (Figure 25A).

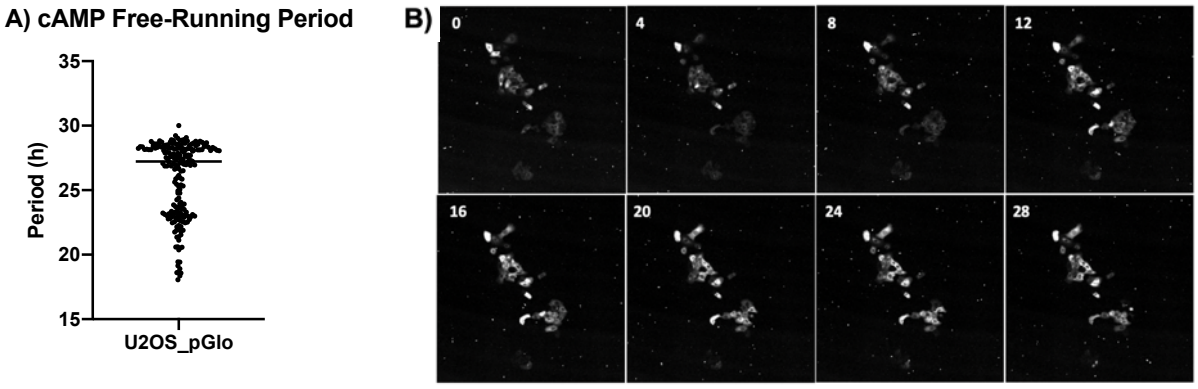

Figure 25: U-2 OS cells with a cAMP luciferase reporter (Promega GloSensor) in constant 30°C after synchronization with dexamethasone.
A) Free-running period of the cAMP rhythms in single cells. About 62% of the cells that showed luminescence signals over several hours were deemed rhythmic by the JTK_Cycle test. Of these, 79% showed a period between 18 and 34 h. The period of those was 25.88 ± 2.924 h, N=207.
B) Example of a time series of U2OS-pGlo in 30°C at time points 0, 4, 8, 12, 16, 20, 24, and 28.

3.2.4.1.2 Impairment of baseline cAMP rhythmicity in RGS16 KD cells

To determine if an abolition of RGS16 in peripheral cells leads to a loss in cAMP rhythms analogous to the SCN, baseline cAMP levels of RGS16 KD cells were compared to controls (U-2 OS-pGlo cells transfected with scrambled shRNA) to look for a change in rhythmicity (see Figure 27). The KD efficiency was 62% (Figure 26).

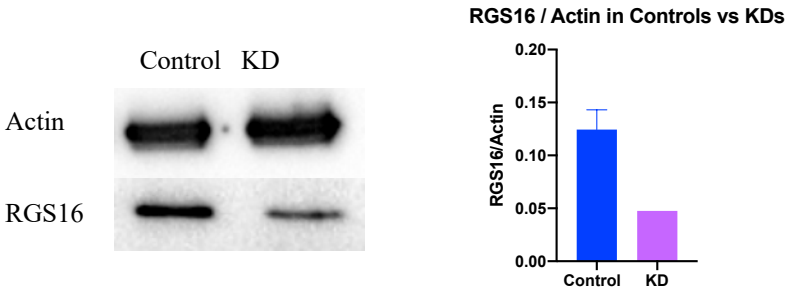

Figure 26: Western blot and bar graph showing the abundance of Actin and RGS16 in U-2 OS pGlo cells stably transfected with scrambled shRNA vs RGS16 shRNA to determine the KD efficiency, which was 62%.

The p-Glo transfected cells were seeded in medium containing dexamethasone and high concentrations of luciferin (1mM). Then they were recorded at 34°C in the luminometer. The first 2 hours, where the cells were acclimating to the conditions, were removed from the dataset. The following 72 hours of data were analyzed (Figure 27). The line graphs are shown in Figure 27B. A JTK_Cycle rhythmicity test was performed (Biodare; Classic JTK, cosine 2H, linear detrending, $p<0.05$ with Benjamini Hochberg correction) and confirmed rhythmicity for 100% of controls and 90% of KDs. The period was calculated for rhythmic wells via FFT-NLLS in Biodare (linear detrending). A period between 18 and 34 hours was considered circadian, which was the case for 58% of rhythmic wells in controls and 44% in KDs. Of these, the average

period was 28.80 ± 3.438 h for the KD cells compared to 24.31 ± 4.805 h in controls (P=0.0057) (Figure 27A). Therefore, a KD of RGS16 seems to lengthen the baseline cAMP rhythm in U-2 OS cells. There seem to be two clusters of cells; one with long and one with short periods (examples of each in Figures 27C-F).

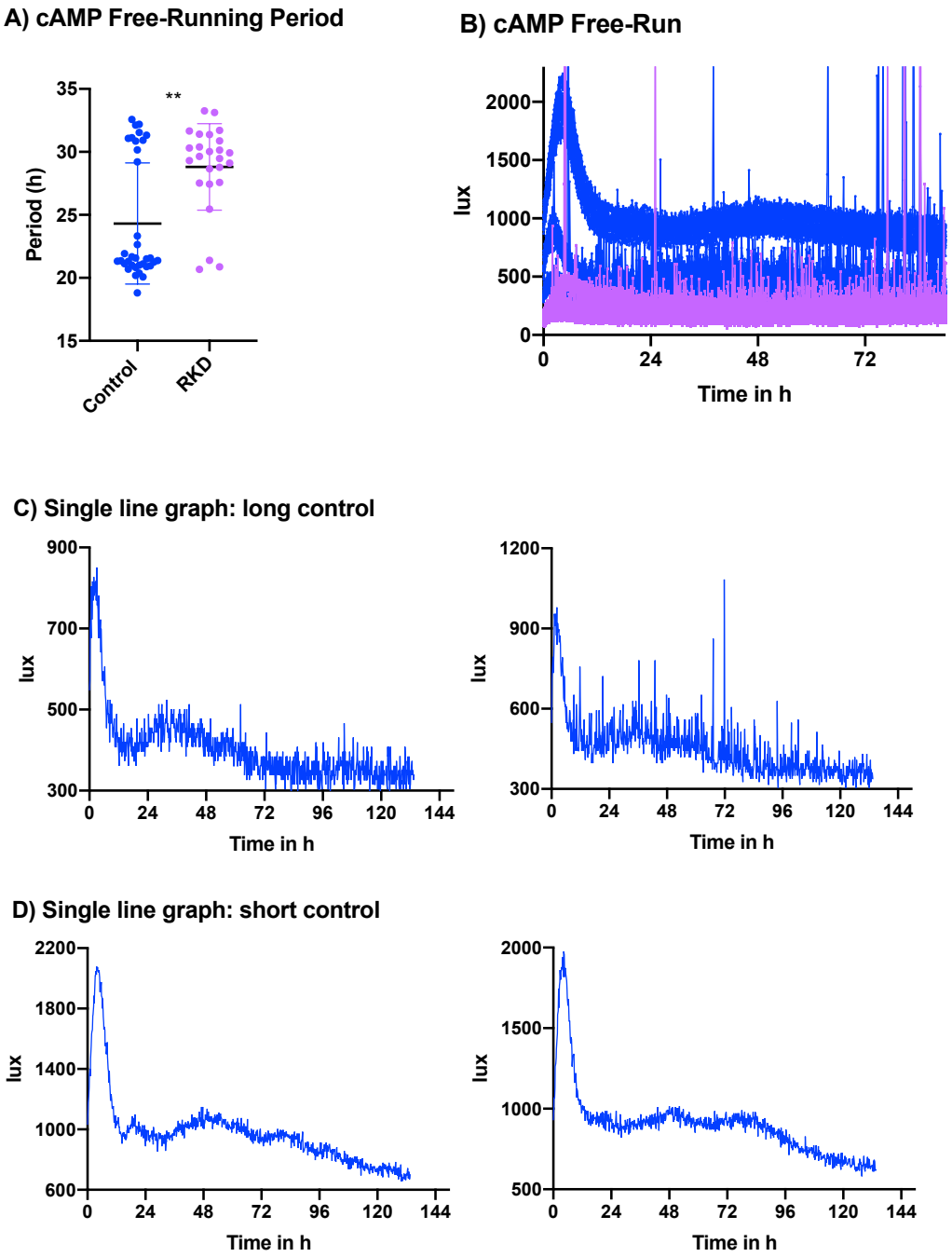

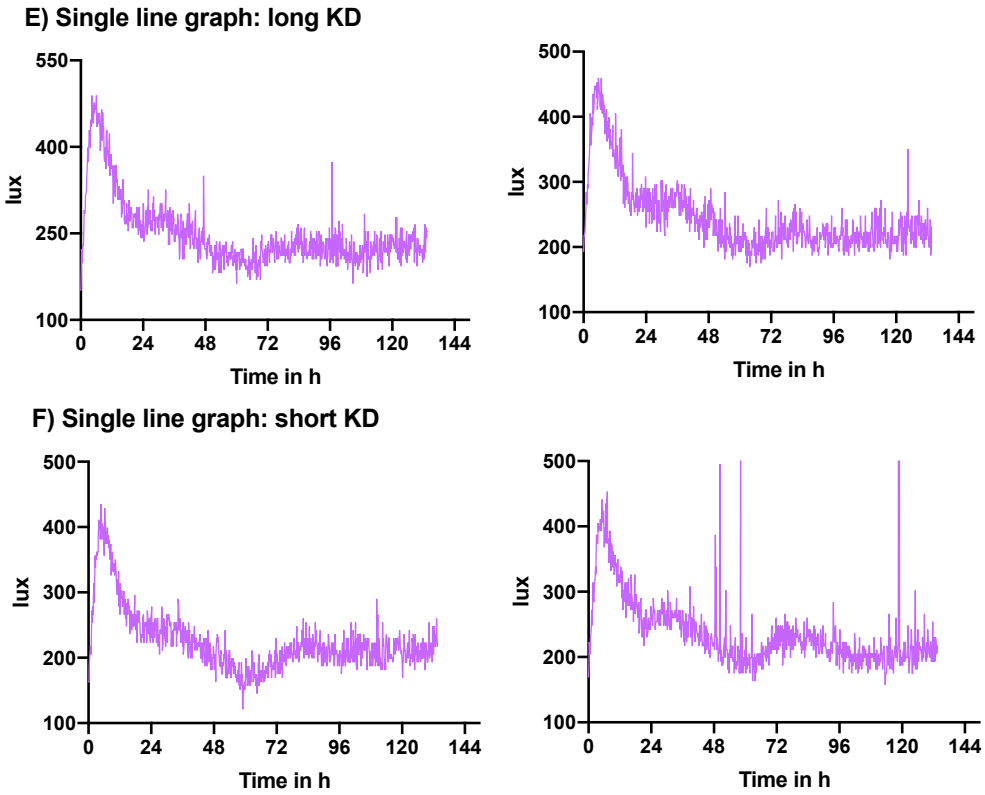

Figure 27: U-2 OS cells containing a cAMP luciferase reporter (Promega GloSensor) in constant 34°C after synchronization with dexamethasone.
Shown is the RGS16 knockdown cell line (pink) vs a control cell line (blue).
*A) The free-running period was 24.31 ± 4.805 h in the controls and 28.80 ± 3.438 h in the KD cells (P=0.0057), * significance determined by Mann-Whitney test. N=35 for controls and N=23 for KDs.*
B) Line graphs. N=60 for both cell lines.
C, D, E, F) 2 single line graphs each from the short and long period cluster.

3.2.4.1.3 Time-dependent cAMP response in the presence and absence of RGS16

Stimulating GPCRs that have been shown to activate pathways in which RGS16 is involved could help shed light onto the regulation of cAMP by RGS16 as well. A simplified model of what is known is shown below in Figure 28. G_i proteins modulate cAMP levels by regulating the activity of the adenylyl cyclase (AC), which produces cAMP (Taussig et al., 1993). When a G_i protein is activated (via activation of its GPCR), it inhibits the AC, thus lowering cAMP levels. RGS16 inactivates G_i proteins, therefore at times of high RGS16 expression, G_i is inactivated and can no longer inhibit the AC, which allows cAMP levels to rise (Bansal et al., 2007; Doi et al., 2011; Koelle, 1997). So, when an agonist of a G_i -coupled GPCR is added, cAMP levels should decrease. But when RGS16 is highly expressed, it should inactivate the activated G_i, so cAMP levels should not be greatly suppressed. When RGS16 is weakly expressed, it cannot inactivate G_i, so cAMP levels should be suppressed.

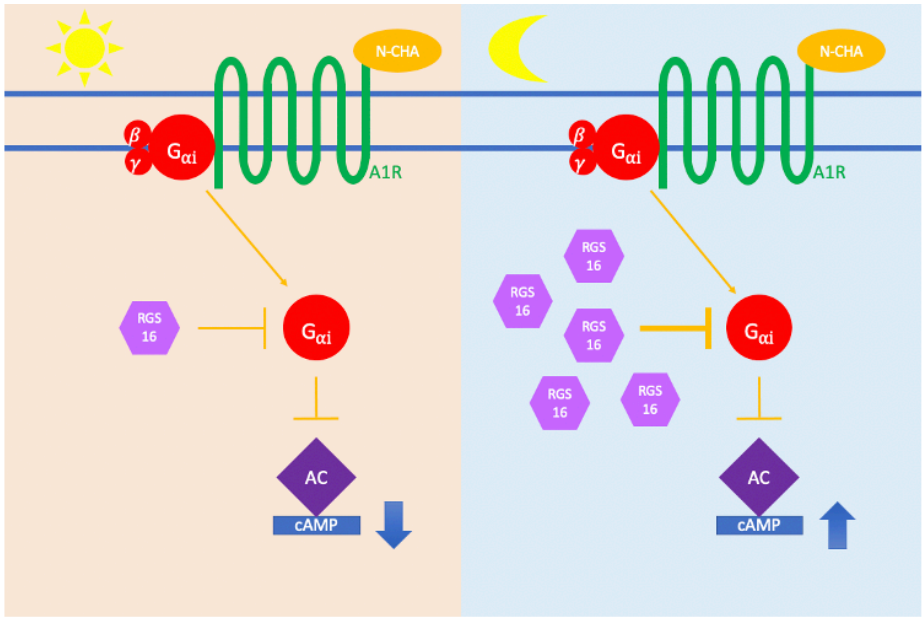

Figure 28: RGS16 involvement in GPCR signaling in U-2 OS cells depending on the time of day.
The selective Adenosine 1 receptor (A1R) agonist N^6-cyclohexyladenosine (N-CHA) binds the Adenosine 1 receptor. This leads to an activation of the G_i subunit, which inhibits the adenylyl cyclase (AC), which then produces less cAMP. RGS16 increases the GTPase-activity of the G_i subunit, thereby increasing GTP hydrolysis and ending the G_i signaling. Consequently, RGS16 activity increases cAMP levels. In these experiments, RGS16 levels were higher in the cold phase than in the warm phase, leading to a difference in cAMP levels after A1R stimulation depending on the time point in the cycling environment. At times of low RGS16 abundance (left), the cAMP suppression after N-CHA addition was higher, since there was less RGS16 to stop the G_i signaling after A1R activation. At times of high RGS16 abundance (right), there was less decrease in cAMP levels. A knockdown of RGS16 abolishes this time-of-day difference.

To test whether this is the case, U-2 OS cells containing the cAMP pGlo sensor system were stimulated at the peak and trough of RGS16 (as determined by the western blot time course, see Figure 16) with the selective A1R agonist N^6-cyclohexyladenosine (N-CHA) (Figure 29). It would be expected that the cAMP levels after addition of the agonist at the peak of RGS16 are higher than at the trough, because RGS16 allows cAMP to rise; therefore, cAMP levels should be in phase with RGS16 levels. When RGS16 is knocked down, this difference is expected to be decreased or gone.

The cells were seeded in 96-well-plates and entrained for 5 days in 34/37°C. Then they were stimulated at the peak and the trough of RGS16 abundance (at ExT 2 and ExT 14, respectively) with 50nM N-CHA, the controls were stimulated with serum-free medium, both on thermally controlled plates. Directly afterwards, luminescence was measured in the luminometer for 1 h in constant 30°C.

Two-way ANOVAs were performed for the fold change agonist/medium stimulation for the controls and for RGS16 KD cells for the peak vs. trough of RGS16 abundance (Figure 29).

There was a significant difference between the time points (Max. vs. Min levels of RGS16) in control cells (F (1, 6372) = 226.1, P<0.0001) (Figures 29A and B). In the RGS16 KD cells, this time-of-day difference was abolished and there was no significant difference between the two time points (F (1,3132) = 2.830, p=0.0926) (Figures 29C and D).

Further it could be observed that cAMP levels after addition of the agonist at the peak of RGS16 were higher than at the trough (Figure 29A). When RGS16 is highly abundant, N-CHA is less effective because RGS16 antagonizes its effect by hydrolyzing the N-CHA-activated G_i, thus cAMP is not decreased as effectively. Additionally, at the peak of RGS16, the difference between stimulation by medium vs. N-CHA is smaller (meaning the stimulated/control ratio is closer to 1) because RGS16 inactivates the activated G_i and lowers the response (Figure 29B). When RGS16 is knocked down, that time-of-day effect is gone and the response to the GPCR stimulation is the same at both times (Figure 29D).

Overall, this suggests that clock-regulated RGS16 protein levels influence the cAMP response to A1R stimulation.

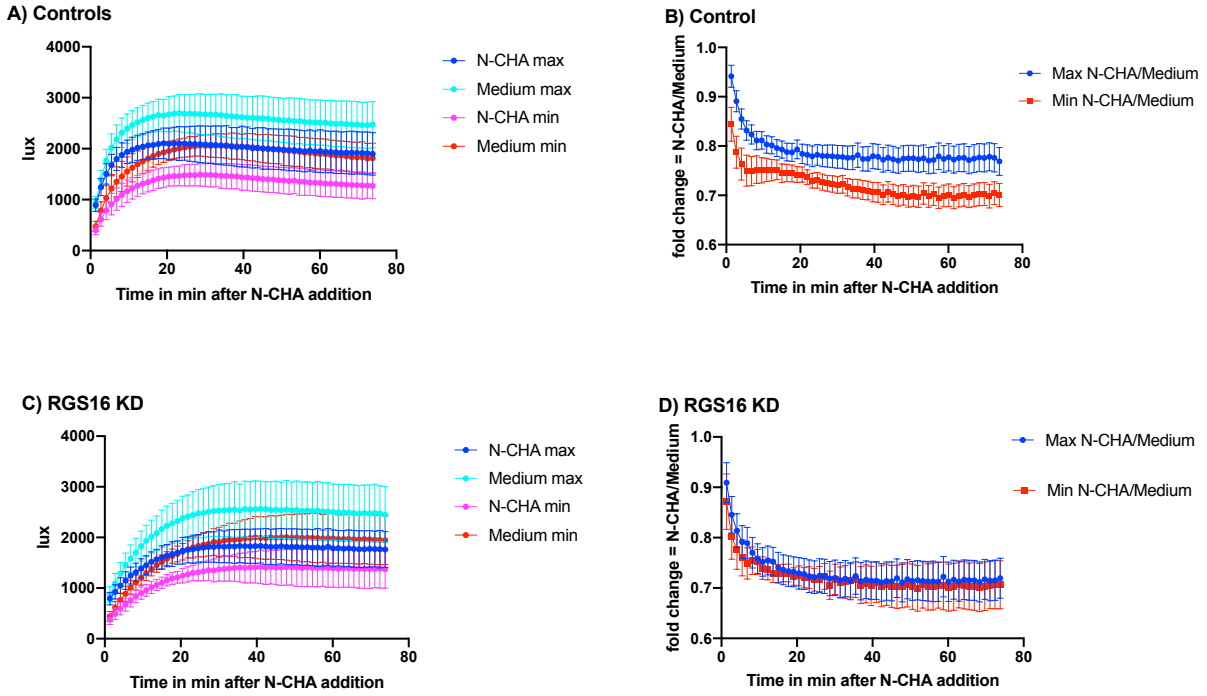

Figure 29: cAMP response depending on RGS16 levels.
U-2 OS cells containing a cAMP luciferase reporter (Promega GloSensor) were stably transfected with shRNA to create a RGS16 KD line. After 5 days of entrainment in 34/37°C in 12:12, both KDs and controls were stimulated with N-6 cyclohexyladenosine (N-CHA) vs. serum-free medium at the times of the peak and trough levels of RGS16 (ExT 2 and ExT 14, respectively).
A+B) Controls, N=60. C+D) RGS16 KDs, N=30. Max = peak of RGS16 (ExT 2, 8 h into the cold phase), Min = trough of RGS16 (ExT 14, 8 h into the warm phase). A+B) show cAMP levels directly following the stimulation (mean ± SD).
B+D) show the cAMP levels of cells stimulated with N-CHA / cAMP levels of cells stimulated with medium. There was a significant difference between the cAMP levels following the stimulations at times of high vs. low RGS16 abundance in controls in the factor Max. vs. Min levels of RGS16 in the two-way ANOVA (P<0.0001). In RGS16 KD cells, there was no significant time-of-day difference, (p=0.0926).

4. Discussion

RGS16 has been proposed to play a role in human chronotype (Hu et al., 2016; Jones et al., 2016; Lane et al., 2016). It regulates cAMP levels in the SCN and plays a role in the food-entrainable oscillator (Doi et al., 2011; Hayasaka et al., 2011; Huang et al., 2006; Pashkov et al., 2011). Thus, RGS16 is involved in the light as well as the food input pathways for the clock. RGS16 is a modulator of GPCR signaling and is ubiquitously expressed in the body. Therefore, we hypothesized that RGS16 function is important not only in the SCN and the liver, but has a generalized role in the clockwork of the circadian clock throughout the body. To determine if this is the case, the following questions were addressed:

1. What effect does a knockdown of RGS16 have on the molecular circadian clock in peripheral (non-SCN) cells, and is this a universal principle?
2. How does RGS16 interact with the circadian clock in peripheral cells?

4.1 What effect does a knockdown of RGS16 have on the molecular circadian clock in non-SCN cells, and is this a universal principle?

RGS16 was knocked down in U-2 OS and ARPE-19 cells containing a BMAL1 luciferase promoter fragment, and stable cell lines were created (one selected and one subcloned U-2 OS KD cell line and one selected ARPE-19 KD cell line, and the respective controls with scrambled shRNA constructs). Then, experiments to determine free-running period, phase of entrainment in several Zeitgeber conditions, and temperature compensation in free-run as well as in entrainment were performed.

In line with previous results, a knockdown of RGS16 impaired key circadian properties (Doi et al., 2011; Hayasaka et al., 2011). The knockdown cell lines show an impairment of the free-running period of the core clock gene *BMAL1* as well as an altered phase of entrainment across several conditions in U-2 OS and ARPE-19 cells. Both U-2 OS and ARPE-19 cells remain temperature-compensated after a KD of RGS16 in both free-run and entrainment.

4.1.1 A KD of RGS16 alters the free-running period

The free-running period was altered in both U-2 OS and ARPE-19 cell lines, but not always in the same way (see Figure 2). In the selected U-2 OS and ARPE-19 cells, the KD shortened the free-running period, while in the subcloned U-2 OS cells, the KD lengthened the period. Doi et al. reported a lengthening of the free-running period in RGS16 knockout mice in constant darkness (Doi et al., 2011). Hayasaka et al. on the other showed a shortening of the free-running period of RGS16 knockdown mice in constant darkness after entrainment (Hayasaka et al.,

2011). Both times, mice with the same genetic background were used, but while RGS16 was completely abolished in Doi et al.'s experiments, the KD efficiencies in Hayasaka et al.'s reports were less than 100% and differed between tissues. Therefore, a loss of RGS16 seems to generally impair circadian rhythms, but the direction seems to vary depending on the environment and experimental setup. The KD also had an opposing effect in the two U-2 OS cell lines that were used here, where there should be no variation in the genetic background either. The same U-2 OS BMAL1::Luc cell line was transfected with the same shRNA to knock down RGS16, and a single clonal cell line was examined, as well as a selected population of cells. The persistence of the shRNA within the cells was monitored by continuous GFP reporter expression. Besides different KD efficiencies, which were similar between the U-2 OS cell lines (60% in the selected U-2 OS cells, 63% in the subcloned U-2 OS cells, and 81.0% in the selected ARPE-19 cells), a 'trivial' explanation for the results in this work could be a changed protocol between the two sets of experiments. The subcloned cell line was tested first, then the phenotype began to decrease, so selected cell lines were created as a more reliable alternative. Then, a COVID-regulations-induced change in protocol was necessary to reduce the time spent in the laboratory. In the new protocol, there was no washing out of dexamethasone, and instead of seeding the cells one day prior to the experiment, they were directly seeded into the luminometry medium including dexamethasone, and measuring began immediately.

Another possibility could be the random selection of a clone exhibiting an especially long free-running period within the subcloned KD cell line, and a comparatively short phenotype in the controls. Kramer et al. showed that U-2 OS cells show a wide range of free-running periods, and even a single clone – when subcloned – yielded free-running periods ranging from 22 to 28 h (Nikhil et al., 2020). This means that even within the same population of cells, there can be very relevant selection effects when only single clones are used. It could be that either the whole population at this point showed a long FRP and the subcloned KD cell line was indeed representative of the average KD population at that time, or this particular clone exhibited an especially long FRP phenotype. Since this was the only surviving clonal cell line, this cannot be ruled out. The creation and comparison of several clonal cell lines could help to differentiate between these possibilities.

Overall, there are several explanations as to why the KD of RGS16 could show various and sometimes unexpected or inconsistent phenotypes. Since this has been shown before in mice, it seems likely that this is not unique to the cellular level. A rescue or overexpression experiment might be helpful to further explore the reasons for the inconsistent results between the cell lines.

4.1.2 A KD of RGS16 influences the phase of entrainment

4.1.2.1 The phase of entrainment in 12:12 cycles is impaired after a KD of RGS16

The phase of entrainment of the center of gravity of the BMAL1 promoter expression also showed differences after a KD of RGS16 (see Figure 3). As was the case for the free running period, the changes in phase did not go in the same direction in all cell lines. While in the selected U-2 OS cell line the KD cells were entraining to a later phase compared to controls, the subcloned U-2 OS KD cells showed an earlier phase. In the selected ARPE-19 cell line, the KD cells were entraining to a later phase, but the difference was not statistically significant. Doi et al. reported a normal 24 h rhythm of RGS16 knockout mice in entrainment, with unchanged responses to light pulses (Doi et al., 2011). However, Hayasaka et al. showed a difference in food-anticipatory activity in RGS16 KD mice under entrainment in a protocol with restricted feeding (Hayasaka et al., 2011). This suggests that RGS16 plays a role in entrainment, but not in all circumstances.

For a long time, it was assumed that a longer free-running period is associated with a later phase of entrainment, while a system that produces a shorter free-running period is expected to show an earlier phase of entrainment (Brown et al., 2008; Duffy & Wright, 2005; Granada et al., 2013; Hoffmann, 1969; Merrow et al., 1999; Vanselow et al., 2006). However, the opposite was observed in these experiments. The selected U-2 OS cells showed a shorter free-running period and a later phase of entrainment. In the subcloned U-2 OS cell line, a longer free-running period and an earlier phase of entrainment were observed. In ARPE-19, the period was shorter, and the phase showed a non-significant trend towards a later phase. We explored entrainment further in order to understand the complex relationship between period and phase in RGS16 knockdown cells.

4.1.2.2 A KD of RGS16 leads to differences in entrainment in different T cycles, thermoperiods and Zeitgeber strengths

RGS16 KD cells generally showed strong signs of temperature-sensitivity and masking. To further investigate the robustness and limits of the system regarding the phase, experiments with different T cycles, thermoperiods and zeitgeber strengths were performed (see Figures 4-10). Changing the structure of the entraining cycle can reveal otherwise masked signs of entrainment (Olmedo et al., 2012).

When the zeitgeber cycle length was shorter than the internal “day” of the cells, the phases of all cell lines got later, as was expected (see Figures 4-6). Especially the subcloned U-2 OS cells, which were tested in T cycles of between 12:12 (24 h) and 8:8 (16 h), yielded interesting results

(see Figure 5). With an intrinsic period of around 24 h, it is generally assumed that humans cannot entrain to extremely long or short cycles (Aschoff, 1960; Bruce, 1960). Therefore, it is possible that cycles of 8:8, meaning a daylength of 16 h, lie out of the range of entrainment of the human U-2 OS cells. Interestingly though, when graphing the phase according to real vs. modulo tau (24/T; the internal clock in relation to the zeitgeber cycle), both KDs and controls show a similar pattern of advance of the phase in longer T cycles, showing that they systematically entrain to the imposed short T cycles. Extreme cycle lengths such as this are usually not assessed, so there is limited understanding of under which conditions human cells can entrain to such short cycles. This may highlight features that groups of cells contribute to organismal clock properties. The parts of the clock have a wider range of entrainment versus the organism as a whole. This hypothesis would benefit from testing in other cell lines.

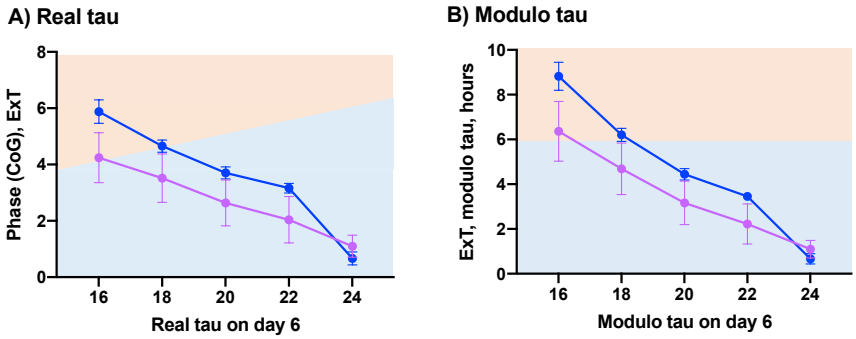

Figure 30: Real and modulo (24/T) tau of the phase of the Center of Gravity of Bmal1 promoter activity in the subcloned U-2 OS cell line in different Zeitgeber (T cycle) lengths in 34/37°C as indicated.
Shown is the phase with mean and SD for the RGS16 knockdowns (pink) vs the controls (blue) for the different cell lines. Time point 0 indicates mid-cold (External time). Outliers were removed by Prism (ROUT = 1).

Further, there was a systematic advance in phase in KDs compared to controls. This was unexpected again, since the subcloned KDs showed a longer free-running period than the controls, suggesting a "slower" internal clock, and therefore one would expect a delay in the phase of entrainment. In 12:12, however, the KDs did entrain to a later phase than the controls in this experiment. This is opposing the earlier findings that the phase of entrainment was earlier with a KD of RGS16 in the subcloned cell line. For this (older) T cycle experiment, 34/37°C was used as a zeitgeber and cells were seeded one day prior to changing the medium and recording, while in the later experiments, a cycle of 35.5/38.5°C was used and the experiments were immediately started after seeding.

In the selected U-2 OS and ARPE-19 cells, the results were less systematic, with the phase of entrainment varying depending on the day analyzed and the cell line that was tested. However,

there was only a limited number of T cycles tested, and ARPE-19 generally had a low well number across all experiments.

A special case of T cycles are the ones where the external zeitgeber cycle is a harmonic of the FRP. This is where frequency demultiplication can occur, where both the innate internal as well as the imposed external rhythms show up. When looking at 6:6 cycles, frequency demultiplication was visible in KDs as well as controls, though generally the controls showed a more persistent internal 24 h rhythm, while the 24 h rhythm of the KDs seemed to be almost overridden by the external 12 h rhythm, even in a low-amplitude zeitgeber cycle, suggesting a decreased robustness of the circadian clock in RGS16 KD cells (see Figure 7). Further, the KDs were more driven by the transitions; cold led to an increase, warm to a decrease in signal. When this effect leads to a change in the apparent phase of entrainment and obscures the real effect of the circadian clock, this phenomenon is called ‘masking’. To determine which effects are from ‘real’ transitions and which are simply temperature effects, one can modify the entraining input, for example by varying the lengths of the cold and warm phases, or ‘thermoperiods’, without changing the overall cycle length, or by exposing the cells to different zeitgeber strengths (Olmedo et al., 2012).

When looking at different thermoperiods, the center of gravity of both U-2 OS and ARPE cells moved closer to the cold-warm transition and further away from the warm-cold transition in cycles with shorter cold phases (see Figures 8 and 9). In both cell lines, the KDs entrained to later phases in long and moderate “nights”, while they showed an earlier phase than controls in short “nights”. There is a progression in the distance of the center of gravity from the cold-warm transitions in both U-2 OS and ARPE cells, indicating a dynamic adaptation, so the phase does not seem to be simply masked by the temperature changes.

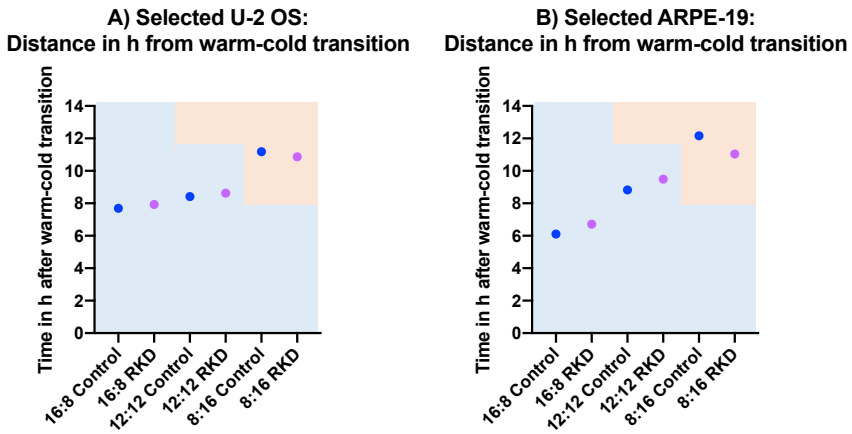

Figure 31: Distance (in hours) of the phase of the Center of Gravity of Bmal1 promoter activity from the warm-cold transition for the different cell lines in different thermoperiods in 35,5/38,5°C as indicated.
Shown is the phase with mean and SD for the RGS16 knockdowns (pink) vs the controls (blue) for the different cell lines. Time point 0 indicates mid-cold (External time). Outliers were removed by Prism (ROUT = 1).
A) U-2 OS cells.
B) ARPE-19 cells.

In cycles with reduced zeitgeber strength, namely a decreased amplitude in the temperature cycles, the KDs reached their stable phase of entrainment faster than controls (see Figure 10). This could be due to a weaker oscillator or to an alteration of the strength and function of the zeitgeber signaling pathway. Since there is no clear and systematic change in the FRP in the KDs and they also show differences in entrainment, it is unlikely that it is simply a weaker oscillator, but more likely an input pathway modification.

4.1.3 U-2 OS and ARPE-19 cells are still temperature-compensated after a KD of RGS16 in both constant and cycling conditions

When temperature-compensation in a circadian system is assessed, usually only the free-running period is taken into account. A slightly modified Q_{10} (the rate of chemical or biological change over 10°C) is calculated by comparing the period at the highest and lowest temperatures. Here, highest and lowest temperature need to be switched as a longer free-running period indicates a slower biochemical process. In most biochemical reactions, the Q_{10} lies around 2-3, while it stays around 1 over a range of physiological temperatures in temperature compensated systems (Avery, 1974; Sweeney & Hastings, 1960). A $Q_{10} < 1$ is termed over-compensation (the period increases in higher temperatures), a $Q_{10} > 1$ under-compensation (the period increases in lower temperatures).

In these experiments, both U-2 OS and ARPE-19 cells remained temperature-compensated, even after a KD of RGS16, even though the KDs showed a trend towards under-compensation in U-2 OS cells (see Figure 11).

Since the standard formula for the Q_{10} only considers the highest and the lowest temperature, an alternative calculation using a non-linear fit was applied as well with comparable results (see Supplementary Materials, 7.1.3). Additionally, the Q_{10} of the longest vs. shortest free-running period was looked at. In most cases, this, too, yielded similar results (see Table 3).

The phase of entrainment is usually not looked at through the lens of temperature compensation. However, as long as the dataset is transposed to +24 to include only positive values, Q_{10} calculations can be performed to gain insights into temperature compensation in cycling conditions. Here, comparing earliest vs. latest phase in addition to highest vs. lowest temperature gives a more accurate picture, since the phase was later in both high and low

temperatures, which is not adequately represented by the linear calculation of the Q_{10} (see Figure 12 and table 5). When comparing the results of the phase calculations with the raw data (shown in Figures 4-6 in the Supplementary Materials), this seems to be adequate and not a masking effect. It could also be observed that both KDs and controls did not always follow the long-assumed rule that longer periods correlate with later phases and that shorter periods correlate with earlier phases (Hamblen-Coyle et al., 1992; Rémi et al., 2010). Especially the ARPE-19 cells showed the opposite behaviour, demonstrating a shorter period and later phase of entrainment in high and low temperatures in controls as well as KDs. In the selected U-2 OS cells, the later phase in high and low temperatures was congruent with the longer free-running period in low temperatures in both controls and KDs, but not with the shorter period in high temperatures in the KDs. The subcloned U-2 OS cells exhibited a later phase in high and low temperatures in both controls and KDs, but the controls showed an over-compensation in period with a shorter period in cold temperatures and a longer period in high temperatures, and vice versa in the KDs. This adds to the growing amount of evidence that earlier phases do not necessarily correlate with shorter periods, and vice versa (Lee et al., 2017). Since RGS16 seems to be involved in the zeitgeber input pathway, it could play a role in this mechanism.

When comparing KDs with controls, there were also significant differences (see Figure 14). In lower temperatures, the KD lengthened the period compared to controls in both U-2 OS cell lines, and the KDs were under-compensated compared to the controls. In ARPE-19 cells, interestingly, the KD cells seem to be slightly better compensated than the controls.
The phases seem to be well compensated in physiological temperatures in both U-2 OS and ARPE-19 cells. In low and especially in high temperatures, however, the cells, especially the KDs, seemed to be less well compensated and showed a later phase of entrainment than controls.
In summary, the KD cells showed a longer free-running period and sometimes a later phase of entrainment in low temperatures. In moderate temperatures, the phase was well-compensated across all cell lines, even when the period was not. In high temperatures, the effect of the KD on the free-running period differed across the cell lines, while the phase was always later in KDs than in controls.

4.1.4 Summary: A KD of RGS16 impacts key circadian properties

Overall, a knockdown of RGS16 resulted in a variety of changes in circadian properties in both U-2 OS and ARPE-19 cells, implying a less specific and more generalized role in clock

processes. The changes were not always systematic and consistent within the same cell type, so the effects seem to be dependent on the environment and circumstances. Overall, the biggest changes were observed in relation to temperature sensitivity, suggesting that a KD of RGS16 leads to a less robust clock and to alterations in the zeitgeber signaling pathway.

4.2 How does RGS16 interact with the circadian clock in peripheral cells?

As opposed to SCN cells, little is yet known of how RGS16 interacts with the molecular clock in peripheral cells. Therefore, a number of experiments was conducted to determine the abundance and localization of RGS16 over the time of day, its localization in response to temperature pulses and to GPCR stimulation, and the relationship between RGS16 and cAMP.

4.2.1 There are fluctuations in RGS16 abundance over the time of day

First, western blot time courses in constant and cycling conditions were performed with U-2 OS cells. The RGS16 levels were normalized to actin or vinculin, which are both considered relatively stable over the day and thus serve as control proteins for normalization.

There was a change in RGS16 peak and trough levels after synchronization with dexamethasone, and also in the time course in entrainment, with a peak at ExT 2 (8 h into the cold phase) and a trough at ExT 14 (8 h into the warm phase) (see Figures 15 and 16).

A free-running rhythm of RGS16 mRNA and protein in the mouse SCN in constant darkness after entrainment has been shown by Doi et al., with a peak 4 h into the day and a trough 4 h into the night (CT 4 and CT 16, respectively, with CT 0 representing the subjective onset of daytime) (Doi et al., 2011). Hayasaka et al. reported a diurnal expression of RGS16 protein and mRNA as well, with high protein levels 5 h into the day (ZT 5) and low levels 5 h into the night (ZT 17) in the SCN, while RGS16 mRNA in the liver peaked 11 h into the day (ZT 11) and showed a trough 11 h into the night (ZT 23) (ZT 0 was defined as the beginning of the light phase) (Hayasaka et al., 2011). Therefore, there are rhythms in RGS16 levels, but the timing of the peak seems to depend on the tissue that was being analyzed.

4.2.2 RGS16 localization changes over the time of day and in response to temperature pulses

Changes in spatiotemporal distribution of proteins can be a way of modifying signaling by exposing or limiting interaction partners. RGS16 has been shown to be present in the cytosol, but it has also been found in the membrane (Chen et al., 1999; Druey et al., 1999; Hiol et al., 2003; Osterhout et al., 2003). Therefore, it was hypothesized that its localization may show

circadian fluctuations. RGS16 was localized primarily in the cytoplasm, as was expected from previous reports (Chatterjee & Fisher, 2000). However, there were some small changes in RGS16 levels and localization to different subcellular areas across the different time points. The RGS16 signal in membrane-adjacent areas appeared to be antiphasic to nuclear and perinuclear levels. The peak RGS16 levels were observed at ExT 2 in the western blot (see Figure 16), which coincides with peak nuclear and perinuclear expression, but interestingly not with peak overall signal intensity in the immunofluorescence time course. There, the peak of signal intensity was at ExT 6. This discrepancy could be due to technical differences between western blot and immunofluorescence. For example, antibody-binding epitopes can be differently exposed by the different preparation methods, and protein levels in the western blot are normalized to control proteins, while the IF signal is averaged across individual cells, where U-2 OS cells show a wide range of cell sizes. To account for this, intracellular analyses were performed comparing ratios of compartment to the whole cell instead of absolute pixel values. Since the microscope used was not a confocal microscope, the exact definition of areas as nuclear and perinuclear is somewhat limited, and regions defined as nuclear may contain overlays of the cytosolic signal above and below. This could explain the comparable changes seen in the areas deemed nuclear and perinuclear. Perinuclear in this context describes the wider cytoplasmatic area 75 pixels around the nucleus.
Overall, the results suggest that the circadian clock influences RGS16 distribution within the cells.

As RGS16 has been shown to be upregulated following heat stress, we hypothesized that it may be part of the cellular response to temperature changes and therefore might change localization in response to heat or cold exposure (Seifert et al., 2015). When the U-2 OS cells were exposed to cold and heat pulses, there were small changes in RGS16 distribution (see Figure 20). Here, again, nuclear and membrane-adjacent signaling levels showed opposing behaviour, indicating a translocation of RGS16 from the nucleus to the membrane-adjacent areas after cold and heat exposure, suggesting a more general response to thermal signals.

4.2.3 RGS16 localization changes slightly after G_i-coupled GPCR stimulation

RGS16 is a regulator of G-protein signaling and can bind $G_{i/o}$ as well as G_q (Masuho et al., 2020). Since some RGS proteins have been shown to change localization after GPCR expression and binding, we hypothesized that RGS16 may also change localization in response

to GPCR stimulation, which in turn can be under circadian regulation (Dulin et al., 1999; Leontiadis et al., 2009; Roy et al., 2003).
The following ligands of GPCRs were tested: caffeine, N^6-cyclohexyladenosine (N-CHA), dopamine, serotonin, phenylephrine, and isoprenaline (see Figures 21-23).

The $G_{i/o}$ -coupled Adenosine 1 receptor (A1R) has been shown to be involved in the circadian clock, sleep and light input pathways, and the administration of the selective A1R agonist N-CHA led to a reduction of light-induced phase delays in mice (Jagannath et al., 2021; Sigworth & Rea, 2003). Caffeine is a known antagonist to the A1R and has been shown to lengthen the circadian rhythm of behavior as well as cellular rhythms in mammals (Burke et al., 2015; Oike et al., 2011). A1R localization and colocalization with RGS16 were also assessed after the administration of the two ligands. In these experiments, the addition of caffeine led to a small change in RGS16, but not A1R signal distribution, while N-CHA did not have any relevant effect on either RGS16 or A1R localization. Both ligands led to small but significant decreases in colocalization in the different subcellular areas.

Dopamine and serotonin also bind with highest affinity to G_i-coupled receptors, the D_2-like dopamine receptors, and the 5-HT_1 (serotonin) receptors, so they are often used for G_i stimulation experiments (Ghavami et al., 2004; Hiol et al., 2003; Masuho et al., 2015; Osterhout et al., 2003; Von Moo et al., 2022). Both dopamine and serotonin have been shown to be intertwined with the clock network on several levels, so an effect of RGS16 through these receptors is possible (Cagampang & Inouye, 1994; Ciarleglio et al., 2011; Le et al., 2024). However, their ligands both had only very small effects on RGS16 distribution.

RGS16 also shows a preference for G_q proteins, so phenylephrine, which primarily activates G_q-coupled α1-adrenergic receptors, was tested as well (Ladds et al., 2007; Masuho et al., 2020; Soundararajan et al., 2008). Phenylephrine has been mainly studied in regards to vasoconstriction, where its administration led to different responses depending on the time of day (Denniff et al., 2014; Görgün et al., 1998). Its effect on RGS16 signal distribution was very small and not significant.

Additionally, RGS16 localization in response to isoprenaline, which stimulates the G_s-coupled β-adrenergic receptor, was assessed. This receptor is not directly associated with RGS16, so its

stimulation served as a negative control (Druey et al., 1999). The addition of isoprenaline did not have any relevant effect on RGS16 localization.

Overall, the addition of GPCR ligands led to only small changes in RGS16 distribution and to no relevant changes in A1R distribution.
When looking at the degree of colocalization of RGS16 and A1R via Pearson's correlation coefficient (PCC), it could be observed that both proteins showed a rather high and mainly even cytosolic expression pattern, thus the degree of correlation was generally very high (see Figure 23). A1R showed higher relative nuclear expression than RGS16, while both proteins showed similar levels of perinuclear and membrane-adjacent localization relative to their overall expression. After stimulation with caffeine or N-CHA, the colocalization was not significantly different when looking at the whole cells, but when the compartments were analyzed separately, small but significant changes became apparent. Caffeine led to a decreased colocalization in the perinuclear and membrane-adjacent areas, while N-CHA decreased the colocalization degree in the nucleus. Interestingly, when the degree of correlation changed after the addition of the ligands, it decreased rather than increased.

To summarize, GPCR stimulation led to only minimal changes in RGS16 and A1R (co-)localization and there was no visible clustering or recruitment to specific regions for either ligand or receptor. However, for these experiments, the U-2 OS cells were treated with the agonists as indicated for 5 min. GPCR stimulation and GTP hydrolysis occur within a few seconds and less, but protein localization changes can be observed even after several minutes to hours (Burgon et al., 2001; Chidiac & Roy, 2003; Dulin et al., 1999; Leontiadis et al., 2009; Psifogeorgou et al., 2007; Ross & Wilkie, 2000). It could be possible that visualization after a shorter treatment time could lead to bigger effects.

In conclusion, while RGS16 presents a mainly cytosolic expression overall, it shows antiphasic (peri-)nuclear vs. membrane-adjacent expression patterns over the day and a translocation from the nucleus to membrane-adjacent regions after cold and heat exposure. More membrane-adjacent localization of RGS16 could in turn lead to faster activation after GPCR stimulation at different times of day, which itself does not seem to play a major role in RGS16 localization.

4.2.4 The effect of caffeine on the free-running period in U-2 OS cells is additive to a KD of RGS16

Caffeine has been shown to lengthen the free-running period on a behavioural as well as on a cellular level (Burke et al., 2015; Oike et al., 2011). To test whether the effect of caffeine was additive to a KD of RGS16, the free-running period was calculated for KDs and controls with and without caffeine. It was observed that both the KD and the addition of caffeine lengthened the free-running period in this experiment, and the effect was additive (see Figure 24). Here, the free-running period of the selected U-2 OS cells with the KD was longer than in controls. The cells were seeded the day before the experiment, and the dexamethasone was removed. This was analogous to the old protocol for the subcloned U-2 OS line which had resulted in a lengthening of the period as well. The effect of caffeine and the KD being additive suggests that they both act in a different way on modifying the period.

Caffeine elevates cAMP levels via the Adenosine 1 receptor by blocking the activation of $G_{i/o}$ by adenosine, thereby indirectly increasing the production of cAMP (Burke et al., 2015; Chen et al., 2013; Nehlig et al., 1992; Shryock et al., 1998). Further it has also been shown to competitively inhibit phosphodiesterase enzymes which degrade cAMP, also leading to elevated cAMP levels (Nehlig et al., 1992). RGS16 KD cells showed lower cAMP levels in other experiments (see Figure 27). RGS16 facilitates the hydrolysis of G_i once it has been activated, and thus increases cAMP levels indirectly as well. Since there should be no specific activation of G_i by the addition of caffeine, RGS16 should not be directly involved in caffeine-induced signaling cascades. As caffeine elevates overall cAMP levels and a KD of RGS16 lowers them, they do not act competitively.

4.2.5 The relationship between RGS16 and cAMP

Since RGS16 has been shown to act through modifying cAMP levels in the SCN, a number of experiments were conducted to explore the relationship between RGS16 and cAMP in peripheral cells (Doi et al., 2011). cAMP itself can then feed back on the clock, for example through CREs (cAMP-response elements) in promoter regions of core clock genes (Allen et al., 2017; Doi et al., 2011; Koyanagi et al., 2011; O'Neill et al., 2008).

4.2.5.1 Detection of free-running cAMP::luciferase rhythms in U-2 OS cells via single-cell live microscopy

So far, there have only been hints about circadian cAMP rhythms in U-2 OS cells, but a clear circadian rhythm has not been shown. Therefore, cAMP reporter cells were assessed via single-cell real-time luminescence to determine if there were any discernible baseline cAMP rhythms in the circadian range (see Figure 25). About 62% of the single cells that showed luminescence signals over several hours were deemed rhythmic by the JTK_Cycle test. Of these, 79% had a circadian period between 18 and 34 hours. The period of these cells was 25.88 ± 2.924 h. Thus, there are indications that there is in fact a baseline circadian cAMP rhythm in U-2 OS cells. However, the experiments had to be carried out in 30°C since the reporter is very sensitive to temperature and higher levels lead to a dramatic decrease in reporter signal.

4.2.5.2 A KD of RGS16 leads to a lengthening of free-running cAMP levels in U-2 OS cells

The cAMP reporter cells were measured in the luminometer to see if it is possible to detect any baseline circadian cAMP rhythms there, and to analyze the effect of a KD of RGS16 on baseline cAMP levels (see Figure 27). In this experiment, 100% of control and 90% of KD wells were deemed rhythmic. 58% of the rhythmic controls and 44% of the rhythmic KDs had a period between 18 and 34 h and were thus considered circadian. Of these, the average period was 28.80 ± 3.438 h for the KD cells compared to 24.31 ± 4.805 h in controls (P=0.0057). Therefore, a KD of RGS16 seems to lengthen the baseline cAMP rhythm in U-2 OS cells.

Interestingly, when looking at the period distribution, there seem to be two clusters of cells in both KDs and controls with distinct phenotypes: one with a shorter period around 22 h and once with a longer period of around 30 h. The KDs almost all fall into the latter category with only few wells exhibiting a short period. The controls are split between both, with the majority of wells presenting a short FRP. This cannot be entirely explained by the use of different luminometers or experimental runs. The KD seems to increase the likelihood that the cells fall into the long FRP cluster.

Overall, the amplitude was very low and the time frame when the rhythm was detectable was short. The reporter is very sensitive to temperature changes and to temperature in general, so the first 2 h were discarded to let the cells adjust as advised in the manufacturer's protocol.

The experiments were carried out in constant 34°C since the loss of reporter signal was too high in higher temperatures.

4.2.5.3 RGS16 abundance influences cAMP levels after G_i-coupled GPCR stimulation

Lastly, the effect of RGS16 levels on the cAMP response after GPCR activation was determined. When a G_i-coupled receptor is activated, the associated G_i protein inhibits the adenylyl cyclase (AC), thereby decreasing cAMP production (Taussig et al., 1993). RGS16 inactivates G_i proteins by facilitating their hydrolysis, therefore at times of high RGS16 abundance, G_i is inactivated faster and can no longer inhibit the AC, which then allows cAMP levels to rise (Bansal et al., 2007; Doi et al., 2011; Koelle, 1997). Consequently, when an agonist of a G_i -coupled GPCR is added, cAMP levels should decrease. But when RGS16 is highly expressed, it should inactivate the activated G_i, so cAMP levels should not be greatly suppressed. When RGS16 is weakly expressed, it cannot inactivate G_i, so cAMP levels should be suppressed more. To test whether this is the case, U-2 OS cells containing the cAMP pGlo sensor system were stimulated at the peak and trough of RGS16 (as determined by the western blot time course) with the selective A1R agonist N^6-cyclohexyladenosine (N-CHA). As was expected, the cAMP levels after addition of the agonist at the peak of RGS16 were higher than at the trough, because RGS16 allows cAMP to rise (see Figure 29). When RGS16 is highly abundant, N-CHA is less effective because RGS16 antagonizes its effect by hydrolyzing the N-CHA-activated G_i, thus cAMP is not decreased as effectively. Additionally, at the peak of RGS16, the difference between the addition of medium vs. N-CHA is smaller (so the stimulated/control ratio is closer to 1) because RGS16 inactivates the activated G_i and lowers the response. When RGS16 is knocked down, that time-of-day effect is gone and the response to the GPCR binding is the same at both times. Therefore, it could be shown that RGS16 abundance influences cAMP levels after G_i-coupled GPCR activation.

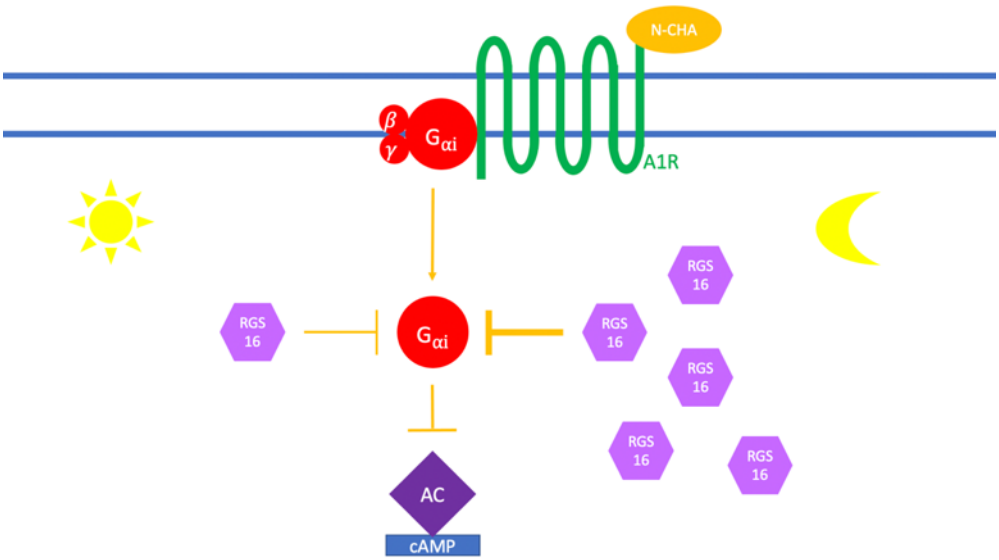

Figure 32: Circadian RGS16 levels influence AC inhibition and thus cAMP production over the day (U-2 OS cells).
The selective Adenosine 1 receptor (A1R) agonist N^6-cyclohexyladenosine (N-CHA) binds the Adenosine 1 receptor. This leads to an activation of the G_i subunit, which inhibits the adenylyl cyclase (AC), which then produces less cAMP. RGS16 increases the GTPase-activity of the G_i subunit, thereby increasing GTP hydrolysis and ending the G_i signaling. Consequently, RGS16 activity increases cAMP levels. In these experiments, RGS16 levels were higher in the cold phase than in the warm phase, leading to a difference in cAMP levels after A1R stimulation depending on the time point in the cycling environment. At times of low RGS16 abundance, the cAMP suppression after N-CHA addition was higher, since there was less RGS16 to stop the G_i signaling after A1R activation. At times of high RGS16 abundance, there was less decrease in cAMP levels. A knockdown of RGS16 abolishes this time-of-day difference.

To further confirm this, it would be interesting to repeat this experiment when blocking the phosphodiesterase (PDE) via isobutylmethylxanthine (IBX), which should lead to an increase in cAMP levels via a different mechanism than RGS16, so the effect should be additive and independent of RGS16 levels.

5. Summary and Conclusion

Taken together, these results suggest that RGS16 is involved in the function of the circadian clock, since its knockdown leads to a variety of changes in the key circadian properties, namely the free-running period and the phase of entrainment in several conditions such as different T cycles and thermoperiods. Changes were observed in U-2 OS cells as wells as ARPE-19 cells, suggesting an involvement in several tissues, although the exact role seems to differ depending on the cell line and the conditions. In turn, RGS16 itself is influenced by the clock by fluctuations in abundance and localization depending on the time of day, thus acting as a so-called zeitnehmer by being both an input and an output of the clock network (McWatters et al., 2000; Roenneberg & Merrow, 2005). Thus, a KD of RGS16 impacts both input and output pathways of the clock (Figure 33). It could also be possible that the KD impairs the overall robustness of the clock oscillator. However, the changes in the FRP are not clear and systematic, and there are also differences in entrainment, therefore a weaker oscillator alone is not enough to explain the changes. Part of the relationship between RGS16 and the circadian clock can be explained by involvement in temperature sensitivity. RGS16 responds to temperature changes, and a KD makes the system more susceptible to temperature variations, which serve as important zeitgebers in the body. Therefore, RGS16 seems to be involved in the zeitgeber input pathway. It acts as a zeitnehmer through several layers of circadian regulation, and passes on timing information to the cells. The effects of RGS16 in peripheral cells seem to be at least in part through influencing cAMP levels, as a KD impairs baseline cAMP levels, and the cAMP response elicited by GPCR activation is influenced by RGS16 levels. cAMP itself can then feed back to the clock via CREs in promoter regions in core clock genes. These findings support

previous research that RGS16 acts on the circadian clock through involvement in the regulation of cAMP levels, and expands the knowledge about its role to other cells and tissues as well. Further research is necessary to determine the exact regulation of RGS16 to explain the diverse consequences of a RGS16 KD on a behavioral as well as a cellular level.

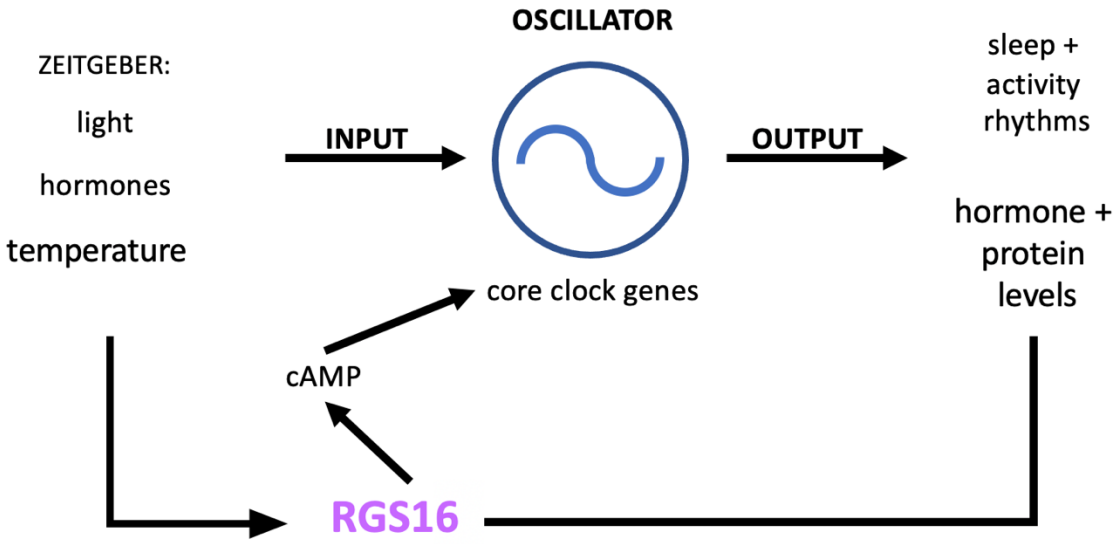

Figure 33: Eskinogram showing a simplified clock model including RGS16, where RGS16 acts as a zeitnehmer, being under circadian control as an output of the clock oscillator as well as part of the zeitnehmer input pathway by responding to temperature changes.

6. Literature

Allebrandt, K. V., Amin, N., Müller-Myhsok, B., Esko, T., Teder-Laving, M., Azevedo, R. V. D. M., Hayward, C., van Mill, J., Vogelzangs, N., Green, E. W., Melville, S. A., Lichtner, P., Wichmann, H. E., Oostra, B. A., Janssens, A. C. J. W., Campbell, H., Wilson, J. F., Hicks, A. A., Pramstaller, P. P., . . . Roenneberg, T. (2013). A KATP channel gene effect on sleep duration: from genome-wide association studies to function in Drosophila. *Molecular Psychiatry*, *18*(1), 122-132. https://doi.org/10.1038/mp.2011.142

Allebrandt, K. V., Teder-Laving, M., Akyol, M., Pichler, I., Müller-Myhsok, B., Pramstaller, P., Merrow, M., Meitinger, T., Metspalu, A., & Roenneberg, T. (2010). CLOCK gene variants associate with sleep duration in two independent populations. *Biol Psychiatry*, *67*(11), 1040-1047. https://doi.org/10.1016/j.biopsych.2009.12.026

Allen, C. N., Nitabach, M. N., & Colwell, C. S. (2017). Membrane Currents, Gene Expression, and Circadian Clocks. *Cold Spring Harb Perspect Biol*, *9*(5). https://doi.org/10.1101/cshperspect.a027714

Aschoff, J. (1960). Exogenous and endogenous components in circadian rhythms. *Cold Spring Harb Symp Quant Biol*, *25*, 11-28. https://doi.org/10.1101/sqb.1960.025.01.004

Aschoff, J. (1983). Circadian control of body temperature. *Journal of Thermal Biology*, *8*(1), 143-147. https://doi.org/https://doi.org/10.1016/0306-4565(83)90094-3

Aschoff, J., & Pohl, H. (1978). Phase relations between a circadian rhythm and its zeitgeber within the range of entrainment. *Naturwissenschaften*, *65*(2), 80-84. https://doi.org/10.1007/bf00440545

Asher, G., Gatfield, D., Stratmann, M., Reinke, H., Dibner, C., Kreppel, F., Mostoslavsky, R., Alt, F. W., & Schibler, U. (2008). SIRT1 regulates circadian clock gene expression through PER2 deacetylation. *Cell*, *134*(2), 317-328. https://doi.org/10.1016/j.cell.2008.06.050

Avery, H. E. (1974). Dependence of Rate on Temperature. In H. E. Avery (Ed.), *Basic Reaction Kinetics and Mechanisms* (pp. 47-58). Macmillan Education UK. https://doi.org/10.1007/978-1-349-15520-0_4

Baggs, J. E., Price, T. S., DiTacchio, L., Panda, S., Fitzgerald, G. A., & Hogenesch, J. B. (2009). Network features of the mammalian circadian clock. *PLoS Biol*, *7*(3), e52. https://doi.org/10.1371/journal.pbio.1000052

Balsalobre, A., Damiola, F., & Schibler, U. (1998). A serum shock induces circadian gene expression in mammalian tissue culture cells. *Cell*, *93*(6), 929-937. https://doi.org/10.1016/s0092-8674(00)81199-x

Bansal, G., Druey, K. M., & Xie, Z. (2007). R4 RGS proteins: regulation of G-protein signaling and beyond. *Pharmacol Ther*, *116*(3), 473-495. https://doi.org/10.1016/j.pharmthera.2007.09.005

Berson, D. M., Dunn, F. A., & Takao, M. (2002). Phototransduction by retinal ganglion cells that set the circadian clock. *Science*, *295*(5557), 1070-1073. https://doi.org/10.1126/science.1067262

Bolte, S., & Cordelières, F. P. (2006). A guided tour into subcellular colocalization analysis in light microscopy. *J Microsc*, *224*(Pt 3), 213-232. https://doi.org/10.1111/j.1365-2818.2006.01706.x

Browman, L. G. (1944). MODIFIED SPONTANEOUS ACTIVITY RHYTHMS IN RATS. *American Journal of Physiology-Legacy Content*, *142*(5), 633-637. https://doi.org/10.1152/ajplegacy.1944.142.5.633

Brown, S. A., Kunz, D., Dumas, A., Westermark, P. O., Vanselow, K., Tilmann-Wahnschaffe, A., Herzel, H., & Kramer, A. (2008). Molecular insights into human daily behavior. *Proc Natl Acad Sci U S A*, *105*(5), 1602-1607. https://doi.org/10.1073/pnas.0707772105

Bruce, V. G. (1960). Environmental entrainment of circadian rhythms. *Cold Spring Harbor Symposia in Quantitative Biology*(25), 29-48.

Buhr, E. D., Yoo, S. H., & Takahashi, J. S. (2010). Temperature as a universal resetting cue for mammalian circadian oscillators. *Science*, *330*(6002), 379-385. https://doi.org/10.1126/science.1195262

Burgon, P. G., Lee, W. L., Nixon, A. B., Peralta, E. G., & Casey, P. J. (2001). Phosphorylation and nuclear translocation of a regulator of G protein signaling (RGS10). *J Biol Chem*, *276*(35), 32828-32834. https://doi.org/10.1074/jbc.M100960200

Burke, T. M., Markwald, R. R., McHill, A. W., Chinoy, E. D., Snider, J. A., Bessman, S. C., Jung, C. M., O'Neill, J. S., & Wright, K. P., Jr. (2015). Effects of caffeine on the human circadian clock in vivo and in vitro. *Sci Transl Med*, *7*(305), 305ra146. https://doi.org/10.1126/scitranslmed.aac5125

Burt, P., Grabe, S., Madeti, C., Upadhyay, A., Merrow, M., Roenneberg, T., Herzel, H., & Schmal, C. (2021). Mechanisms Underlying the Complex Dynamics of Temperature Entrainment by a Circadian Clock. *bioRxiv*, 2021.2004.2028.441752. https://doi.org/10.1101/2021.04.28.441752

Cagampang, F. R. A., & Inouye, S.-I. T. (1994). Diurnal and circadian changes of serotonin in the suprachiasmatic nuclei: regulation by light and an endogenous pacemaker. *Brain Research*, *639*(1), 175-179. https://doi.org/https://doi.org/10.1016/0006-8993(94)91780-9

Chatterjee, T. K., & Fisher, R. A. (2000). Cytoplasmic, Nuclear, and Golgi Localization of RGS Proteins: EVIDENCE FOR N-TERMINAL AND RGS DOMAIN SEQUENCES AS INTRACELLULAR TARGETING MOTIFS*. *Journal of Biological Chemistry*, *275*(31), 24013-24021. https://doi.org/https://doi.org/10.1074/jbc.M002082200

Chen, C., Seow, K. T., Guo, K., Yaw, L. P., & Lin, S.-C. (1999). The Membrane Association Domain of RGS16 Contains Unique Amphipathic Features That Are Conserved in RGS4 and RGS5*. *Journal of Biological Chemistry*, *274*(28), 19799-19806. https://doi.org/https://doi.org/10.1074/jbc.274.28.19799

Chen, J. F., Eltzschig, H. K., & Fredholm, B. B. (2013). Adenosine receptors as drug targets--what are the challenges? *Nat Rev Drug Discov*, *12*(4), 265-286. https://doi.org/10.1038/nrd3955

Chidiac, P., & Roy, A. A. (2003). Activity, regulation, and intracellular localization of RGS proteins. *Recept Channels*, *9*(3), 135-147.

Ciarleglio, C. M., Resuehr, H. E. S., & McMahon, D. G. (2011). Interactions of the serotonin and circadian systems: nature and nurture in rhythms and blues. *Neuroscience*, *197*, 8-16. https://doi.org/https://doi.org/10.1016/j.neuroscience.2011.09.036

Daan, S., Merrow, M., & Roenneberg, T. (2002). External time--internal time. *J Biol Rhythms*, *17*(2), 107-109. https://doi.org/10.1177/074873002129002375

Daniels, L. J., Kay, D., Marjot, T., Hodson, L., & Ray, D. W. (2023). Circadian regulation of liver metabolism: experimental approaches in human, rodent, and cellular models. *Am J Physiol Cell Physiol*, *325*(5), C1158-c1177. https://doi.org/10.1152/ajpcell.00551.2022

Denniff, M., Turrell, H. E., Vanezis, A., & Rodrigo, G. C. (2014). The time-of-day variation in vascular smooth muscle contractility depends on a nitric oxide signalling pathway. *Journal of Molecular and Cellular Cardiology*, *66*, 133-140. https://doi.org/https://doi.org/10.1016/j.yjmcc.2013.11.009

DeVera, C., Dixon, J., Chrenek, M. A., Baba, K., Le, Y. Z., Iuvone, P. M., & Tosini, G. (2022). The Circadian Clock in the Retinal Pigment Epithelium Controls the Diurnal Rhythm of Phagocytic Activity. *Int J Mol Sci*, *23*(10). https://doi.org/10.3390/ijms23105302

Díez-Noguera, A. (2013). Methods for serial analysis of long time series in the study of biological rhythms. *J Circadian Rhythms*, *11*(1), 7. https://doi.org/10.1186/1740-3391-11-7

Dodd, A. N., Salathia, N., Hall, A., Kévei, E., Tóth, R., Nagy, F., Hibberd, J. M., Millar, A. J., & Webb, A. A. (2005). Plant circadian clocks increase photosynthesis, growth, survival, and competitive advantage. *Science*, *309*(5734), 630-633. https://doi.org/10.1126/science.1115581

Doi, M., Ishida, A., Miyake, A., Sato, M., Komatsu, R., Yamazaki, F., Kimura, I., Tsuchiya, S., Kori, H., Seo, K., Yamaguchi, Y., Matsuo, M., Fustin, J. M., Tanaka, R., Santo, Y., Yamada, H., Takahashi, Y., Araki, M., Nakao, K., . . . Okamura, H. (2011). Circadian regulation of intracellular G-protein signalling mediates intercellular synchrony and rhythmicity in the suprachiasmatic nucleus. *Nat Commun*, *2*, 327. https://doi.org/10.1038/ncomms1316

Druey, K. M., Ugur, O., Caron, J. M., Chen, C. K., Backlund, P. S., & Jones, T. L. (1999). Amino-terminal cysteine residues of RGS16 are required for palmitoylation and modulation of Gi- and Gq-mediated signaling. *J Biol Chem*, *274*(26), 18836-18842. https://doi.org/10.1074/jbc.274.26.18836

Dubocovich, M. L. (2007). Melatonin receptors: Role on sleep and circadian rhythm regulation. *Sleep Medicine*, *8*, 34-42. https://doi.org/https://doi.org/10.1016/j.sleep.2007.10.007

Duffy, J. F., Rimmer, D. W., & Czeisler, C. A. (2001). Association of intrinsic circadian period with morningness-eveningness, usual wake time, and circadian phase. *Behav Neurosci*, *115*(4), 895-899. https://doi.org/10.1037//0735-7044.115.4.895

Duffy, J. F., & Wright, K. P., Jr. (2005). Entrainment of the human circadian system by light. *J Biol Rhythms*, *20*(4), 326-338. https://doi.org/10.1177/0748730405277983

Dulin, N. O., Sorokin, A., Reed, E., Elliott, S., Kehrl, J. H., & Dunn, M. J. (1999). RGS3 inhibits G protein-mediated signaling via translocation to the membrane and binding to Galpha11. *Mol Cell Biol*, *19*(1), 714-723. https://doi.org/10.1128/mcb.19.1.714

Ebisawa, T., Uchiyama, M., Kajimura, N., Mishima, K., Kamei, Y., Katoh, M., Watanabe, T., Sekimoto, M., Shibui, K., Kim, K., Kudo, Y., Ozeki, Y., Sugishita, M., Toyoshima, R., Inoue, Y., Yamada, N., Nagase, T., Ozaki, N., Ohara, O., . . . Yamauchi, T. (2001). Association of structural polymorphisms in the human period3 gene with delayed sleep phase syndrome. *EMBO Rep*, *2*(4), 342-346. https://doi.org/10.1093/embo-reports/kve070

Edery, I. (2000). Circadian rhythms in a nutshell. *Physiological Genomics*, *3*(2), 59-74. https://doi.org/10.1152/physiolgenomics.2000.3.2.59

Escobar, C., Cailotto, C., Angeles-Castellanos, M., Delgado, R. S., & Buijs, R. M. (2009). Peripheral oscillators: the driving force for food-anticipatory activity. *European Journal of Neuroscience*, *30*(9), 1665-1675. https://doi.org/https://doi.org/10.1111/j.1460-9568.2009.06972.x

Eskin, A. (1979). Identification and physiology of circadian pacemakers. Introduction. *Fed Proc*, *38*(12), 2570-2572.

Ghavami, A., Hunt, R. A., Olsen, M. A., Zhang, J., Smith, D. L., Kalgaonkar, S., Rahman, Z., & Young, K. H. (2004). Differential effects of regulator of G protein signaling (RGS) proteins on serotonin 5-HT1A, 5-HT2A, and dopamine D2 receptor-mediated signaling and adenylyl cyclase activity. *Cell Signal*, *16*(6), 711-721. https://doi.org/10.1016/j.cellsig.2003.11.006

Görgün, C. Z., Keskil, Z. A., Hodoglugil, U., Ercan, Z. S., Abaciog'lu, N., & Zengil, H. (1998). In Vitro Evidence of Tissue Susceptibility Rhythms. I. Temporal Variation in Effect of Potassium Chloride and

Phenylephrine on Rat Aorta. *Chronobiology International*, *15*(1), 39-48. https://doi.org/10.3109/07420529808998668

Granada, A. E., Bordyugov, G., Kramer, A., & Herzel, H. (2013). Human chronotypes from a theoretical perspective. *PLoS One*, *8*(3), e59464. https://doi.org/10.1371/journal.pone.0059464

Hamblen-Coyle, M. J., Wheeler, D. A., Rutila, J. E., Rosbash, M., & Hall, J. C. (1992). Behavior of period-altered circadian rhythm mutants ofDrosophila in light: Dark cycles (Diptera: Drosophilidae). *Journal of Insect Behavior*, *5*(4), 417-446. https://doi.org/10.1007/BF01058189

Hamet, P., & Tremblay, J. (2006). Genetics of the sleep-wake cycle and its disorders. *Metabolism*, *55*(10 Suppl 2), S7-12. https://doi.org/10.1016/j.metabol.2006.07.006

Hayasaka, N., Aoki, K., Kinoshita, S., Yamaguchi, S., Wakefield, J. K., Tsuji-Kawahara, S., Horikawa, K., Ikegami, H., Wakana, S., Murakami, T., Ramabhadran, R., Miyazawa, M., & Shibata, S. (2011). Attenuated food anticipatory activity and abnormal circadian locomotor rhythms in Rgs16 knockdown mice. *PLoS One*, *6*(3), e17655. https://doi.org/10.1371/journal.pone.0017655

Hiol, A., Davey, P. C., Osterhout, J. L., Waheed, A. A., Fischer, E. R., Chen, C. K., Milligan, G., Druey, K. M., & Jones, T. L. (2003). Palmitoylation regulates regulators of G-protein signaling (RGS) 16 function. I. Mutation of amino-terminal cysteine residues on RGS16 prevents its targeting to lipid rafts and palmitoylation of an internal cysteine residue. *J Biol Chem*, *278*(21), 19301-19308. https://doi.org/10.1074/jbc.M210123200

Hirota, T., Lewis, W. G., Liu, A. C., Lee, J. W., Schultz, P. G., & Kay, S. A. (2008). A chemical biology approach reveals period shortening of the mammalian circadian clock by specific inhibition of GSK-3beta. *Proc Natl Acad Sci U S A*, *105*(52), 20746-20751. https://doi.org/10.1073/pnas.0811410106

Hoffmann, K. (1963). Zur Beziehung zwischen Phasenlage und Spontanfrequenz bei der endogenen Tagesperiodik. *Zeitschrift für Naturforschung B*, *18*(2), 154-157. https://doi.org/doi:10.1515/znb-1963-0211

Hoffmann, K. (1969). *Zum Einfluß der Zeitgeberstärke auf die Phasenlage der synchronisierten circadianen Periodik*.

Hu, Y., Shmygelska, A., Tran, D., Eriksson, N., Tung, J. Y., & Hinds, D. A. (2016). GWAS of 89,283 individuals identifies genetic variants associated with self-reporting of being a morning person. *Nat Commun*, *7*, 10448. https://doi.org/10.1038/ncomms10448

Huang, J., Pashkov, V., Kurrasch, D. M., Yu, K., Gold, S. J., & Wilkie, T. M. (2006). Feeding and fasting controls liver expression of a regulator of G protein signaling (Rgs16) in periportal hepatocytes. *Comp Hepatol*, *5*, 8. https://doi.org/10.1186/1476-5926-5-8

Jagannath, A., Varga, N., Dallmann, R., Rando, G., Gosselin, P., Ebrahimjee, F., Taylor, L., Mosneagu, D., Stefaniak, J., Walsh, S., Palumaa, T., Di Pretoro, S., Sanghani, H., Wakaf, Z., Churchill, G. C., Galione, A., Peirson, S. N., Boison, D., Brown, S. A., . . . Vasudevan, S. R. (2021). Adenosine integrates light and sleep signalling for the regulation of circadian timing in mice. *Nat Commun*, *12*(1), 2113. https://doi.org/10.1038/s41467-021-22179-z

Jones, C. R., Campbell, S. S., Zone, S. E., Cooper, F., DeSano, A., Murphy, P. J., Jones, B., Czajkowski, L., & Ptácek, L. J. (1999). Familial advanced sleep-phase syndrome: A short-period circadian rhythm variant in humans. *Nat Med*, *5*(9), 1062-1065. https://doi.org/10.1038/12502

Jones, S. E., Lane, J. M., Wood, A. R., van Hees, V. T., Tyrrell, J., Beaumont, R. N., Jeffries, A. R., Dashti, H. S., Hillsdon, M., Ruth, K. S., Tuke, M. A., Yaghootkar, H., Sharp, S. A., Jie, Y., Thompson, W. D., Harrison, J. W., Dawes, A., Byrne, E. M., Tiemeier, H., . . . Weedon, M. N. (2019). Genome-wide association analyses of chronotype in 697,828 individuals provides insights into circadian rhythms. *Nat Commun*, *10*(1), 343. https://doi.org/10.1038/s41467-018-08259-7

Jones, S. E., Tyrrell, J., Wood, A. R., Beaumont, R. N., Ruth, K. S., Tuke, M. A., Yaghootkar, H., Hu, Y., Teder-Laving, M., Hayward, C., Roenneberg, T., Wilson, J. F., Del Greco, F., Hicks, A. A., Shin, C., Yun, C. H., Lee, S. K., Metspalu, A., Byrne, E. M., . . . Weedon, M. N. (2016). Genome-Wide Association Analyses in 128,266 Individuals Identifies New Morningness and Sleep Duration Loci. *PLoS Genet*, *12*(8), e1006125. https://doi.org/10.1371/journal.pgen.1006125

Katzenberg, D., Young, T., Finn, L., Lin, L., King, D. P., Takahashi, J. S., & Mignot, E. (1998). A CLOCK polymorphism associated with human diurnal preference. *Sleep*, *21*(6), 569-576. https://doi.org/10.1093/sleep/21.6.569

Kleitman, N., & Kleitman, E. (1953). Effect of non-twenty-four-hour routines of living on oral temperature and heart rate. *J Appl Physiol*, *6*(5), 283-291. https://doi.org/10.1152/jappl.1953.6.5.283

Koelle, M. R. (1997). A new family of G-protein regulators - the RGS proteins. *Curr Opin Cell Biol*, *9*(2), 143-147. https://doi.org/10.1016/s0955-0674(97)80055-5

Koyanagi, S., Hamdan, A. M., Horiguchi, M., Kusunose, N., Okamoto, A., Matsunaga, N., & Ohdo, S. (2011). cAMP-response element (CRE)-mediated transcription by activating transcription factor-4 (ATF4) is essential for circadian expression of the Period2 gene. *J Biol Chem*, *286*(37), 32416-32423. https://doi.org/10.1074/jbc.M111.258970

Ladds, G., Goddard, A., Hill, C., Thornton, S., & Davey, J. (2007). Differential effects of RGS proteins on G alpha(q) and G alpha(11) activity. *Cell Signal*, *19*(1), 103-113. https://doi.org/10.1016/j.cellsig.2006.05.027

Lane, J. M., Vlasac, I., Anderson, S. G., Kyle, S. D., Dixon, W. G., Bechtold, D. A., Gill, S., Little, M. A., Luik, A., Loudon, A., Emsley, R., Scheer, F. A., Lawlor, D. A., Redline, S., Ray, D. W., Rutter, M. K., & Saxena, R. (2016). Genome-wide association analysis identifies novel loci for chronotype in 100,420 individuals from the UK Biobank. *Nat Commun*, *7*, 10889. https://doi.org/10.1038/ncomms10889

Le, J. Q., Ma, D., Dai, X., & Rosbash, M. (2024). Light and dopamine impact two circadian neurons to promote morning wakefulness. *Curr Biol*. https://doi.org/10.1016/j.cub.2024.07.056

Lee, K., Shiva Kumar, P., McQuade, S., Lee, J. Y., Park, S., An, Z., & Piccoli, B. (2017). Experimental and Mathematical Analyses Relating Circadian Period and Phase of Entrainment in Neurospora crassa. *J Biol Rhythms*, *32*(6), 550-559. https://doi.org/10.1177/0748730417738611

Leontiadis, L. J., Papakonstantinou, M. P., & Georgoussi, Z. (2009). Regulator of G protein signaling 4 confers selectivity to specific G proteins to modulate mu- and delta-opioid receptor signaling. *Cell Signal*, *21*(7), 1218-1228. https://doi.org/10.1016/j.cellsig.2009.03.013

Liu, A. C., Welsh, D. K., Ko, C. H., Tran, H. G., Zhang, E. E., Priest, A. A., Buhr, E. D., Singer, O., Meeker, K., Verma, I. M., Doyle, F. J., 3rd, Takahashi, J. S., & Kay, S. A. (2007). Intercellular coupling confers robustness against mutations in the SCN circadian clock network. *Cell*, *129*(3), 605-616. https://doi.org/10.1016/j.cell.2007.02.047

Maier, B., Wendt, S., Vanselow, J. T., Wallach, T., Reischl, S., Oehmke, S., Schlosser, A., & Kramer, A. (2009). A large-scale functional RNAi screen reveals a role for CK2 in the mammalian circadian clock. *Genes Dev*, *23*(6), 708-718. https://doi.org/10.1101/gad.512209

Masuho, I., Balaji, S., Muntean, B. S., Skamangas, N. K., Chavali, S., Tesmer, J. J. G., Babu, M. M., & Martemyanov, K. A. (2020). A Global Map of G Protein Signaling Regulation by RGS Proteins. *Cell*, *183*(2), 503-521.e519. https://doi.org/10.1016/j.cell.2020.08.052

Masuho, I., Ostrovskaya, O., Kramer, G. M., Jones, C. D., Xie, K., & Martemyanov, K. A. (2015). Distinct profiles of functional discrimination among G proteins determine the actions of G protein-coupled receptors. *Sci Signal*, *8*(405), ra123. https://doi.org/10.1126/scisignal.aab4068

McWatters, H. G., Bastow, R. M., Hall, A., & Millar, A. J. (2000). The ELF3 zeitnehmer regulates light signalling to the circadian clock. *Nature*, *408*(6813), 716-720. https://doi.org/10.1038/35047079

Mendoza, J. (2007). Circadian Clocks: Setting Time By Food. *Journal of Neuroendocrinology*, *19*(2), 127-137. https://doi.org/https://doi.org/10.1111/j.1365-2826.2006.01510.x

Merrow, M., Brunner, M., & Roenneberg, T. (1999). Assignment of circadian function for the Neurospora clock gene frequency. *Nature*, *399*(6736), 584-586. https://doi.org/10.1038/21190

Milev, N. B., Rey, G., Valekunja, U. K., Edgar, R. S., O'Neill, J. S., & Reddy, A. B. (2015). Analysis of the redox oscillations in the circadian clockwork. *Methods Enzymol*, *552*, 185-210. https://doi.org/10.1016/bs.mie.2014.10.007

Mistlberger, R. E. (2009). Food-anticipatory circadian rhythms: concepts and methods. *European Journal of Neuroscience*, *30*(9), 1718-1729. https://doi.org/https://doi.org/10.1111/j.1460-9568.2009.06965.x

Mrosovsky, N. (1999). Masking: history, definitions, and measurement. *Chronobiol Int*, *16*(4), 415-429. https://doi.org/10.3109/07420529908998717

Nakagawa, S., Nguyen Pham, K. T., Shao, X., & Doi, M. (2020). Time-Restricted G-Protein Signaling Pathways via GPR176, G(z), and RGS16 Set the Pace of the Master Circadian Clock in the Suprachiasmatic Nucleus. *Int J Mol Sci*, *21*(14). https://doi.org/10.3390/ijms21145055

Nehlig, A., Daval, J. L., & Debry, G. (1992). Caffeine and the central nervous system: mechanisms of action, biochemical, metabolic and psychostimulant effects. *Brain Res Brain Res Rev*, *17*(2), 139-170. https://doi.org/10.1016/0165-0173(92)90012-b

Nikhil, K. L., Korge, S., & Kramer, A. (2020). Heritable gene expression variability and stochasticity govern clonal heterogeneity in circadian period. *PLOS Biology*, *18*(8), e3000792. https://doi.org/10.1371/journal.pbio.3000792

O'Neill, J. S., Maywood, E. S., Chesham, J. E., Takahashi, J. S., & Hastings, M. H. (2008). cAMP-dependent signaling as a core component of the mammalian circadian pacemaker. *Science*, *320*(5878), 949-953. https://doi.org/10.1126/science.1152506

Oike, H., Kobori, M., Suzuki, T., & Ishida, N. (2011). Caffeine lengthens circadian rhythms in mice. *Biochem Biophys Res Commun*, *410*(3), 654-658. https://doi.org/10.1016/j.bbrc.2011.06.049

Olmedo, M., O'Neill, J. S., Edgar, R. S., Valekunja, U. K., Reddy, A. B., & Merrow, M. (2012). Circadian regulation of olfaction and an evolutionarily conserved, nontranscriptional marker in Caenorhabditis elegans. *Proceedings of the National Academy of Sciences*, *109*(50), 20479-20484. https://doi.org/10.1073/pnas.1211705109

Osterhout, J. L., Waheed, A. A., Hiol, A., Ward, R. J., Davey, P. C., Nini, L., Wang, J., Milligan, G., Jones, T. L. Z., & Druey, K. M. (2003). Palmitoylation Regulates Regulator of G-protein Signaling (RGS) 16 Function: II. PALMITOYLATION OF A CYSTEINE RESIDUE IN THE RGS BOX IS CRITICAL

FOR RGS16 GTPase ACCELERATING ACTIVITY AND REGULATION OF Gi-COUPLED SIGNALING*. *Journal of Biological Chemistry*, *278*(21), 19309-19316. https://doi.org/https://doi.org/10.1074/jbc.M210124200

Ouyang, Y., Andersson, C. R., Kondo, T., Golden, S. S., & Johnson, C. H. (1998). Resonating circadian clocks enhance fitness in cyanobacteria. *Proc Natl Acad Sci U S A*, *95*(15), 8660-8664. https://doi.org/10.1073/pnas.95.15.8660

Panda, S., Nayak, S. K., Campo, B., Walker, J. R., Hogenesch, J. B., & Jegla, T. (2005). Illumination of the melanopsin signaling pathway. *Science*, *307*(5709), 600-604. https://doi.org/10.1126/science.1105121

Pashkov, V., Huang, J., Parameswara, V. K., Kedzierski, W., Kurrasch, D. M., Tall, G. G., Esser, V., Gerard, R. D., Uyeda, K., Towle, H. C., & Wilkie, T. M. (2011). Regulator of G protein signaling (RGS16) inhibits hepatic fatty acid oxidation in a carbohydrate response element-binding protein (ChREBP)-dependent manner. *J Biol Chem*, *286*(17), 15116-15125. https://doi.org/10.1074/jbc.M110.216234

Peirson, S. N., & Foster, R. G. (2009). Photoreceptors and Circadian Clocks. In L. R. Squire (Ed.), *Encyclopedia of Neuroscience* (pp. 669-676). Academic Press. https://doi.org/https://doi.org/10.1016/B978-008045046-9.01602-8

Pévet, P., Agez, L., Bothorel, B., Saboureau, M., Gauer, F., Laurent, V., & Masson-Pévet, M. (2006). Melatonin in the multi-oscillatory mammalian circadian world. *Chronobiology International*, *23*(1-2), 39-51. https://doi.org/10.1080/07420520500482074

Pittendrigh, C. S. (1960). Circadian rhythms and the circadian organization of living systems. *Cold Spring Harb Symp Quant Biol*, *25*, 159-184. https://doi.org/10.1101/sqb.1960.025.01.015

Pittendrigh, C. S. (1981). Circadian Systems: Entrainment. In J. Aschoff (Ed.), *Biological Rhythms* (pp. 95-124). Springer US. https://doi.org/10.1007/978-1-4615-6552-9_7

Pittendrigh, C. S., & Daan, S. (1976). A functional analysis of circadian pacemakers in nocturnal rodents. *Journal of comparative physiology*, *106*(3), 223-252. https://doi.org/10.1007/BF01417856

Prolo, L. M., Takahashi, J. S., & Herzog, E. D. (2005). Circadian rhythm generation and entrainment in astrocytes. *J Neurosci*, *25*(2), 404-408. https://doi.org/10.1523/jneurosci.4133-04.2005

Provencio, I., Rodriguez, I. R., Jiang, G., Hayes, W. P., Moreira, E. F., & Rollag, M. D. (2000). A novel human opsin in the inner retina. *J Neurosci*, *20*(2), 600-605. https://doi.org/10.1523/jneurosci.20-02-00600.2000

Psifogeorgou, K., Papakosta, P., Russo, S. J., Neve, R. L., Kardassis, D., Gold, S. J., & Zachariou, V. (2007). RGS9-2 is a negative modulator of mu-opioid receptor function. *J Neurochem*, *103*(2), 617-625. https://doi.org/10.1111/j.1471-4159.2007.04812.x

Rask-Andersen, M., Almén, M. S., & Schiöth, H. B. (2011). Trends in the exploitation of novel drug targets. *Nat Rev Drug Discov*, *10*(8), 579-590. https://doi.org/10.1038/nrd3478

Rémi, J., Merrow, M., & Roenneberg, T. (2010). A circadian surface of entrainment: varying T, τ, and photoperiod in Neurospora crassa. *J Biol Rhythms*, *25*(5), 318-328. https://doi.org/10.1177/0748730410379081

Roenneberg, T., Daan, S., & Merrow, M. (2003). The art of entrainment. *J Biol Rhythms*, *18*(3), 183-194. https://doi.org/10.1177/0748730403018003001

Roenneberg, T., Dragovic, Z., & Merrow, M. (2005). Demasking biological oscillators: Properties and principles of entrainment exemplified by the Neurospora circadian clock. *Proceedings of the National Academy of Sciences*, *102*(21), 7742-7747. https://doi.org/10.1073/pnas.0501884102

Roenneberg, T., Kuehnle, T., Juda, M., Kantermann, T., Allebrandt, K., Gordijn, M., & Merrow, M. (2007). Epidemiology of the human circadian clock. *Sleep Med Rev*, *11*(6), 429-438. https://doi.org/10.1016/j.smrv.2007.07.005

Roenneberg, T., & Merrow, M. (2005). Circadian Clocks: Translation Lost. *Current Biology*, *15*(12), R470-R473. https://doi.org/https://doi.org/10.1016/j.cub.2005.06.014

Roenneberg, T., & Merrow, M. (2016). The Circadian Clock and Human Health. *Curr Biol*, *26*(10), R432-443. https://doi.org/10.1016/j.cub.2016.04.011

Roenneberg, T., Wirz-Justice, A., & Merrow, M. (2003). Life between clocks: daily temporal patterns of human chronotypes. *J Biol Rhythms*, *18*(1), 80-90. https://doi.org/10.1177/0748730402239679

Ross, E. M., & Wilkie, T. M. (2000). GTPase-activating proteins for heterotrimeric G proteins: regulators of G protein signaling (RGS) and RGS-like proteins. *Annu Rev Biochem*, *69*, 795-827. https://doi.org/10.1146/annurev.biochem.69.1.795

Roy, A. A., Lemberg, K. E., & Chidiac, P. (2003). Recruitment of RGS2 and RGS4 to the plasma membrane by G proteins and receptors reflects functional interactions. *Mol Pharmacol*, *64*(3), 587-593. https://doi.org/10.1124/mol.64.3.587

Schindelin, J., Arganda-Carreras, I., Frise, E., Kaynig, V., Longair, M., Pietzsch, T., Preibisch, S., Rueden, C., Saalfeld, S., Schmid, B., Tinevez, J.-Y., White, D. J., Hartenstein, V., Eliceiri, K., Tomancak, P., & Cardona, A. (2012). Fiji: an open-source platform for biological-image analysis. *Nature Methods*, *9*(7), 676-682. https://doi.org/10.1038/nmeth.2019

Seifert, A., Schofield, P., Barton, G. J., & Hay, R. T. (2015). Proteotoxic stress reprograms the chromatin landscape of SUMO modification. *Sci Signal*, *8*(384), rs7. https://doi.org/10.1126/scisignal.aaa2213

Shryock, J. C., Ozeck, M. J., & Belardinelli, L. (1998). Inverse agonists and neutral antagonists of recombinant human A1 adenosine receptors stably expressed in Chinese hamster ovary cells. *Mol Pharmacol*, *53*(5), 886-893.

Sigworth, L. A., & Rea, M. A. (2003). Adenosine A1 receptors regulate the response of the mouse circadian clock to light. *Brain Res*, *960*(1-2), 246-251. https://doi.org/10.1016/s0006-8993(02)03896-9

Soundararajan, M., Willard, F. S., Kimple, A. J., Turnbull, A. P., Ball, L. J., Schoch, G. A., Gileadi, C., Fedorov, O. Y., Dowler, E. F., Higman, V. A., Hutsell, S. Q., Sundström, M., Doyle, D. A., & Siderovski, D. P. (2008). Structural diversity in the RGS domain and its interaction with heterotrimeric G protein alpha-subunits. *Proc Natl Acad Sci U S A*, *105*(17), 6457-6462. https://doi.org/10.1073/pnas.0801508105

Sriram, K., & Insel, P. A. (2018). G Protein-Coupled Receptors as Targets for Approved Drugs: How Many Targets and How Many Drugs? *Mol Pharmacol*, *93*(4), 251-258. https://doi.org/10.1124/mol.117.111062

Sweeney, B. M., & Hastings, J. W. (1960). Effects of temperature upon diurnal rhythms. *Cold Spring Harb Symp Quant Biol*, *25*, 87-104. https://doi.org/10.1101/sqb.1960.025.01.009

Takahashi, J. S. (2017). Transcriptional architecture of the mammalian circadian clock. *Nat Rev Genet*, *18*(3), 164-179. https://doi.org/10.1038/nrg.2016.150

Tan, Y., Merrow, M., & Roenneberg, T. (2004). Photoperiodism in Neurospora crassa. *J Biol Rhythms*, *19*(2), 135-143. https://doi.org/10.1177/0748730404263015

Taussig, R., Iñiguez-Lluhi, J. A., & Gilman, A. G. (1993). Inhibition of adenylyl cyclase by Gi alpha. *Science*, *261*(5118), 218-221. https://doi.org/10.1126/science.8327893

Tian, M., Ma, Y., Li, T., Wu, N., Li, J., Jia, H., Yan, M., Wang, W., Bian, H., Tan, X., & Qi, J. (2022). Functions of regulators of G protein signaling 16 in immunity, inflammation, and other diseases. *Front Mol Biosci*, *9*, 962321. https://doi.org/10.3389/fmolb.2022.962321

Toh, K. L., Jones, C. R., He, Y., Eide, E. J., Hinz, W. A., Virshup, D. M., Ptácek, L. J., & Fu, Y. H. (2001). An hPer2 phosphorylation site mutation in familial advanced sleep phase syndrome. *Science*, *291*(5506), 1040-1043. https://doi.org/10.1126/science.1057499

Vanselow, K., Vanselow, J. T., Westermark, P. O., Reischl, S., Maier, B., Korte, T., Herrmann, A., Herzel, H., Schlosser, A., & Kramer, A. (2006). Differential effects of PER2 phosphorylation: molecular basis for the human familial advanced sleep phase syndrome (FASPS). *Genes Dev*, *20*(19), 2660-2672. https://doi.org/10.1101/gad.397006

Von Moo, E., Harpsøe, K., Hauser, A. S., Masuho, I., Bräuner-Osborne, H., Gloriam, D. E., & Martemyanov, K. A. (2022). Ligand-directed bias of G protein signaling at the dopamine D(2) receptor. *Cell Chem Biol*, *29*(2), 226-238.e224. https://doi.org/10.1016/j.chembiol.2021.07.004

Welsh, D. K., Imaizumi, T., & Kay, S. A. (2005). Real-Time Reporting of Circadian-Regulated Gene Expression by Luciferase Imaging in Plants and Mammalian Cells. In M. W. Young (Ed.), *Methods in Enzymology* (Vol. 393, pp. 269-288). Academic Press. https://doi.org/https://doi.org/10.1016/S0076-6879(05)93011-5

Yamazaki, S., & Takahashi, J. S. (2005). Real-Time Luminescence Reporting of Circadian Gene Expression in Mammals. In M. W. Young (Ed.), *Methods in Enzymology* (Vol. 393, pp. 288-301). Academic Press. https://doi.org/https://doi.org/10.1016/S0076-6879(05)93012-7

Zhang, R., Lahens, N. F., Ballance, H. I., Hughes, M. E., & Hogenesch, J. B. (2014). A circadian gene expression atlas in mammals: implications for biology and medicine. *Proc Natl Acad Sci U S A*, *111*(45), 16219-16224. https://doi.org/10.1073/pnas.1408886111

Zielinski, T., Moore, A. M., Troup, E., Halliday, K. J., & Millar, A. J. (2014). Strengths and limitations of period estimation methods for circadian data. *PLoS One*, *9*(5), e96462. https://doi.org/10.1371/journal.pone.0096462

7. Appendix and Supplementary Materials

7.1 Circadian properties

Line graphs of the circadian properties experiments in free-run and entrainment, overlays of all single wells without smoothing or trend correction.

7.1.1 Free-running period

Selected U-2 OS cells

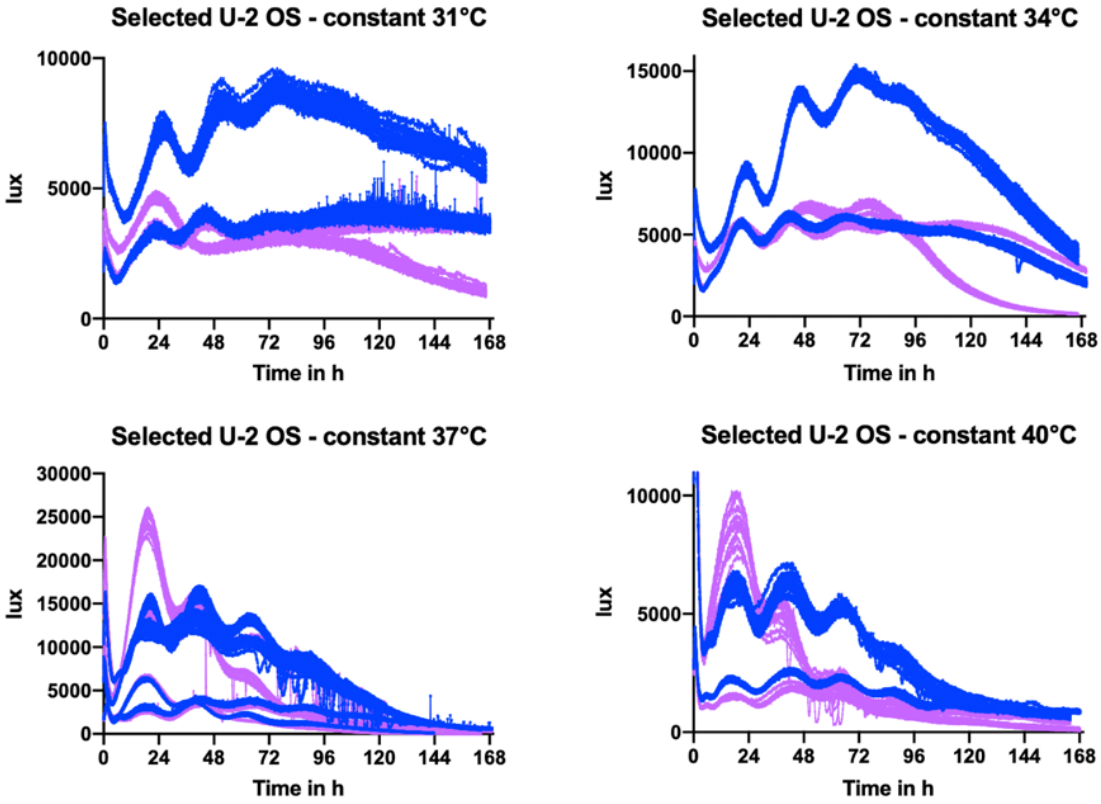

Figure S 1: Line graphs of a luciferase reporter of Bmal1 promoter activity in selected U-2 OS cells in different constant temperatures as indicated after synchronization with dexamethasone.
RGS16 knockdowns (pink) vs the controls (blue). No detrending, no smoothing.

Subcloned U-2 OS cells

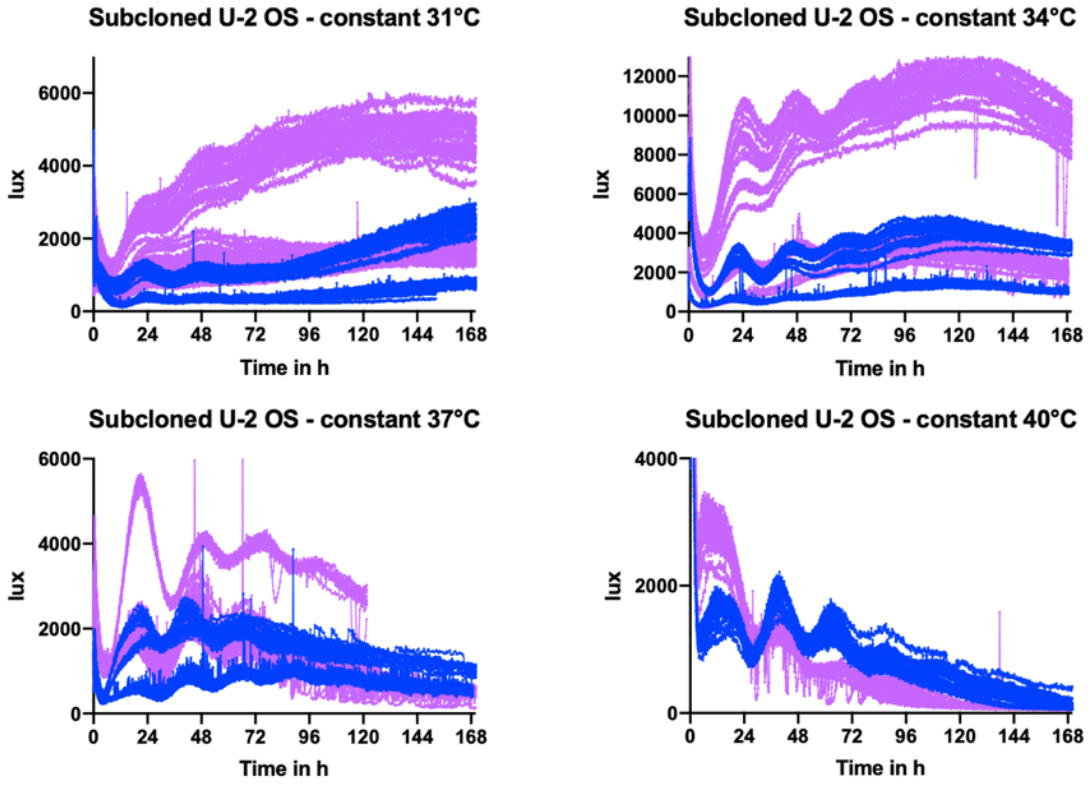

Figure S 2: Line graphs of a luciferase reporter of Bmal1 promoter activity in subcloned U-2 OS in different constant temperatures as indicated after synchronization with dexamethasone.
RGS16 knockdowns (pink) vs the controls (blue). No detrending, no smoothing.

Selected ARPE-19 cells

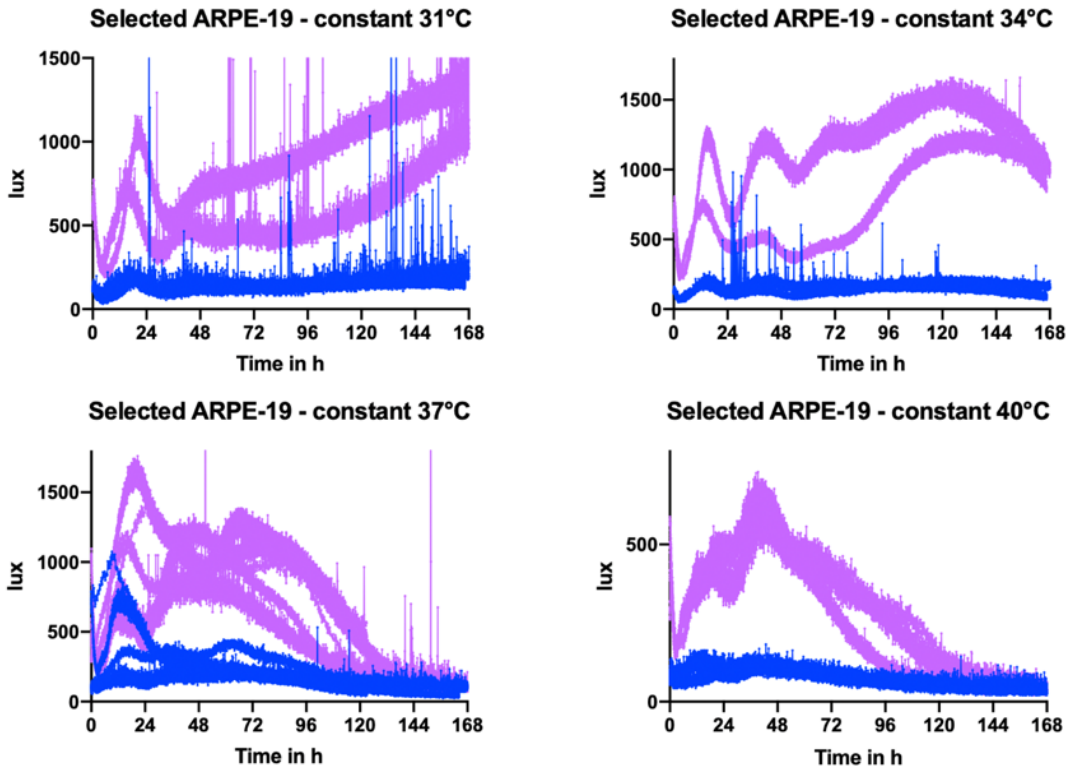

Figure S 3: Line graphs of a luciferase reporter of Bmal1 promoter activity in selected ARPE-19 cells in different constant temperatures as indicated after synchronization with dexamethasone.
RGS16 knockdowns (pink) vs the controls (blue). No detrending, no smoothing.

7.1.2 Phase of entrainment:

Selected U-2 OS cells

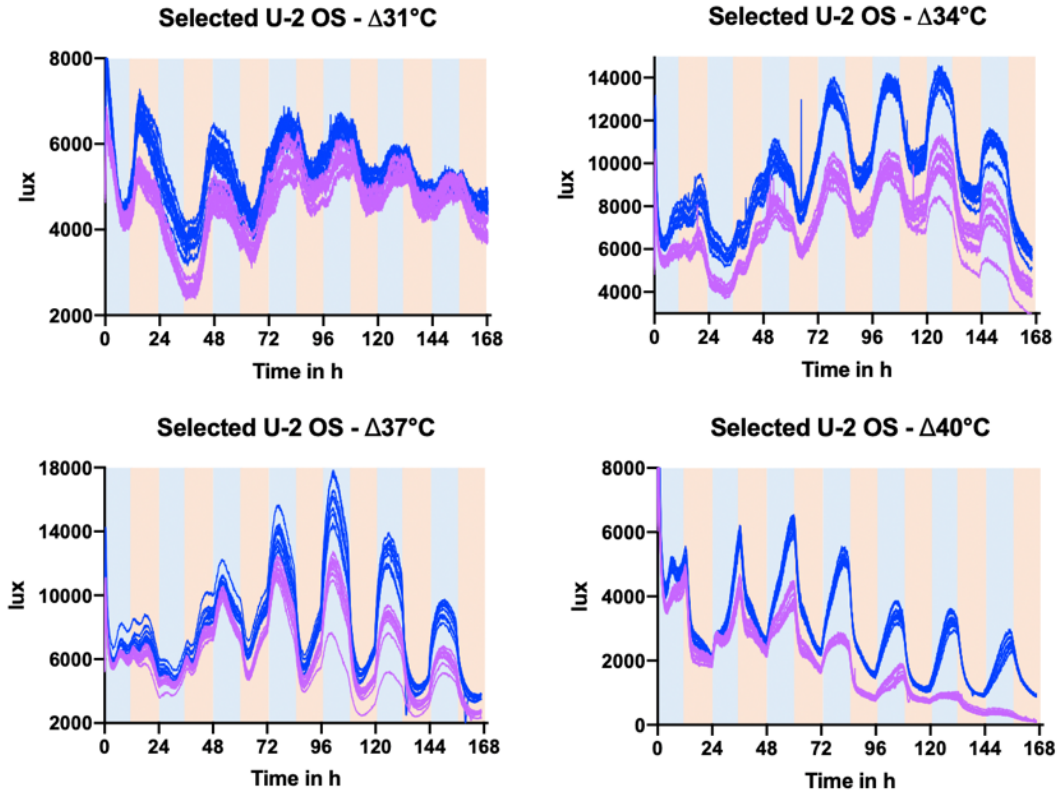

Figure S 4: Line graphs of a luciferase reporter of Bmal1 promoter activity in selected U-2 OS cells in 29.5/32.5°C, 32.5/35.5°C, 35.5/38.5°C, 38.5/41.5°C, in 12:12 as indicated.
RGS16 knockdowns (pink) vs the controls (blue). No detrending, no smoothing.

Subcloned U-2 OS cells

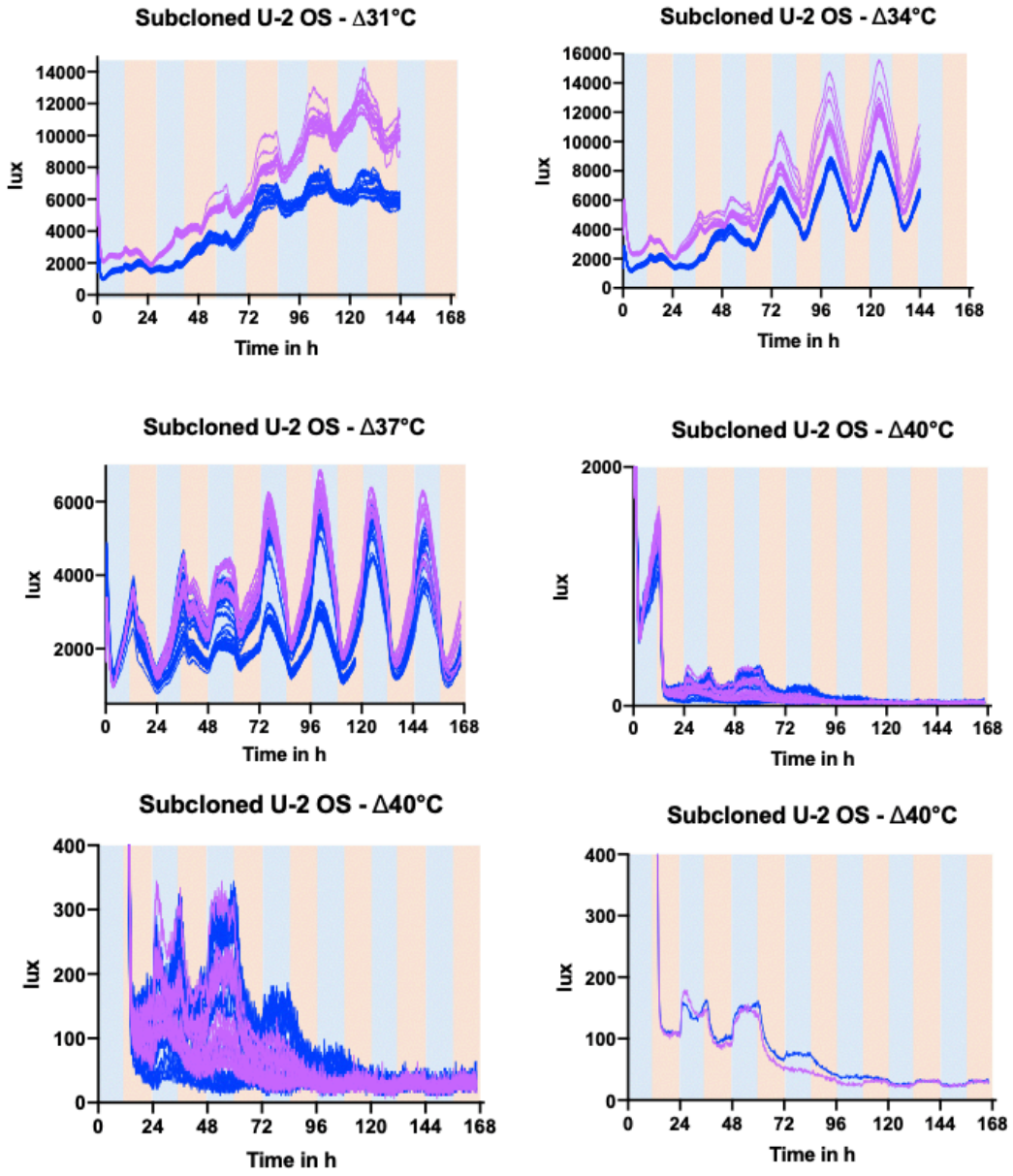

Figure S 5: Line graphs of a luciferase reporter of Bmal1 promoter activity in subcloned U-2 OS cells in 29.5/32.5°C, 32.5/35.5°C, 35.5/38.5°C, 38.5/41.5°C, in 12:12 as indicated.
RGS16 knockdowns (pink) vs the controls (blue). No detrending, no smoothing.

Selected ARPE-19 cells

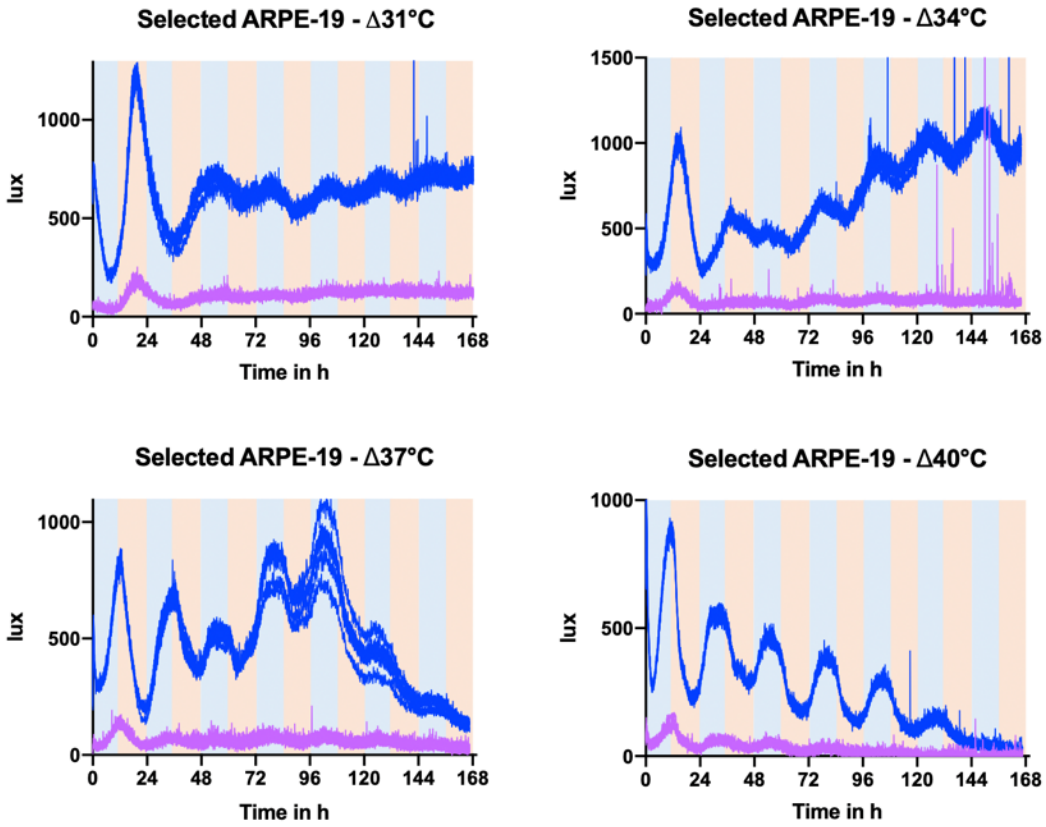

Figure S 6: Line graphs of a luciferase reporter of Bmal1 promoter activity in selected ARPE-19 cells in 29.5/32.5°C, 32.5/35.5°C, 35.5/38.5°C, 38.5/41.5°C, in 12:12 as indicated.
RGS16 knockdowns (pink) vs the controls (blue). No detrending, no smoothing.

7.1.3 Temperature Compensation: Alternative Q_{10} calculation

Period: Selected U-2 OS cell line

Controls: 1.027 ± 0.031

KDs: 1.333 ± 0.102

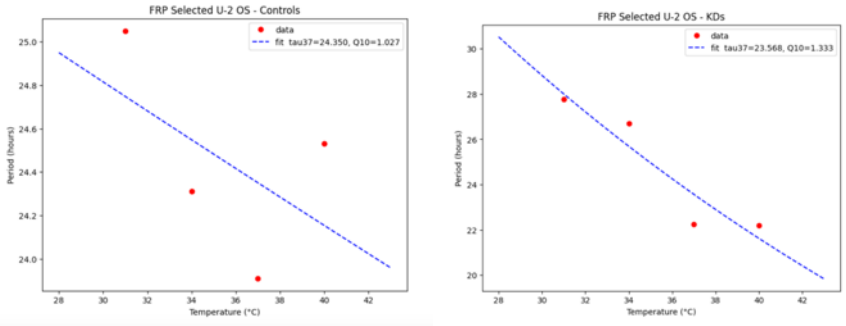

Period: Subcloned U-2 OS cell line

Controls: 0.977 ± 0.005

KDs: 1.319 ± 0.085

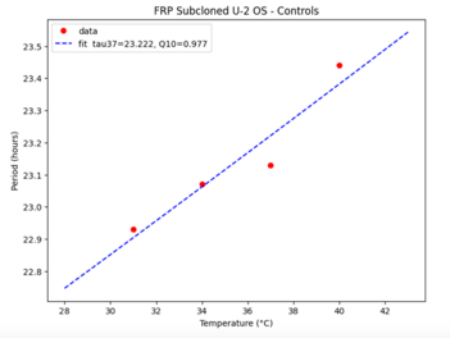

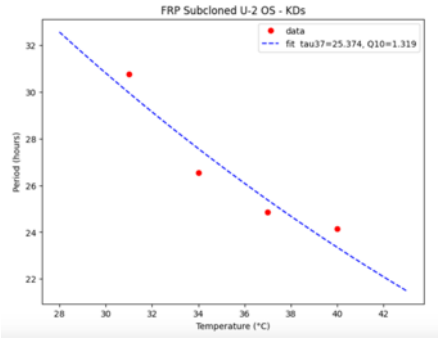

Period: Selected ARPE-19 cell line

Controls: 1.015 ± 0.141

KDs: 1.046 ± 0.066

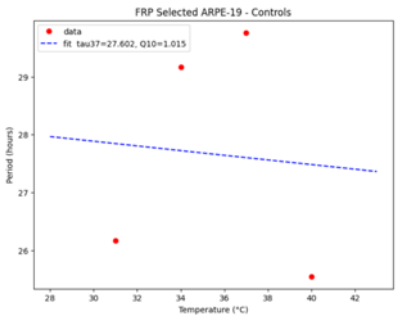

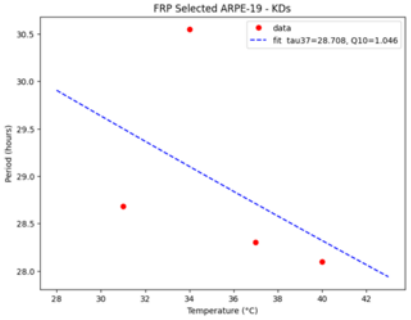

Phase: Selected U-2 OS cell line

Controls: 1.038 ± 0.071

KDs: 1.019 ± 0.102

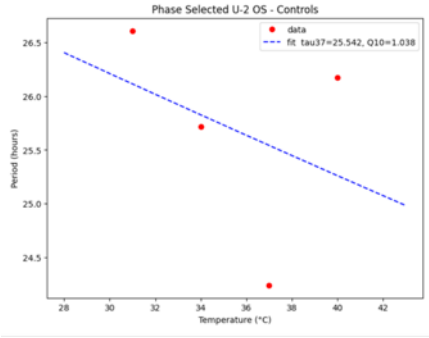

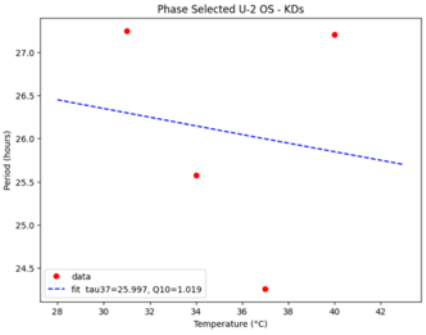

Phase: Subcloned U-2 OS cell line

Controls: 0.824 ± 0.234

KDs: 0.628 ± 0.243

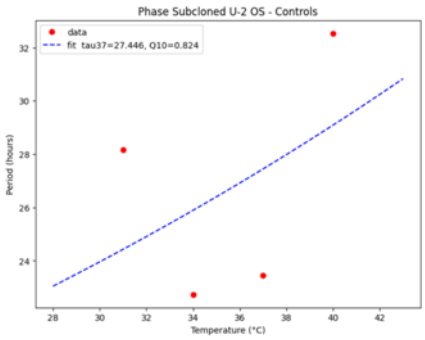

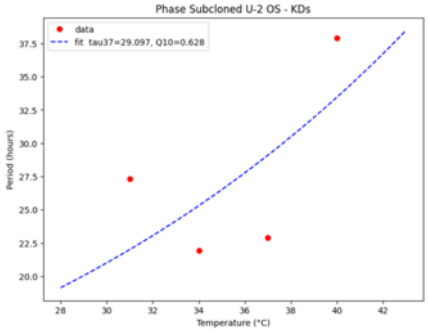

Phase: Selected ARPE-19 cell line

Controls: 1.048 ± 0.113

KDs: 1.214 ± 0.556

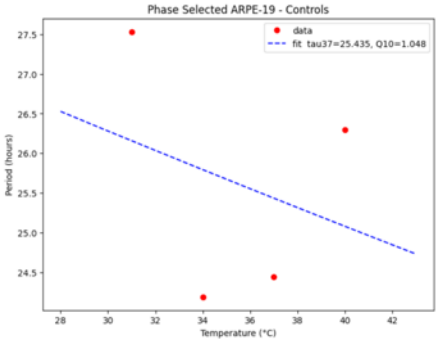

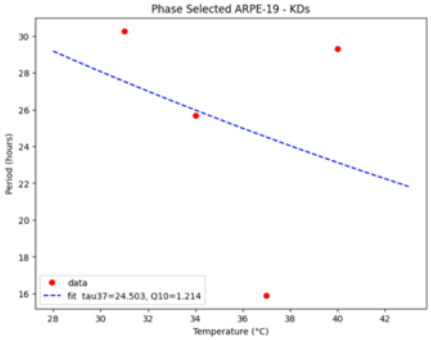

7.2 Immunofluorescence Experiments

7.2.1 IF Time course

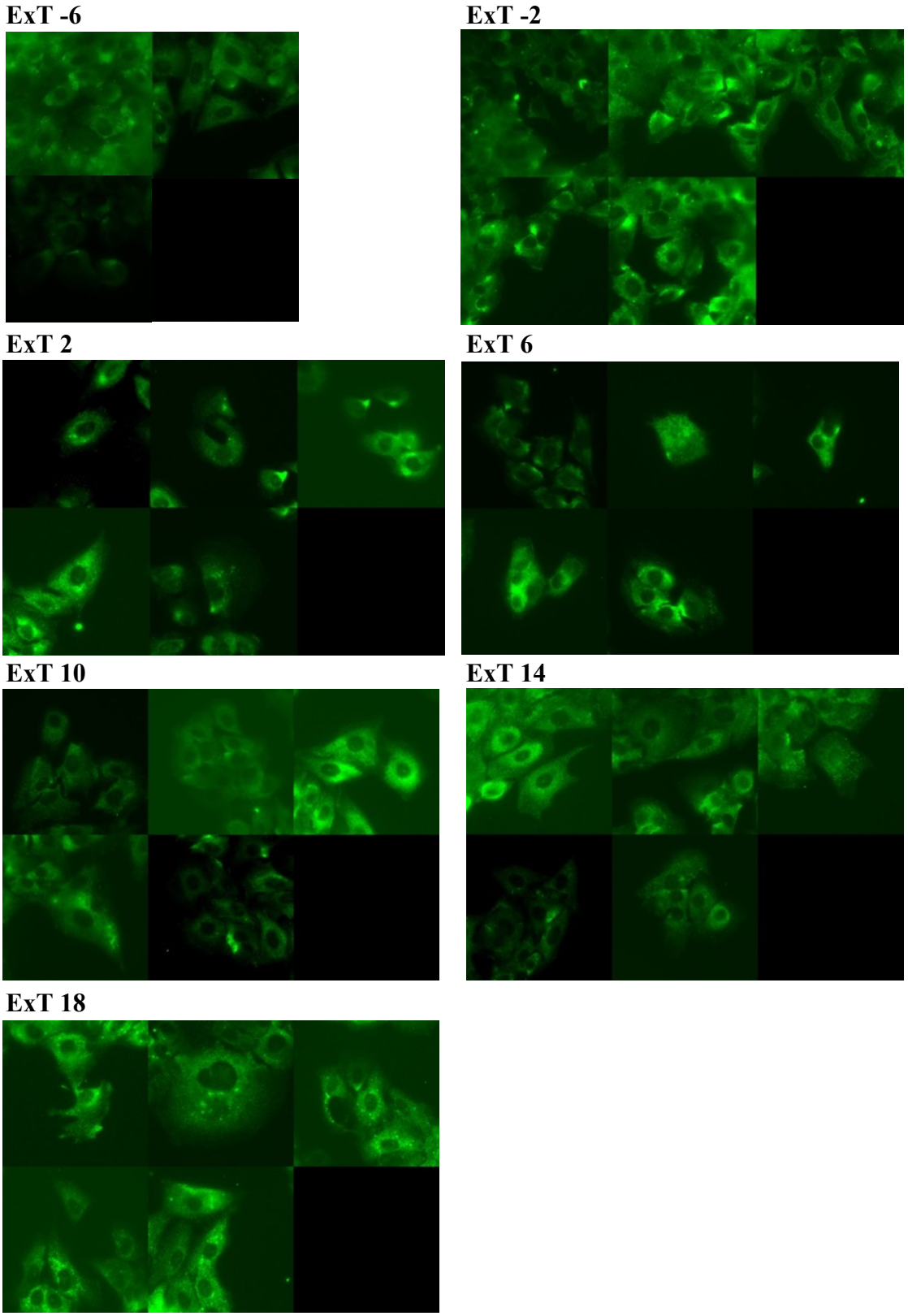

Figure S 7: Immunofluorescence of GFP-stained RGS16 protein over 24 h in entrainment.
The cells were entrained in 34/37°C 12:12 and then released into 34°C or 37°C for 3 days before harvesting.
ExT = External Time; time point 0 indicates mid-cold.

7.2.2 Temperature Pulses

27°C for 4 h

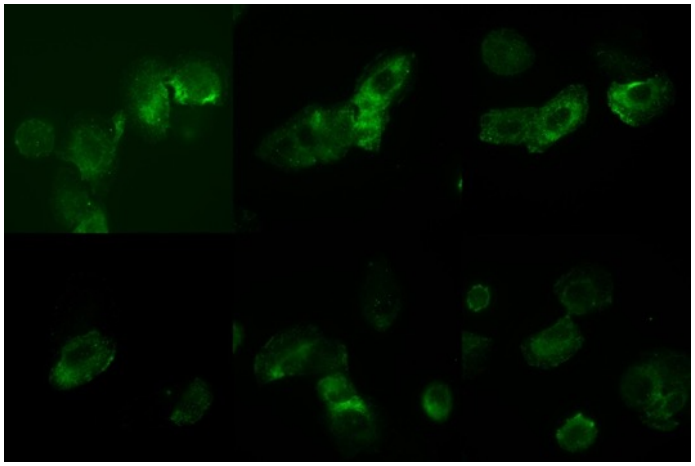

37°C for 4 h (control)

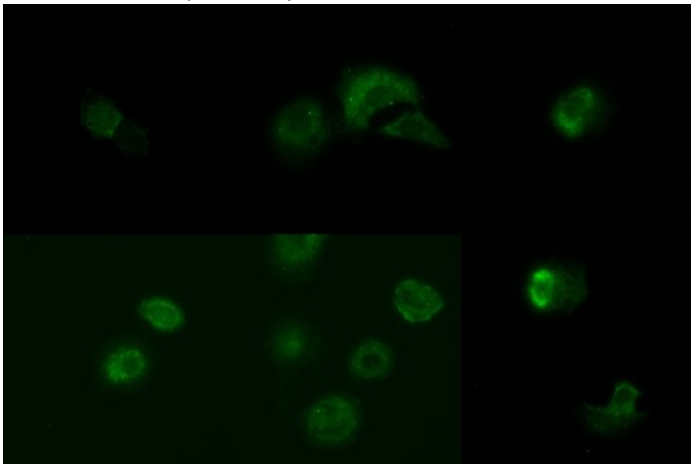

43°C for 4 h

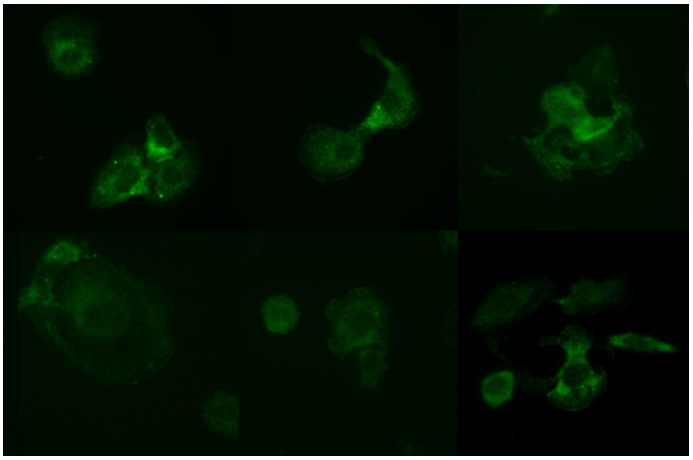

Figure S 8: Immunofluorescence of GFP-stained RGS16 protein after temperature pulses of 27°C and 43°C for 4 h.
The cells were kept in 37°C and then exposed to the indicated temperatures for 4 hours.

7.2.3 GPCR Stimulation

Control

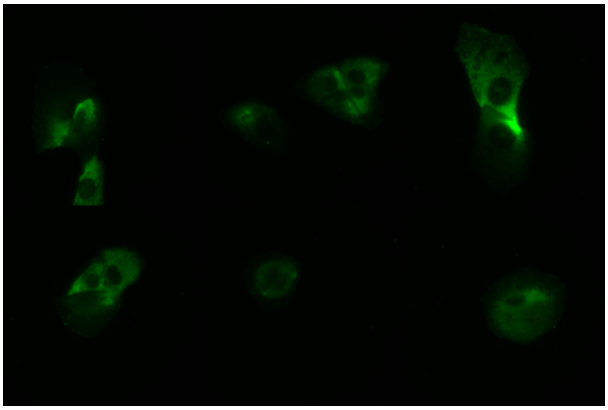

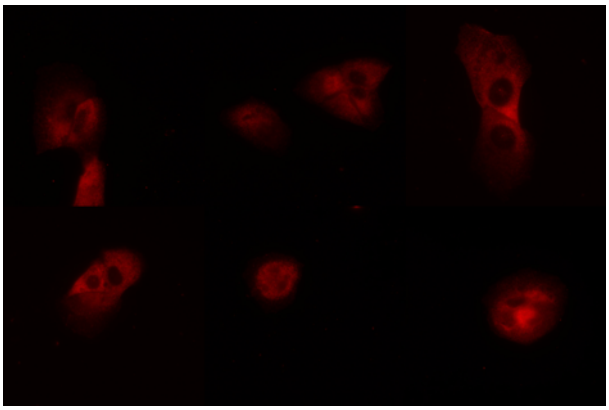

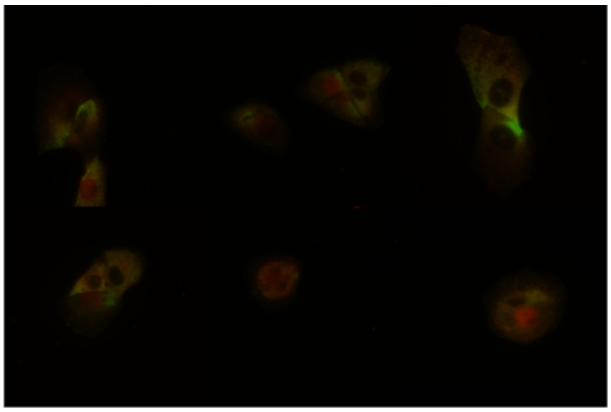

Caffeine

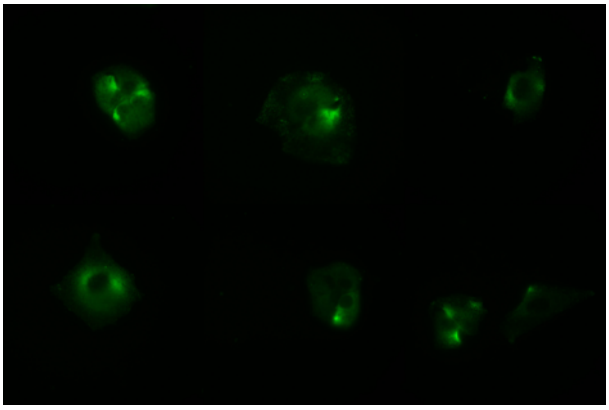

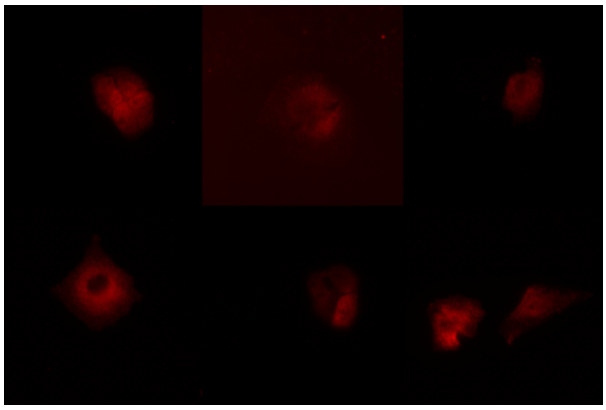

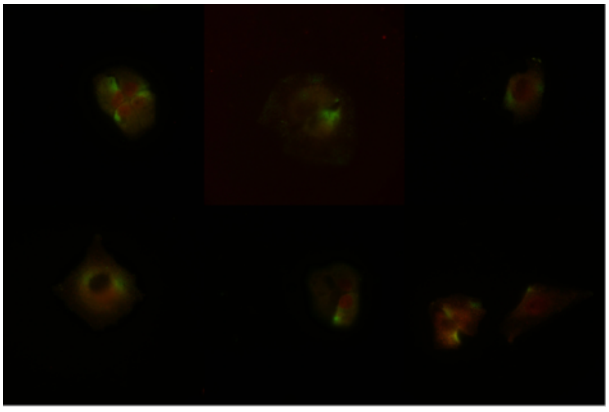

N-CHA

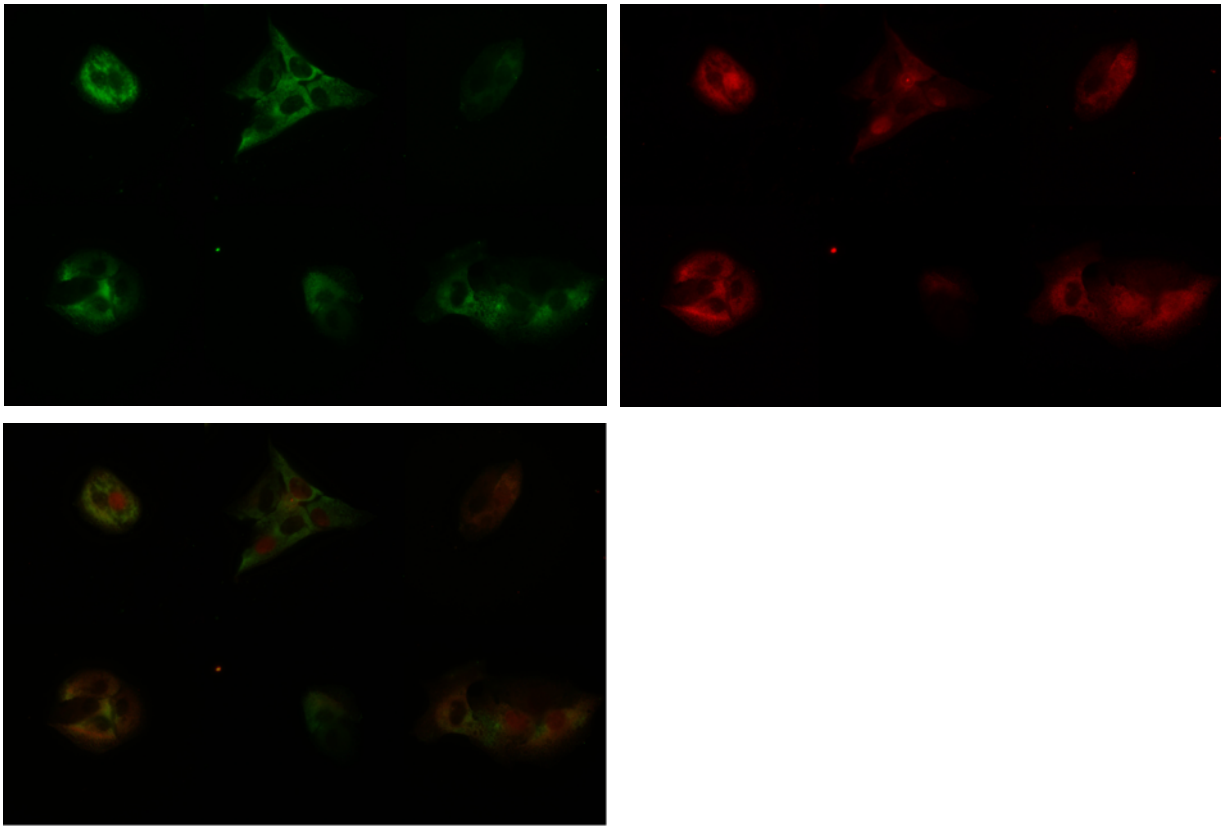

Dopamine

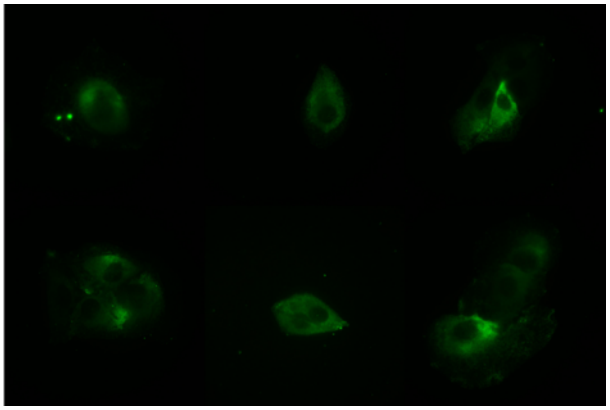

Serotonin

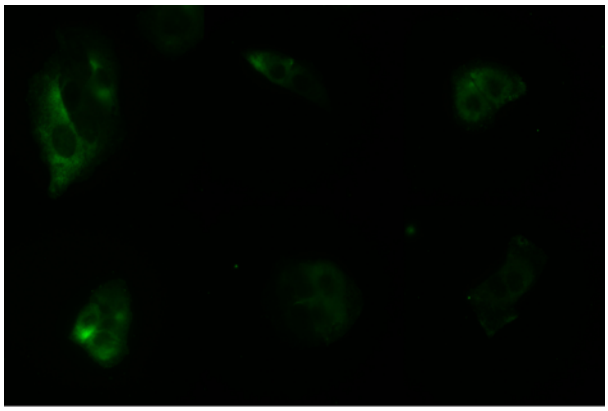

Phenylephrine

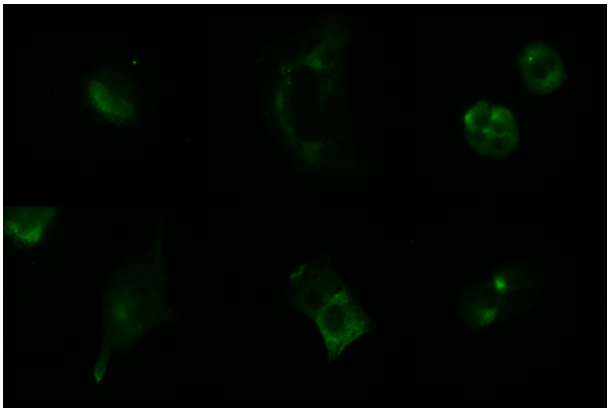

Isoprenaline

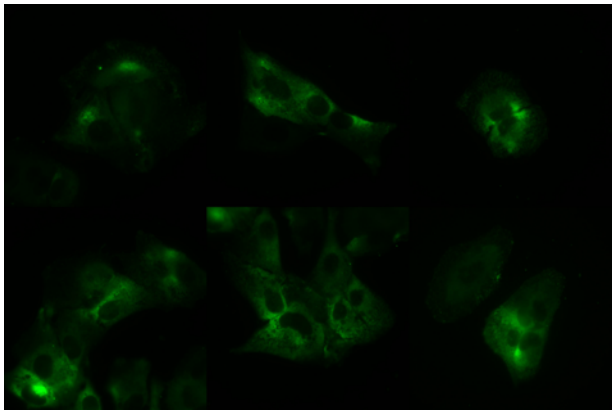

Figure S 9: Immunofluorescence RGS16 (green, GFP) and A1R (red, RFP) after treatment with 100 µM of caffeine, N6-cyclohexyladenosine, dopamine, serotonin, phenylephrine, or isoprenaline as indicated for 5 min. Controls, Caffeine, N-CHA: left: RGS16, right: A1R, below: overlay. Dopamine, serotonin, phenylephrine, and isoprenaline: RGS16 only.

7.2.4 Distribution of RGS16 via visual scoring system:

Scoring of 1 to 5 for each individual cell.
Questions 1 to 4 exclude bright spots.

1.) Distribution within the cell: nuclear
(1) no nuclear signal
(2) low signal in the nucleus
(3) equal signal in nucleus as in overall cytoplasm
(4) more signal in nucleus than in overall cytoplasm
(5) only nuclear signal

2.) Distribution within the cell: perinuclear
(1) no perinuclear signal
(2) low perinuclear signal
(3) equal perinuclear signal as in overall cytoplasm
(4) more perinuclear signal than in overall cytoplasm
(5) only perinuclear signal

3.) Distribution within the cell: membrane-near
(1) no membrane-near signal
(2) low membrane-near signal
(3) equal membrane-near signal as in overall cytoplasm
(4) more membrane-near signal than in overall cytoplasm
(5) only membrane-near signal

4.) Distribution within the cytoplasm:
(1) homogenous distribution of the signal
(2) more signal around the nucleus
(3) more signal in one side/corner of the cell
(4) more signal in two sides/corners of the cell
(5) multifocal (3+) bright areas

5.) Homogeneity of the signal (bright spots):
(1) no bright spots
(2) one to three bright spots
(3) few bright spots
(4) many bright spots
(5) only bright spots
(then summarized as ≤ 3 and > 3)

7.2.4.1 RGS16 distribution in response to temperature pulses

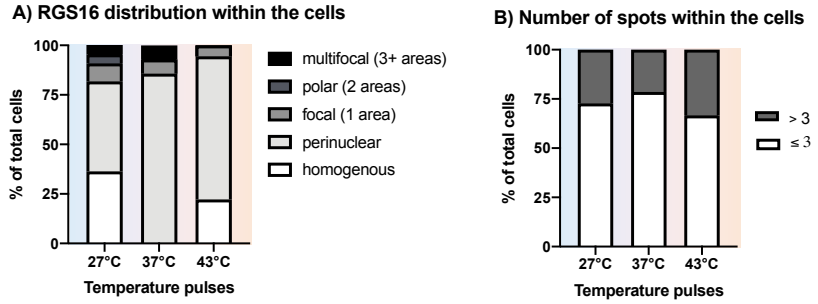

Figure S 10: Immunofluorescence of GFP-stained RGS16 protein after temperature pulses of 27°C and 43°C for 4 h.
The cells were kept in 37°C and then exposed to the indicated temperatures for 4 hours. The cells were scored visually via the visual scoring system above to determine signal and spot distribution.
A) Percentage of cells that (visually) had their main signal concentrated in the indicated area(s).
B) Percentage of cells that had more than 3 (gray) vs. up to 3 (white) bright spots.

7.2.4.2 RGS16 distribution in response to GPCR stimulation

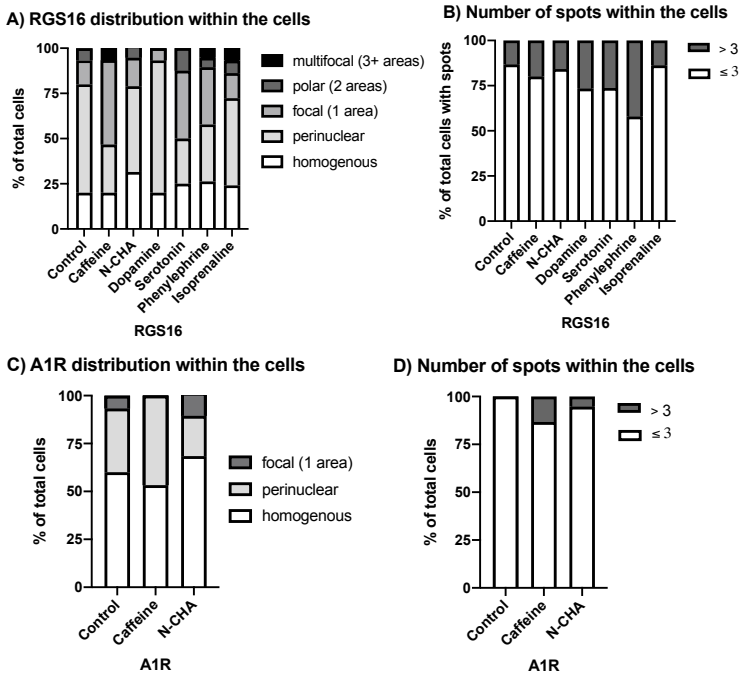

Figure S 11: Immunofluorescence of GFP-stained RGS16 protein and RFP-stained A1R protein after treatment with 100 µM of caffeine, N6-cyclohexyladenosine, dopamine, serotonin, phenylephrine, or isoprenaline as indicated for 5 min.
The cells were scored visually to determine signal and spot distribution.
A) Percentage of cells that (visually) had their main RGS16 signal concentrated in the indicated area(s).
B) Percentage of cells that had more than 3 (gray) vs. up to 3 (white) bright spots of RGS16 antibody signal.
C) Percentage of cells that (visually) had their main A1R signal concentrated in the indicated area(s).
D) Percentage of cells that had more than 3 (gray) vs. up to 3 (white) bright spots of A1R antibody signal.

7.3 Line graphs cAMP free-run (luminometry)

There seem to be two populations within the different cell lines that show either a long (around 30 h) or a short period (around 22 h). Shown below are the single line graphs of all wells that were deemed rhythmic and circadian.

Controls - Long

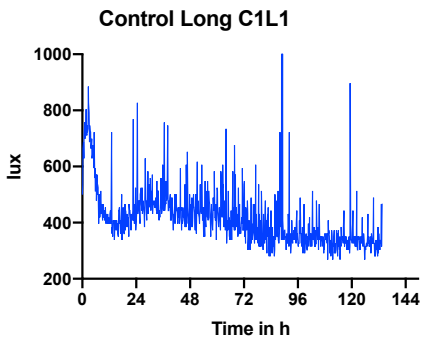

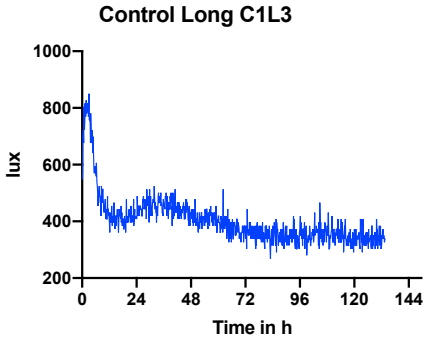

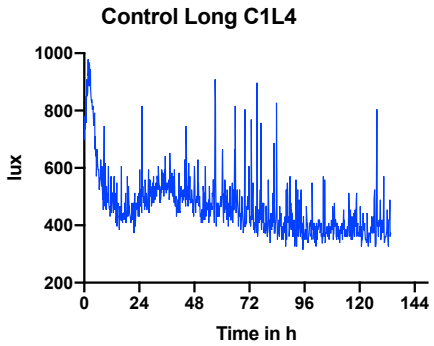

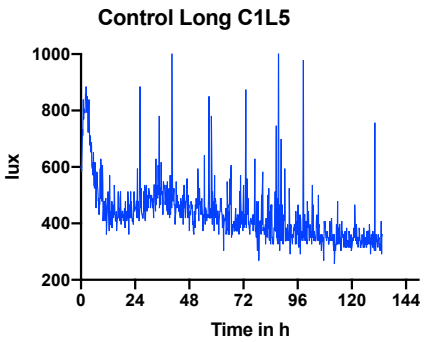

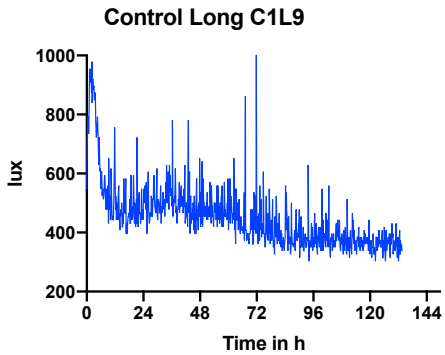

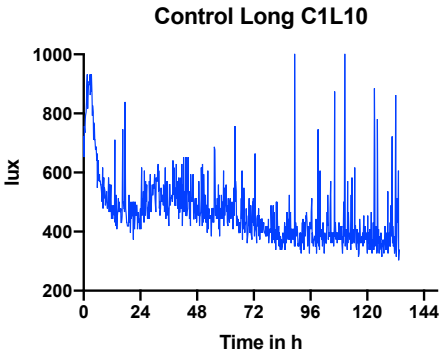

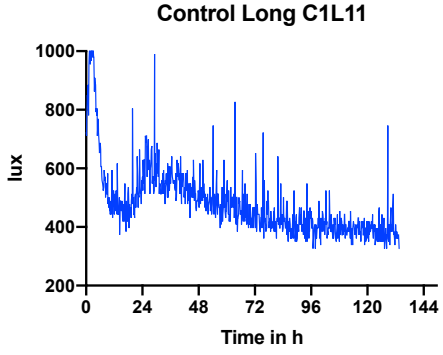

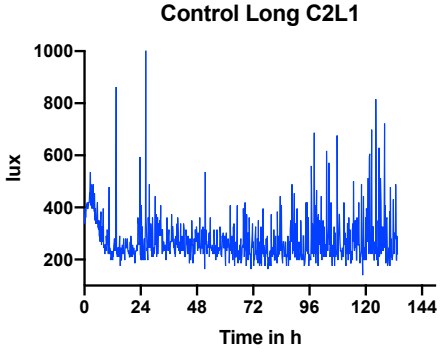

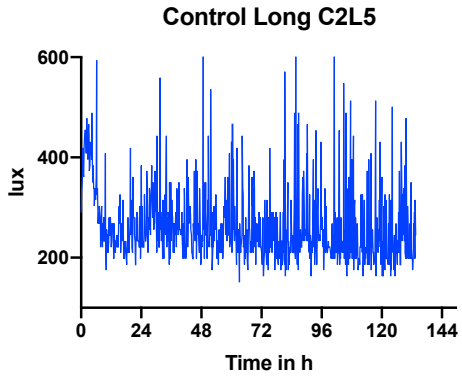

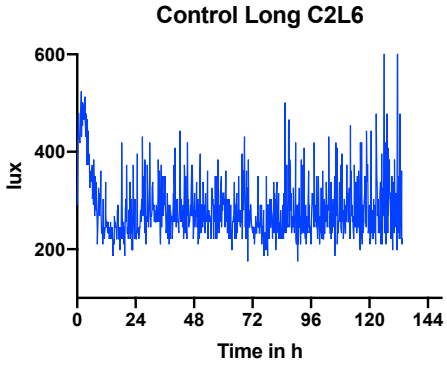

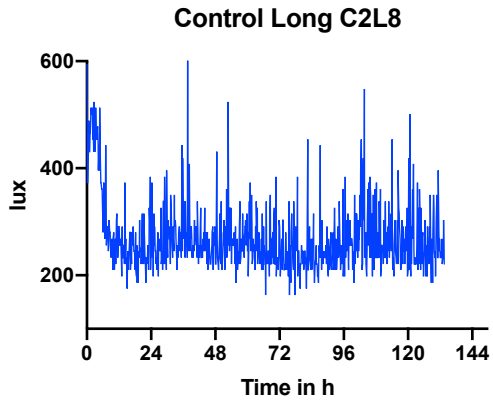

Controls – Short

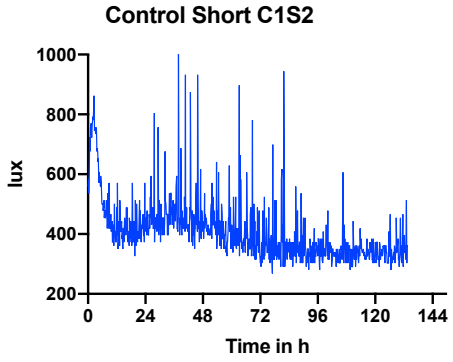

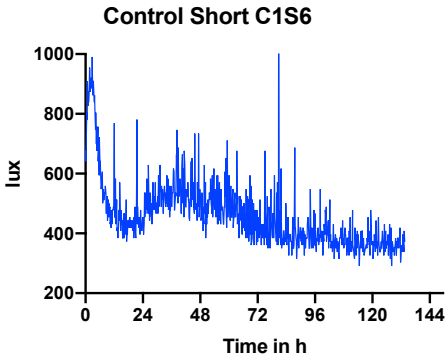

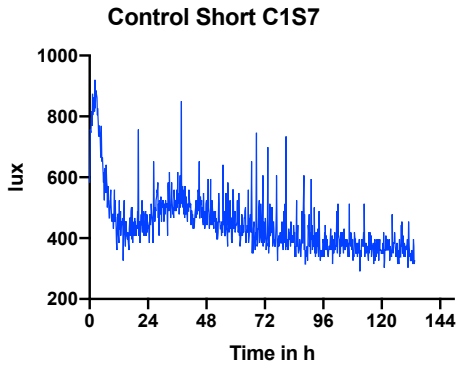

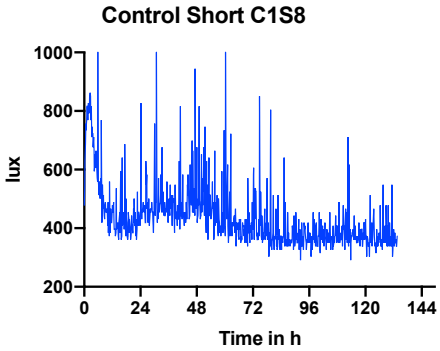

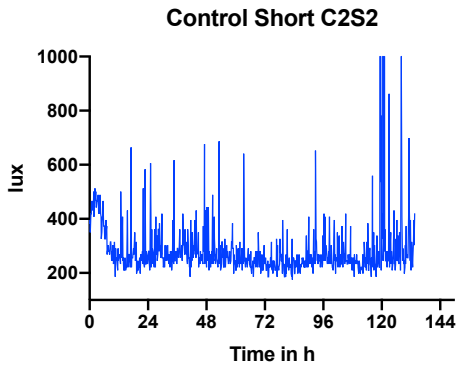
Control Short C2S2
lux
1000
800
600
400
200
0
24
48
72
96
120
144
Time in h

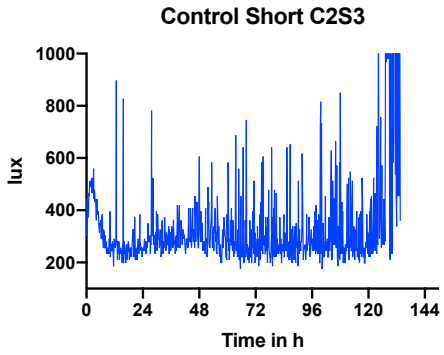
Control Short C2S3
lux
1000
800
600
400
200
0
24
48
72
96
120
144
Time in h

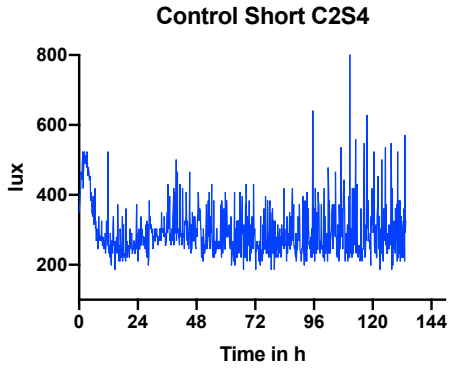
Control Short C2S4
lux
800
600
400
200
0
24
48
72
96
120
144
Time in h

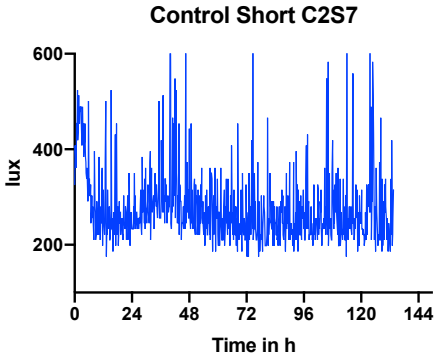
Control Short C2S7
lux
600
400
200
0
24
48
72
96
120
144
Time in h

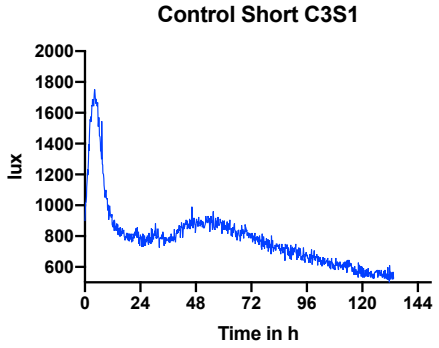
Control Short C3S1
lux
2000
1800
1600
1400
1200
1000
800
600
0
24
48
72
96
120
144
Time in h

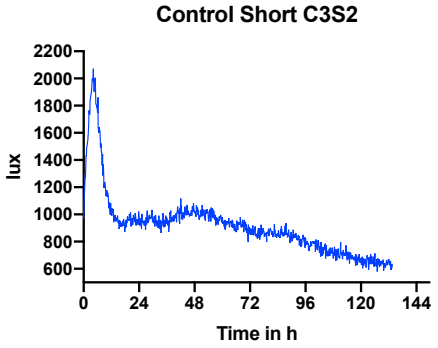
Control Short C3S2
lux
2200
2000
1800
1600
1400
1200
1000
800
600
0
24
48
72
96
120
144
Time in h

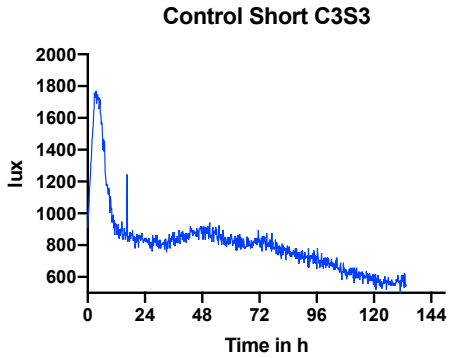
Control Short C3S3
lux
2000
1800
1600
1400
1200
1000
800
600
0
24
48
72
96
120
144
Time in h

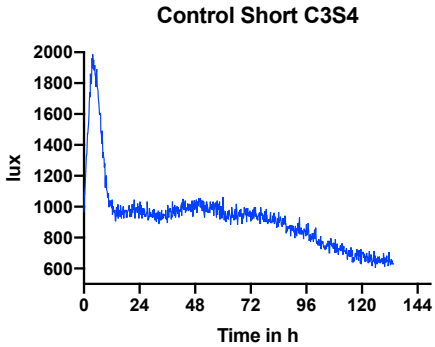
Control Short C3S4
lux
2000
1800
1600
1400
1200
1000
800
600
0
24
48
72
96
120
144
Time in h

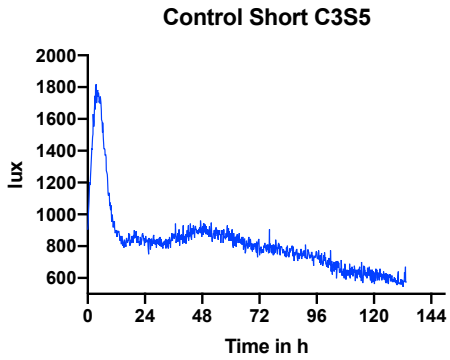
Control Short C3S5
lux
2000
1800
1600
1400
1200
1000
800
600
0
24
48
72
96
120
144
Time in h

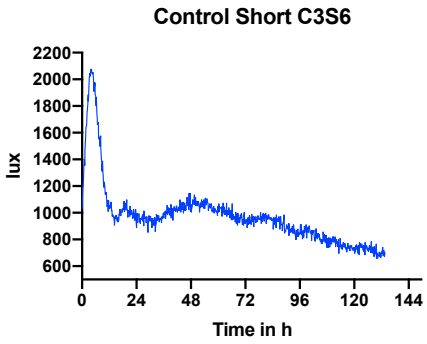
Control Short C3S6
lux
2200
2000
1800
1600
1400
1200
1000
800
600
0
24
48
72
96
120
144
Time in h

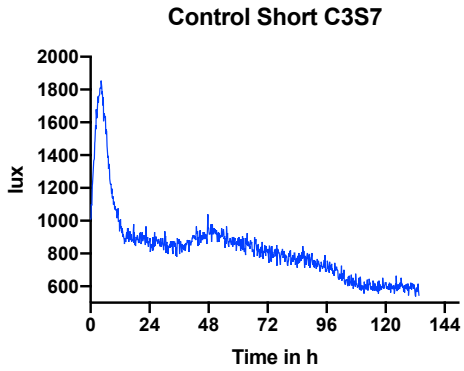
Control Short C3S7
lux
2000
1800
1600
1400
1200
1000
800
600
0
24
48
72
96
120
144
Time in h

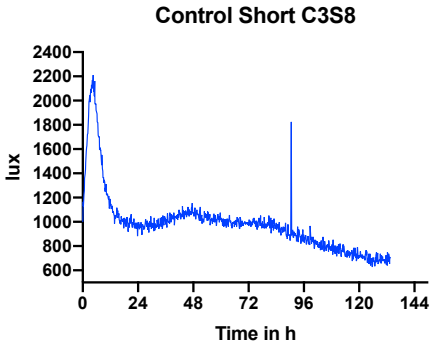
Control Short C3S8
lux
2400
2200
2000
1800
1600
1400
1200
1000
800
600
0
24
48
72
96
120
144
Time in h

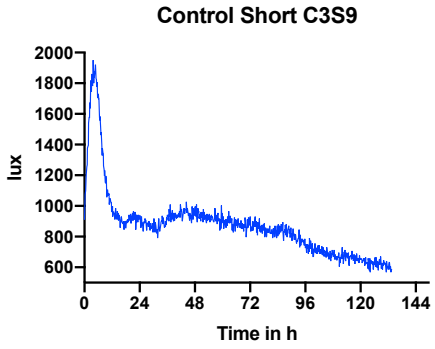
Control Short C3S9
lux
2000
1800
1600
1400
1200
1000
800
600
0
24
48
72
96
120
144
Time in h

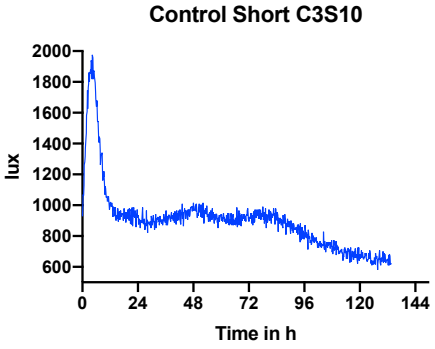
Control Short C3S10
lux
2000
1800
1600
1400
1200
1000
800
600
0
24
48
72
96
120
144
Time in h

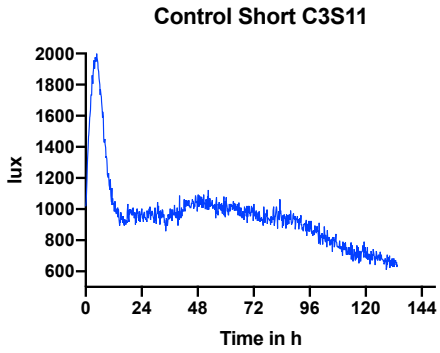
Control Short C3S11
lux
2000
1800
1600
1400
1200
1000
800
600
0
24
48
72
96
120
144
Time in h

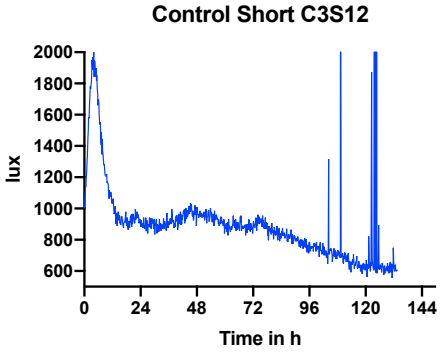
Control Short C3S12
lux
2000
1800
1600
1400
1200
1000
800
600
0
24
48
72
96
120
144
Time in h

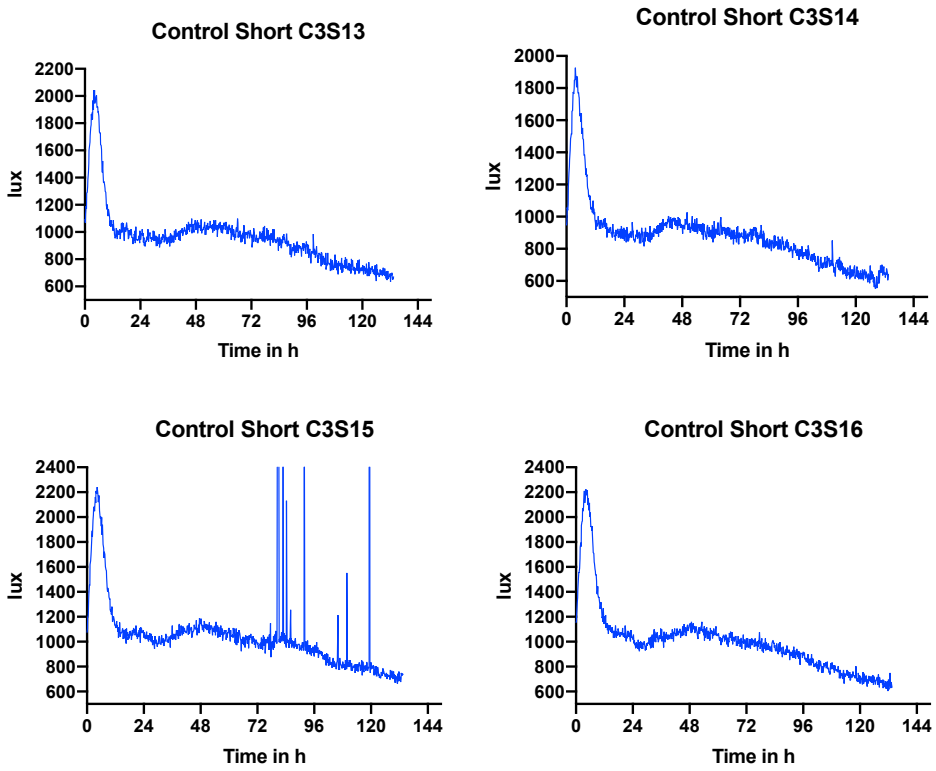
Control Short C3S13
lux
Time in h
Control Short C3S14
lux
Time in h
Control Short C3S15
lux
Time in h
Control Short C3S16
lux
Time in h

RKD - Long

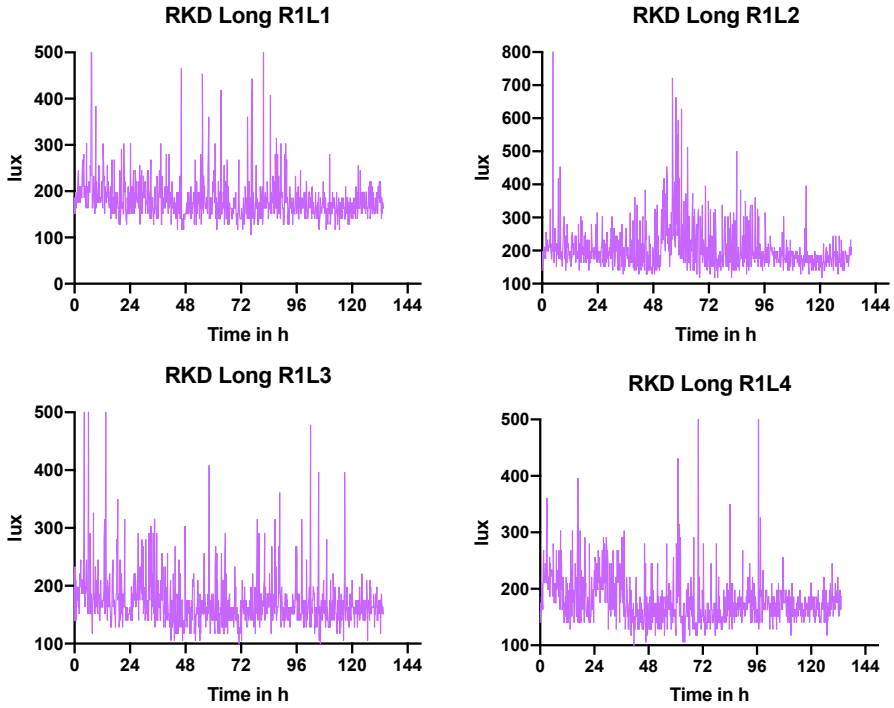
RKD Long R1L1
lux
Time in h
RKD Long R1L2
lux
Time in h
RKD Long R1L3
lux
Time in h
RKD Long R1L4
lux
Time in h

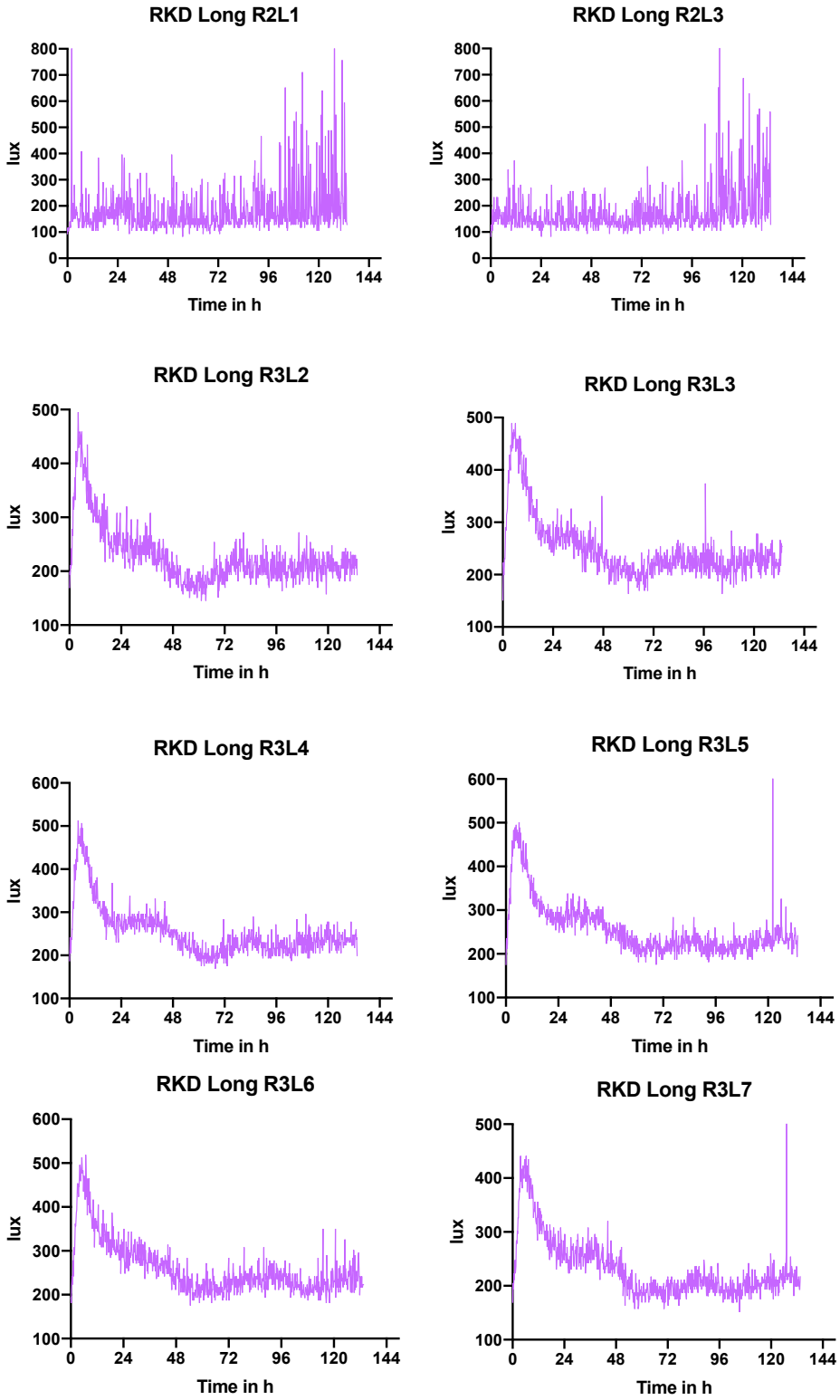
RKD Long R2L1
RKD Long R2L3
RKD Long R3L2
RKD Long R3L3
RKD Long R3L4
RKD Long R3L5
RKD Long R3L6
RKD Long R3L7
lux
Time in h
0
24
48
72
96
120
144

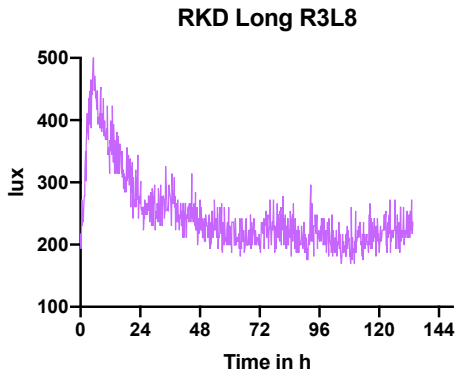
RKD Long R3L8
lux
500
400
300
200
100
0
24
48
72
96
120
144
Time in h

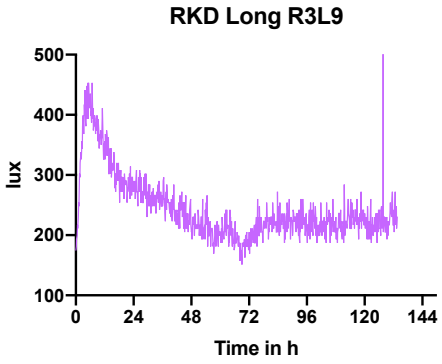
RKD Long R3L9
lux
500
400
300
200
100
0
24
48
72
96
120
144
Time in h

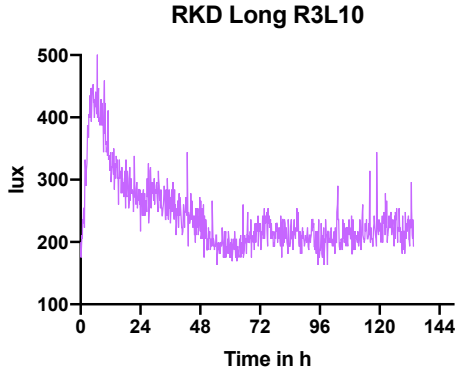
RKD Long R3L10
lux
500
400
300
200
100
0
24
48
72
96
120
144
Time in h

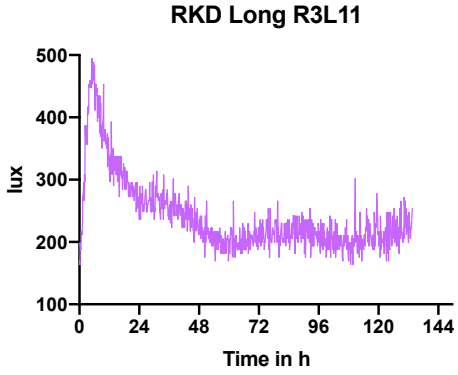
RKD Long R3L11
lux
500
400
300
200
100
0
24
48
72
96
120
144
Time in h

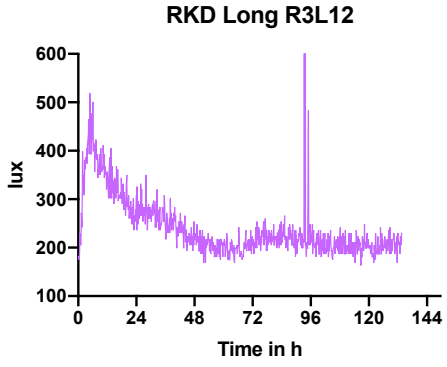
RKD Long R3L12
lux
600
500
400
300
200
100
0
24
48
72
96
120
144
Time in h

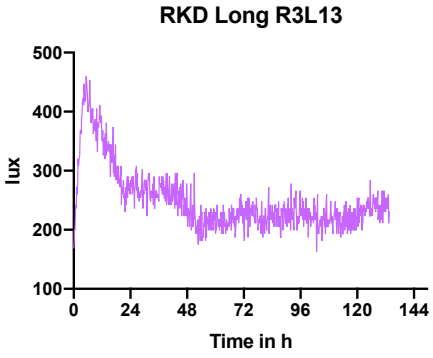
RKD Long R3L13
lux
500
400
300
200
100
0
24
48
72
96
120
144
Time in h

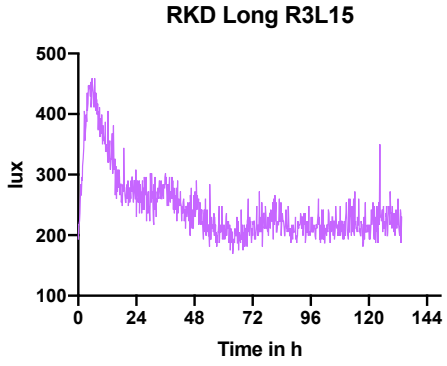
RKD Long R3L15
lux
500
400
300
200
100
0
24
48
72
96
120
144
Time in h

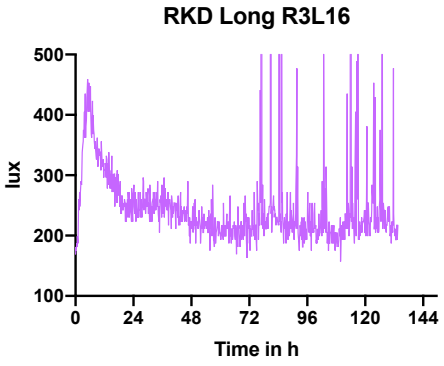
RKD Long R3L16
lux
500
400
300
200
100
0
24
48
72
96
120
144
Time in h

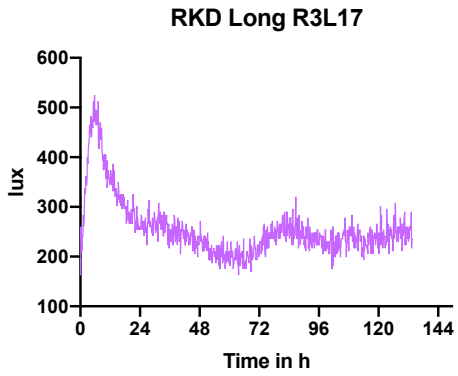

RKD - Short

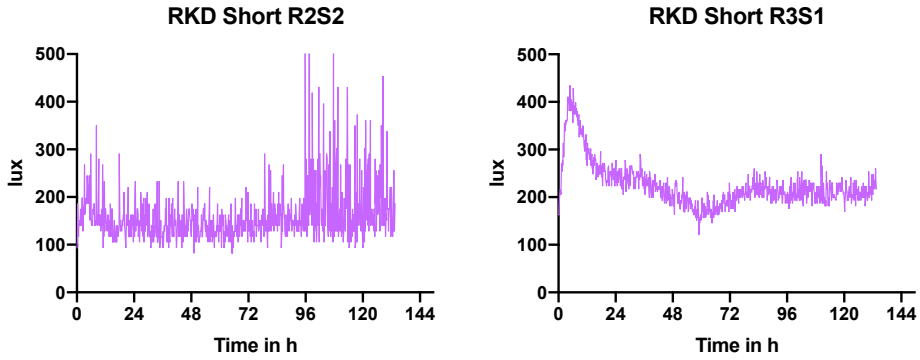

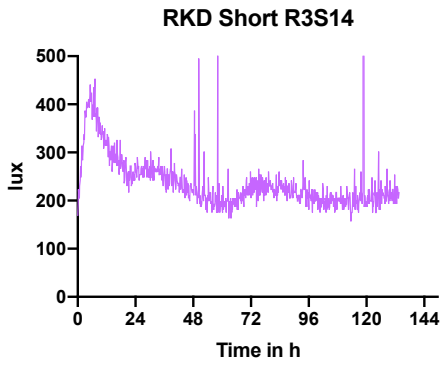

Figure S 12: Line graphs of U-2 OS cells containing a cAMP luciferase reporter (Promega GloSensor) in constant 34°C after synchronization with dexamethasone.
Shown is the RGS16 knockdown cell line (pink) vs a control cell line (blue), short and long phenotypes as indicated.

Acknowledgements

Thank you to everyone who supported me throughout this journey – my family, friends, and supervisors. Your encouragement, guidance, and support have been invaluable, and without them, this would not have been possible.

I would like to especially thank Martha for introducing me to the world of science and for guiding me through this process with patience and expertise.

I am forever grateful to my daughter, Emilia, who reminds my daily of why it is important to pursue and persevere, to stay curious and open-minded, and strive to be my best self.

Eidesstattliche Versicherung

Schwarzmeier, Tanja

Name, Vorname

Ich erkläre hiermit an Eides statt, dass ich die vorliegende Dissertation mit dem Titel

The circadian clock and G-protein-coupled receptor signaling: RGS16 and how it controls chronotype

selbständig verfasst, mich außer der angegebenen keiner weiteren Hilfsmittel bedient und alle Erkenntnisse, die aus dem Schrifttum ganz oder annähernd übernommen sind, als solche kenntlich gemacht und nach ihrer Herkunft unter Bezeichnung der Fundstelle einzeln nachgewiesen habe.

Ich erkläre des Weiteren, dass die hier vorgelegte Dissertation nicht in gleicher oder in ähnlicher Form bei einer anderen Stelle zur Erlangung eines akademischen Grades eingereicht wurde.

München, 20.11.2025

Ort, Datum

Tanja Schwarzmeier

Unterschrift Tanja Schwarzmeier

LMU LUDWIG-MAXIMILIANS-UNIVERSITÄT MÜNCHEN

Dekanat Medizinische Fakultät
Promotionsbüro

Erklärung zur Übereinstimmung der gebundenen Ausgabe der Dissertation mit der elektronischen Fassung

Schwarzmeier, Tanja

Name, Vorname

Hiermit erkläre ich, dass die elektronische Version der eingereichten Dissertation mit dem Titel:

The circadian clock and G-protein-coupled receptor signaling: RGS16 and how it controls chronotype

in Inhalt und Formatierung mit den gedruckten und gebundenen Exemplaren übereinstimmt.

München, 20.11.2025	Tanja Schwarzmeier
Ort, Datum	Unterschrift Tanja Schwarzmeier

List of Publications

Haag, M., Igel, C., & Fischer, M. (2018). Digital Teaching and Digital Medicine: A national initiative is needed. GMS Journal for Medical Education, 35.
https://doi.org/10.3205/zma001189
(Als Mitglied des Ausschusses für Digitalisierung der GMA)

Haspel, J., Kim, M., Zee, P., Schwarzmeier, T., Montagnese, S., Panda, S., Albani, A., & Merrow, M. (2021). A Timely Call to Arms: COVID-19, the Circadian Clock, and Critical Care. Journal of Biological Rhythms, 36(1), 55-70.
https://doi.org/10.1177/0748730421992587

Posters:

The circadian clock and G-protein-coupled receptor signaling: RGS16 and how it controls chronotype; 13th Harvard-LMU Young Scientists' forum, ONLINE from July 12-14, 2021

The circadian clock and G-protein-coupled receptor signaling: RGS16 and how it controls chronotype; EBRS 2022 conference Zürich